UNIVERSITY OF CALIFORNIA
RIVERSIDE

Neuronal Activity in the Auditory System of the *Fmr1* KO Mouse

A Dissertation submitted in partial satisfaction
of the requirements for the degree of

Doctor of Philosophy

in

Bioengineering

by

Anna O. Nguyen

December 2019

Dissertation Committee:
Dr. Khaleel Abdulrazak, Chairperson
Dr. B. Hyle Park
Dr. Devin K. Binder

The Dissertation of Anna O. Nguyen is approved:

_____

_____

_____

Committee Chairperson

University of California, Riverside

Acknowledgements

I would like to acknowledge my guidance and dissertation committee members Drs. Khaleel A. Razak, Hyle B. Park, and Devin K. Binder. In addition, Drs. Peter Hickmott and Iryna Ethell have been instrumental to my oral qualifying committee. Every one of their valuable feedback, guidance, and enthusiasm about my work had aided my professional growth and shaped my research into its present form. I am humbled by their hard work and grateful for the mentorship they have provided.

In addition, I would like to acknowledge Dr. Wei Dong at the Loma Linda, VA for all of the accommodations that she had provided for me in her lab and her expertise on ABR and DPOAE. The members of her lab have been extremely generous with their time. I would like to especially thank Glenna Stomackin for her patience in training me on the protocols and Bart Stagner for his help on the ABR and DPOAE analysis.

I would like to thank the members of the Razak Lab (past and present) and the members of the neighboring lab of Dr. Peter Hickmott for their friendship and good company throughout the late nights and early mornings in the lab and office.

I wish to thank the support staff in both the Bioengineering and Psychology department: Renee Young, Annette Meneses, Reneisha Wilkes, and Nancy Ford for all of their hard work to keep the department affairs running smoothly and their support for the graduate students.

And lastly, I wish to thank my family for all their support and kindness. My grandparents, parents, uncle, and sister have always placed my education as their priority. Because of the confidence they have in me, I was able to pursue my PhD.

Chapter 4, Effects of Noise-induced Hearing Loss on Parvalbumin and Perineuronal Net Expression in the Mouse Primary Auditory Cortex, had been previously published in 2017 in the journal, Hearing Research. The entire text and figures of the article is reproduced in this dissertation with editing of the format to match this disseration. The primary author is myself and the primary investigator is Dr. Khaleel A. Razak.

Dedication

To my family, for their unconditional love and support.

ABSTRACT OF THE DISSERTATION

Neuronal Activity in the Auditory System of the *Fmr1* KO Mouse

by

Anna O. Nguyen

Doctor of Philosophy, Graduate Program in Bioengineering
University of California, Riverside, December 2019
Dr. Khaleel A. Razak, Chairperson

This dissertation examined how the auditory system in the *Fmr1* KO mouse, a model of Fragile X Syndrome (FXS), processes sounds as a way to examine mechanisms that cause auditory hypersensitivity in this autism spectrum disorder. Using a molecular marker for neuronal activity, cFos, and single unit electrophysiology recordings in response to auditory stimuli, we sought to understand auditory hypersensitivity in the *Fmr1* KO mouse. We found a difference in cFos expression between WT and *Fmr1* KO mice that is both age and region specific. Single-unit recording in the inferior colliculus revealed higher spontaneous activity, higher response magnitude, broader tuning, longer latency, greater minimum threshold, and greater response to SAM tones in neurons tuned to CF< 20 kHz in the inferior colliculus. These results suggest an overall excitability or lack of inhibition in the inferior colliculus of the mouse model for FXS.

In addition, this dissertation describes two areas in the auditory processing of FXS, audiogenic seizure and conventional audiology tests (auditory brainstem response (ABR) and distortion product otoacoustic emissions (DPOAE)). Our results show a correlation between audiogenic seizure severity and sound intensity. We did not see a difference in ABR amplitudes between genotypes; however, there was latency deficits in peak III and V of the ABR waveform. The DPOAE reveal no difference between *Fmr1* KO and WT mice in Input/Output functions of magnitude and phase. These findings suggest that no auditory deficits can be detected with conventional audiology tests except for latency of peak III and peak V in the ABR waveform.

Overall, we interpret the increase in response magnitude as hyperexcitability in the inferior colliculus that is present during development; particularly at P21, which may explain the increase in susceptibility to audiogenic seizure at this age. The proposed mechanism is impairments in GABAergic functions because many of the deficits we found are in neurons with CF< 20 kHz, a region which is higher in GABA terminals than in region with CF>= 20 kHz.

Table of Contents

List of Tables

List of Figures

Chapter 2: Abnormal development of auditory responses in the inferior colliculus of a mouse model of Fragile X Syndrome

Chapter 1

Dysfunctions in the auditory system

1.1 Introduction

There are many areas throughout the auditory system pathway from the peripheral cochlea to the auditory cortex. A disruption at one or more of these auditory pathway nuclei can influence how sounds are processed. The two main dysfunctions to the auditory system in this dissertation are first, a disruption to the auditory system by environmental factors, loud sounds that damage the hair cells in the cochlea, which leads to noise-induced hearing loss. The second disruption to the auditory system is a genetic neurodevelopmental disorder called Fragile X Syndrome (FXS), which affects the auditory system in addition to causing a multitude of behavioral phenotypes. Noise-induced hearing loss and FXS cause dysfunctions in the auditory system but with different mechanisms of pathologies to the auditory circuit. A brief introduction will be presented about the noise-induced hearing loss study; however, a more extensive introduction will be presented about the FXS study.

1.2 Auditory system development

Even though the framework for capacity to hear sounds is present after birth, the auditory system continues to develop during infancy, adolescence, and into adulthood. In the mouse model of this study, the onset of hearing begins when the ear canal opens; thus, allowing sound to enter into the ear at approximately postnatal (P)10-11 (Mikaelian and Ruben, 1965). Before the onset of hearing at P10-P11, the basic circuity for hearing had already been developed and spontaneous activities throughout

the auditory system are present. The spontaneous activities before hearing onset play a role in stabilizing and forming synapses (Tritsch et al., 2007). During this developmental time point, protein factors and exposure to environmental sounds can affect the circuit development of the auditory system. An unrefined tonotopic map is present before hearing onset through genetic coordination. However, the refinement of the tonotopic map is required from exposure to environmental sounds and proper translation of developmental protein factors. The tonotopic map has malleable borders that can be influenced through experience during the critical period of development (Kandler et al., 2009; Sanes and Bao, 2009). At P10, there are broad tuning curves, longer response latencies, and increased thresholds, until P16-20 when the tuning curve narrows, response latencies shorten, and thresholds decrease to values similar to adult levels (Ehret and Romand, 1992). Functionally, responses to low frequency sounds develop first at approximately P10 and then responses to higher frequency sounds develop at P13. There is a gradual increase in neuronal responses to higher CFs from P10-P20 (Romand and Ehret, 1990). During development, there is also a change in inhibitory and excitatory balance in the auditory system (King, 2010). As development progresses, there is a decrease in spontaneous activity.

1.3 Auditory Deficits in Fragile X Syndrome

1.3.1 Neurodevelopmental disorder, Fragile X Syndrome

Fragile X Syndrome (FXS) is the leading cause of intellectual disability and genetic cause of autism spectrum disorder. This X-chromosome linked disorder affects 1:4000 males and 1:8000 females. The disorder results from expansion and hypermethylation of the trinucleotide CGG repeats in the Fragile X Mental Retardation 1 gene region (*Fmr1*) on the X chromosome. The hypermethylation of the region leads to silencing of the *Fmr1* gene and results in inadequate production of the Fragile X Mental Retardation Protein (FMRP). Symptoms of FXS include intellectual disability, hyperactivity, language impairments, and sensory hypersensitivity. Despite efforts to identify drug targets and development of pharmaceutical treatments, there is no effective medication for the wide-ranging symptoms of FXS (Bagni et al., 2012; Hagerman and Stafstrom, 2009; Hagerman et al., 2012).

FMRP is widely distributed throughout the brain, testes, ovaries, esophagus, spleen, and eyes (Hinds et al., 1993). The activity of FMRP is necessary for normal development but little is known about how the lack of FMRP impacts behavioral phenotypes. FMRP is highly expressed after the first postnatal week, and then the FMRP expression level gradually declines (Till, 2010). The main role of FMRP is a translational regulator to over 432 mRNAs (Brown et al., 2001), which suggests that the protein has an important influence on the expression levels of many mRNAs during critical times in development. There is abnormal dendritic spine development in FXS; *Fmr1* KO mice

show greater density and spine length compared to WT (Wild-type) mice (Nimchinsky et al., 2001). There is a delay in the GABA polarity switch from depolarizing to hyperpolarizing in the cortex of *Fmr1* KO mice during the first two postnatal weeks (He et al., 2014). mRNAs and proteins associated with circadian rhythm are disrupted in FXS (Zhang et al., 2008). In the *Fmr1* KO mice, there is an increased number of excitatory fibers onto one lateral superior olive neurons (Garcia-Pino et al., 2017). Previous studies have shown an impairment in *Fmr1* KO mice's ability to generate a Kv3.1b channel gradient in MNTB for quiet condition and in response to sound stimulation (Strumbos et al., 2010). The common findings in many studies in FXS are hyperexcitability (Contractor et al., 2015).

A recent review by Rais et al. (2018) covers the sensory systems (the auditory, visual, and somatosensory system) deficits in FXS. Out of the sensory deficits, auditory hypersensitivity is the most pronounced in individuals with FXS (O'Donnell and Warren, 2002; Rogers et al., 2003). However, it is still unclear what role FMRP plays in the development of the auditory system. There are clear evidences for dysfunction in auditory processing in humans (Castrén et al., 2003; Rogers et al., 2003) and rodent models of FXS (Engineer et al., 2014; Rotschafer and Razak, 2013, 2014). One approach to understanding the development of neurobiological abnormalities in FXS is to investigate the underlying mechanisms of sensory processing deficits. In the somatosensory cortex, there is a decrease in the number of inhibitory GABAergic PV-expressing interneurons in layers II/III/IV and an increase in layers V/VI (Selby et al.,

2007). WT mice exposed to 16 kHz sound from P9 to P20 develop an enlarged representation to 16 kHz in the auditory cortex, meanwhile *Fmr1* KO mice lack the enlarged representation (Kim et al., 2013), suggesting an impaired or delayed critical period plasticity in FXS. Sound-evoked electrophysiological experiments of the auditory cortex suggest abnormal neuronal response properties (Lovelace et al., 2016; Rotschafer and Razak, 2013). In vitro electrophysiological recording of the somatosensory barrel cortex revealed local circuit deficit with enhanced excitatory drive in *Fmr1* KO mice (Gibson et al., 2008). In addition, there is reduced cortical long term potentiation in *Fmr1* KO mice compared to WT mice (Li et al., 2002). EEG studies showed similar deficits in auditory processing in human with FXS and the mouse model of FXS (Ethridge et al., 2017; Lovelace et al., 2018). In addition, there are habituation deficits to repeated sounds (Ethridge et al., 2016; Lovelace et al., 2016), altered N1 wave response (Castrén et al., 2003; Knoth and Lippe, 2012; Knoth et al., 2014), and abnormal resting-state functional connectivity in FXS (Molen et al., 2014). EEG recordings in *Fmr1* KO mice showed an increase in resting state gamma power (Lovelace et al., 2018), which are consistent with findings in human's EEG recordings (Wang et al., 2017). Individuals with FXS have higher N100m component than normal controls with magnetoencephalography imaging to acoustic stimuli (Rojas et al., 2001). Individuals with FXS showed greater amounts of brain activation in a temporal discrimination task in the fMRI study (Hall et al., 2009). *Fmr1* KO mice has higher baseline and evoked gamma power compared to WT mice (Sinclair et al., 2017).

Thus, auditory deficits are a consistent, robust, and translationally relevant phenotype in FXS that will provide insights onto the mechanism of sensory hypersensitivity and may be a model for studying autistic features (Bernardet and Crusio, 2006).

1.3.2 What do we know now?

Here, I will only briefly mention the main studies that motivated this dissertation because Rotschafer and Razak, 2014 and Rais et al., 2018 are excellent reviews of the auditory system and sensory deficits in FXS. In conjunction, I will introduce relevant studies since the publication of Rotschafer and Razak, 2014's review with an emphasis in the area of development and subcortical studies and how this dissertation fits into the overall progress of the field. There are many other publications that focus on therapeutic targets and clinical trials in FXS which will not be in the scope of this chapter.

Recent findings in the brainstem of *Fmr1* KO animal models showed deficits in many nuclei and abnormal neuronal morphology. In the *Fmr1* KO rat, neurons in the medial superior olive (MSO), medial nucleus of the trapezoid body (MNTB), and superior periolivary nucleus (SPON) nuclei were abnormally smaller than in WT rat (Ruby et al., 2015), which are comparable to smaller cell size in the LSO and MNTB *Fmr1* KO mice showed by Rotschafer and Cramer, (2017)'s results. In a chicken model of FXS with reduced FMRP expression, the cell size in the nucleus magnocellularis (NM) was also

reduced (Wang et al., 2018). In addition, the MNTB contained fewer GAD67 and the SPON contained fewer calretinin terminals in the *Fmr1* KO rat (Ruby et al., 2015). Meanwhile, there is enhanced VGAT expression in the MNTB (Rotschafer et al., 2015), which is inconsistent with (Garcia-Pino et al., 2017)'s results of unaltered glycinergic input from the MNTB to the LSO. The discrepancy may be attributed to a compensatory mechanism in *Fmr1* KO mice to enhance inhibition because of a less effective inhibitory input. These studies demonstrate neurochemical and morphological impairments in the brainstem which may be passed on to higher auditory nuclei and contribute to the behavioral phenotypes present in FXS.

The maximal EPSC (all VCN axons) from the ventral cochlear nucleus (VCN) to the lateral superior olive (LSO) is greater in *Fmr1* KO than WT mice at P21 and P33. However, there was no difference between *Fmr1* KO and WT mice in input strength of minimal EPSC (one VCN axon) from the VCN to LSO. There was no alternations in inhibitory MNTB to LSO glycinergic synaptic strength. In addition, Garcia-Pino et al., (2017) showed *Fmr1* KO mice have an increased number of excitatory fibers onto the lateral superior olive, which suggest that the increase in EPSC is from an increase in excitatory synapse to the LSO rather than a decrease in glycinergic inhibition. The calyces, a large relay synapse in the MNTB, in *Fmr1* KO mice have increased volume and surface area (Wang et al., 2015).

It is expected that FMRP plays an important role in downstream protein regulation in brain regions that contain high levels of FMRP. When FMRP is lost or

reduced, these brain regions that contain high levels of FMRP may experience the strongest impact in abnormal functions. FMRP density appeared as a gradient in the LSO and MNTB, with a higher density of expression in the medial than lateral region of the LSO and MNTB (corresponding to high and low frequency regions) (Ruby et al., 2015). There was a tonotopy-dependent decrease of glycinergic presynaptic structures in the MNTB of *Fmr1* KO mice (McCullagh et al., 2017). This density gradient of FMRP along the tonotopic axis in the brainstem nuclei may suggest a tonotopic-specific deficits, because loss of FMRP in regions that normally contain a high density of FMRP may impact the frequency region to a greater extent than a region that contained lesser FMRP levels. There is still little knowledge about how the tonotopic-specific deficits in the brainstem influence higher processes upstream in the auditory system. This leads to the question, is the frequency specific deficits in the brainstem are carried to the IC, medical geniculate body and the auditory cortex or are the tonotopic deficits intrinsic to the local loss of FMRP in the region?

In the auditory cortex at P21, there are impairments to PNNs around PV cells and an increase in spiking activity in *Fmr1* KO mice compared to WT mice (Wen et al., 2018). Work in the superior colliculus suggest a wider visual receptive field, hyperexcitability in axis selective neurons, and a poorly refined descending projection from the visual cortex to the superior colliculus (Kay et al., 2018). The cortical impairments may lead to deficits in the efferent auditory pathway. The auditory cortex had been shown to modulate

outer hair cell activity (León et al., 2012). This leads us to ask if there are peripheral deficits that can be detected using the DPOAE method.

There are substantial evidence for cortical and brainstem auditory deficits in *Fmr1* KO mice. However, there is a gap in knowledge about the auditory midbrain, the inferior colliculus. Audiogenic seizure in *Fmr1* KO mice appear to be developmentally regulated with sensitivity to seizure greatest at P21. Little is known about the response properties in the IC across development which may underlie the mechanism of auditory hypersensitivity.

1.4 The Inferior colliculus

1.4.1 Background

The inferior colliculus (IC) is the major auditory processing center in the midbrain, with almost all auditory brainstem nuclei projecting to the IC (Coleman and Clerici, 1987). The IC receives descending projections from the auditory cortex and receives major ascending projections from the cochlear nucleus, superior olivary complex, and nuclei of the lateral lemniscus. In addition to the IC's role as the main auditory processing center in the midbrain, it is also a sensory multimodal region with connections to the somatosensory and visual areas. There are three main areas in the IC that can be defined: the dorsal IC (ICd), the central IC (ICc), and the external IC (ICx). There are no distinct borders for these regions of the IC but rather there is a transition area from one area to the next. The tonotopic region of the IC is the ICc; this region

projects to the ventral division of the medical geniculate nucleus, where the tonotopy is preserved. The inferior colliculus contains the largest density of GABAergic markers (Edgar and Schwartz, 1990). Approximately 20-40% of all projections from the IC to the thalamus are GABAergic (Beebe et al., 2018). The ICx projects to the superior colliculus and ventral/medial subdivisions of the MGB (Kudo and Niimi, 1980). The ICd region of the inferior colliculus contains modular zones, which receives input from the somatosensory cortex, dorsal column nuclei, and auditory cortex (Lesicko et al., 2016). Moreover, there is a thin area of that has broad tonotopy in the ICd. The ICc mainly contains two type of cells, flat disk-like cells that have laminar structure along the tonotopic axis and stellate cells that branches across laminae (Oliver and Morest, 1984). Overall, one of the important roles of the IC is consolidating signals from multiple subnuclei as well as multimodally from the somatosensory, limbic, and amygdala areas.

The tonotopic gradient in the IC is in the dorsal-lateral to the ventral-medial direction representing low to high frequency. The IC contains both GABAergic and glycinergic inhibition that appears to be in a concentration gradient throughout the ICc (Choy Buentello et al., 2015). The GABAergic terminals are relatively higher in the dorsal-medial region then decrease to a lower concentration in the ventral-lateral region, aligning with the low to high frequency tonotopy. For the inhibitory glycinergic neurotransmitter, the density gradient of glycinergic terminals was high in the ventral-lateral region and low in the dorsal-medial region, going from high to low along the tonotopic axis.

1.4.2 The inferior colliculus and Fragile X Syndrome

Many cortical deficits in FXS may be inherited from subcortical structures. While the focus in the literature has been on cortical dysfunction and recently, the brainstem, very little work has tested the hypothesis that midbrain abnormalities are present in FXS. FMRP is widely distributed in the human auditory brainstem suggesting a lack of FMRP in these regions would affect auditory processing (Beebe et al., 2014; Wang et al., 2014). The hypothesis tested here is that there is altered auditory processing in FXS at the IC and it is age-dependent, leading to auditory symptoms (e.g., increased seizure susceptibility and altered startle response). The main goals of my dissertation are to: 1) identify the density of neurons activated in response to a sound stimuli in the IC, medial geniculate body, and auditory cortex during developmental stages (P21 and P34) and 2) investigate the functional response properties of the IC neurons in response to sound stimuli at developmental ages (P14, P21, and P34).

The IC is of interest because it is one of the understudied auditory regions in FXS. One of the most commonly used behavioral phenotypes to determine potential drug efficacy is audiogenic seizure in FXS. Audiogenic seizure sensitivity is age dependent with P20-P30 being the most susceptible (Musumeci et al., 2000). Auditory response patterns of cFos expression is age-dependent (Friauf, 1992; Keilmann and Herdegen, 1997; Pierson and Snyder-Keller, 1994; Snyder-Keller and Pierson, 1992) suggesting differential auditory processing during development. The auditory midbrain, the IC in particular, is the progenitor of audiogenic seizures (Sakamoto and Niki, 2001). However,

little is known about how the IC functions in FXS but it is clearly an important integration center in the auditory pathway. Humans and mice with FXS have a ~20% increased susceptibility to seizure compared to the normal population (Berry-Kravis, 2002; Chen and Toth, 2001; Musumeci et al., 2000; Wisniewski et al., 1991). Audiogenic seizure was inhibited when the IC was lesioned in seizure prone rodents, in contrast, audiogenic seizures were still present when the medial geniculate body or the auditory cortex was lesioned (Kesner, 1966). One study showed enhanced cFos expression in the dorsal nucleus of the lateral lemniscus, posterior intralaminar nucleus, periaqueductal gray, and medial part of the geniculate nucleus after the induction of audiogenic seizure in *Fmr1* KO mice (Chen and Toth, 2001). In addition, GABA plays an important role in the IC of audiogenic seizure susceptible rodents (Faingold, 2002; Faingold et al., 1994) which parallels GABA abnormalities in FXS (D'Hulst et al., 2006; El Idrissi et al., 2005). There is downregulated tonic GABAa current and a decrease in GABAa receptors in *Fmr1* KO mice (Curia et al., 2009; D'Hulst et al., 2006). The IC has the most GABAa receptors (Edgar and Schwartz, 1990) compared to other parts of the brain, which implies that impaired GABAa functions will greatly affect the IC's activities.

In an acoustic startle paradigm, there is a reduction in prepulse inhibition in humans with FXS (Hessl et al., 2009), conversely, there is an increase in prepulse inhibition in FXS mice (Chen and Toth, 2001; Frankland et al., 2004). Although the acoustic startle response is inverted between the humans and mice, the underlying mechanism suggest a deficit in the fundamental acoustic processing in FXS. In another

study, adult *Fmr1* KO mice exhibit a decrease in startle response to a lower intensity sound (Nielsen et al., 2002) which is consistent with Kokash et al.'s, (2019)'s finding in P23-25 *Fmr1* KO mice. Damage to the IC enhanced startle amplitude in rats (Leitner and Cohen, 1985).

Fmr1 KO mice showed increased audiogenic seizure susceptibility, enhanced auditory startle response and greater pre-pulse inhibition (Chen and Toth, 2001; Nielsen et al., 2002; de Vrij et al., 2008; Yun et al., 2006); however Spencer et al., (2006) showed decrease startle response in *Fmr1* KO compared to WT mice. Many studies have used auditory startle response, pre-pulse inhibition, audiogenic seizure and cortical evoked responses; all of these phenotypes involve the IC, but little is known about how the IC processes sound in FXS. The dysregulation of the IC may cause the deficits observed in the auditory cortex (Castrén et al., 2003; Engineer et al., 2014; Gibson et al., 2008; Kim et al., 2013; Lovelace et al., 2016; Rotschafer and Razak, 2013) because these impaired response properties could be inherited from the lower nuclei. In addition, there is an age-dependent seizure susceptibility in the IC which guides the question, is there auditory hypersensitivity in the IC of the *Fmr1* KO mouse.

Despite the clear evidence for auditory deficits, little is known about the subcortical auditory development in FXS. The role of the IC is in auditory filtering, which is often used to determines relevant sounds from background noise (Casseday and Covey, 1996). Disruption of the IC and the auditory filtering process may lead to many of the auditory symptoms such as inability to filter out repeated sounds (a habituation

deficit). Ethridge et al., (2016) showed a habituation deficit in individuals with FXS; however, the mechanism is unclear. The second chapter aims to answer the question, what is the response properties in the IC across developmental ages in WT and *Fmr1* KO mice?

1.5 Peripheral deficits in *Fmr1* KO mice and Fragile X Syndrome

Orefice et al., 2016 suggests that changes during development in the peripheral sensory receptors lead to more central social-cognitive deficits. In FXS, the literature for testing peripheral hearing sensitivity have conflicting results. The auditory brainstem response (ABR), a measure of threshold and amplitude in response to sounds, is a test commonly used in infants and animal models to test hearing ability. There is prolonged III-V interpeak latency in ABR of human with FXS (Arinami et al., 1988). While ABR and DPOAE in humans with FXS showed no difference from normal controls in another report (Roberts et al., 2005). In mice, there is higher threshold in FXS, smaller amplitude for peak 1 and peak 3 in click responses (Rotschafer et al., 2015). The difference in results among the literature might be attributed to the medications the FXS population was taking at the time of testing, the different strains in the animal models, housing conditions, and experimental protocols. mRNA sequencing from the inner and outer hair cells from the cochlea indicates that there are mRNAs in both the inner and outer hair cells; however, there is not a relatively high amounts of *Fmr1* mRNAs (it is not within the 200 most abundant mRNA expressed in the inner and outer hair cells) (Li et al., 2016).

This suggest that there may be FMRP present but not at a very high number in the auditory sensory periphery. However, it is important to test outer hair cells functions in the cochlea to determine normal functions or impairments. The outer hair cells receives efferent connections from the auditory pathway. The auditory cortex had been shown to modulate the outer hair cell responses so if deficits arise in the otoacoustic emissions measurement, it can be attributed to impaired auditory efferent pathway.

1.6 Noise-induced hearing loss

Noise-induced hearing loss affects as many as 40 million adults in the United States (Carroll, 2017). Due to the exposure to loud sounds and the consequential hearing impairments, some effects may include tinnitus (ringing in the ear), hypo or hyper sensitivity to sounds, poor sound discrimination in noisy environments and poor temporal resolution. The exposure to loud sound leads to peripheral damage such as cell death in the spiral ganglion cells, inner hair cell loss in the cochlea and lack of synapses in the inner ear. Even though hearing threshold detected with conventional audiology tests may not be impaired, there can be a loss of spiral ganglion cells and synapses (Kujawa and Liberman, 2009). As a result of the insult to the periphery, many auditory nuclei downstream can affect how sounds are processed, even after normal hearing threshold have been regained. A gain in threshold can affect the neuronal structures, we explored if the molecular structures in the central auditory system can be affected by hearing loss. In Chapter 4, we investigated parvalbumin (PV) and

perineuronal nets (PNNs) in the auditory cortex after noise-induced hearing loss. PV is a calcium binding protein expressed in inhibitory interneurons. PNNs are extracellular matrix proteins that are commonly found surrounding inhibitory interneuron (PV). PV-expressing interneurons are fast spiking cells who's inhibition suppresses gamma oscillations in the neocortex (Sohal et al., 2009). Perineuronal nets provide structural support and enhance excitability (Balmer, 2016; Dansie and Ethell, 2011). Dysregulation of either PV-expressing interneurons or perineuronal nets can impact the regulation of the neocortex. This study tested the hypothesis that noise-induced hearing loss disrupts PNN which may reduce cortical inhibition.

1.7 Summary

The auditory system is a complex and dynamic structure. A rough tonotopic map is present even before the onset of hearing from genetic guidance, while others require activity dependent experience to fully develop normal function. This dissertation presents effects of noise-induced hearing loss on PV+ and PNN+ neurons in the auditory cortex and auditory dysfunctions in Fragile X Syndrome. FXS is a neurodevelopmental disorder, affecting the development of sensory processes. There are clear auditory deficits in FXS. Investigating how auditory information is processed in the auditory system gives insight into the dysfunction present in FXS. Common results across the literature are abnormal GABAergic properties, higher response activity, higher spontaneous activity, and seizures. Understanding auditory disorders can give new

insight into the functions of how the brain process auditory information. In this dissertation, the goal was to investigate auditory abnormality from noise induced hearing loss and a genetically inherited neurodevelopmental disorder, FXS.

References

Arinami, T., Sato, M., Nakajima, S., and Kondo, I. (1988). Auditory brain-stem responses in the fragile X syndrome. Am. J. Hum. Genet. *43*, 46–51.

Bagni, C., Tassone, F., Neri, G., and Hagerman, R. (2012). Fragile X syndrome: causes, diagnosis, mechanisms, and therapeutics. J. Clin. Invest. *122*, 4314–4322.

Balmer, T.S. (2016). Perineuronal nets enhance the excitability of fast-spiking neurons. Eneuro.

Beebe, K., Wang, Y., and Kulesza, R. (2014). Distribution of fragile X mental retardation protein in the human auditory brainstem. Neuroscience *273*, 79–91.

Beebe, N.L., Mellott, J.G., and Schofield, B.R. (2018). Inhibitory Projections from the Inferior Colliculus to the Medial Geniculate body Originate from Four Subtypes of GABAergic Cells. ENeuro *5*, ENEURO.0406-18.2018.

Bernardet, M., and Crusio, W.E. (2006). Fmr1 KO Mice as a Possible Model of Autistic Features. Sci. World J. *6*, 1164–1176.

Berry-Kravis, E. (2002). Epilepsy in fragile X syndrome. Dev. Med. Child Neurol. *44*, 724–728.

Brown, V., Jin, P., Ceman, S., Darnell, J.C., O'Donnell, W.T., Tenenbaum, S.A., Jin, X., Feng, Y., Wilkinson, K.D., Keene, J.D., et al. (2001). Microarray Identification of FMRP-Associated Brain mRNAs and Altered mRNA Translational Profiles in Fragile X Syndrome. Cell *107*, 477–487.

Carroll, Y.I. (2017). Vital Signs: Noise-Induced Hearing Loss Among Adults — United States 2011–2012. MMWR Morb. Mortal. Wkly. Rep. *66*.

Casseday, J.H., and Covey, E. (1996). A neuroethological theory of the operation of the inferior colliculus. Brain. Behav. Evol. *47*, 311–336.

Castrén, M., Pääkkönen, A., Tarkka, I.M., Ryynänen, M., and Partanen, J. (2003). Augmentation of Auditory N1 in Children with Fragile X Syndrome. Brain Topogr. *15*, 165–171.

Chen, L., and Toth, M. (2001). Fragile X mice develop sensory hyperreactivity to auditory stimuli. Neuroscience *103*, 1043–1050.

Choy Buentello, D., Bishop, D.C., and Oliver, D.L. (2015). Differential distribution of GABA and glycine terminals in the inferior colliculus of rat and mouse. J. Comp. Neurol. *523*, 2683–2697.

Coleman, J.R., and Clerici, W.J. (1987). Sources of projections to subdivisions of the inferior colliculus in the rat. J. Comp. Neurol. *262*, 215–226.

Contractor, A., Klyachko, V.A., and Portera-Cailliau, C. (2015). Altered Neuronal and Circuit Excitability in Fragile X Syndrome. Neuron *87*, 699–715.

Curia, G., Papouin, T., Séguéla, P., and Avoli, M. (2009). Downregulation of tonic GABAergic inhibition in a mouse model of fragile X syndrome. Cereb. Cortex N. Y. N 1991 *19*, 1515–1520.

Dansie, L.E., and Ethell, I.M. (2011). Casting a net on dendritic spines: the extracellular matrix and its receptors. Dev. Neurobiol. *71*, 956–981.

D'Hulst, C., De Geest, N., Reeve, S.P., Van Dam, D., De Deyn, P.P., Hassan, B.A., and Kooy, R.F. (2006). Decreased expression of the GABAA receptor in fragile X syndrome. Brain Res. *1121*, 238–245.

Edgar, P.P., and Schwartz, R.D. (1990). Localization and characterization of 35S-t-butylbicyclophosphorothionate binding in rat brain: an autoradiographic study. J. Neurosci. *10*, 603–612.

Ehret, G., and Romand, R. (1992). Development of tone response thresholds, latencies and tuning in the mouse inferior colliculus. Dev. Brain Res. *67*, 317–326.

El Idrissi, A., Ding, X.-H., Scalia, J., Trenkner, E., Brown, W.T., and Dobkin, C. (2005). Decreased GABAA receptor expression in the seizure-prone fragile X mouse. Neurosci. Lett. *377*, 141–146.

Engineer, C.T., Centanni, T.M., Im, K.W., Rahebi, K.C., Buell, E.P., and Kilgard, M.P. (2014). Degraded speech sound processing in a rat model of fragile X syndrome. Brain Res. *1564*, 72–84.

Ethridge, L.E., White, S.P., Mosconi, M.W., Wang, J., Byerly, M.J., and Sweeney, J.A. (2016). Reduced habituation of auditory evoked potentials indicate cortical hyper-excitability in Fragile X Syndrome. Transl. Psychiatry *6*, e787.

Ethridge, L.E., White, S.P., Mosconi, M.W., Wang, J., Pedapati, E.V., Erickson, C.A., Byerly, M.J., and Sweeney, J.A. (2017). Neural synchronization deficits linked to cortical hyper-excitability and auditory hypersensitivity in fragile X syndrome. Mol. Autism *8*, 22.

Faingold, C.L. (2002). Role of GABA abnormalities in the inferior colliculus pathophysiology – audiogenic seizures. Hear. Res. *168*, 223–237.

Faingold, C.L., Marcinczyk, M.J., Casebeer, D.J., Randall, M.E., Arneric´, S.P., and Browning, R.A. (1994). GABA in the inferior colliculus plays a critical role in control of audiogenic seizures. Brain Res. *640*, 40–47.

Frankland, P.W., Wang, Y., Rosner, B., Shimizu, T., Balleine, B.W., Dykens, E.M., Ornitz, E.M., and Silva, A.J. (2004). Sensorimotor gating abnormalities in young males with fragile X syndrome and Fmr1-knockout mice. Mol. Psychiatry *9*, 417–425.

Friauf, E. (1992). Tonotopic Order in the Adult and Developing Auditory System of the Rat as Shown by c-fos Immunocytochemistry. Eur. J. Neurosci. *4*, 798–812.

Garcia-Pino, E., Gessele, N., and Koch, U. (2017). Enhanced Excitatory Connectivity and Disturbed Sound Processing in the Auditory Brainstem of Fragile X Mice. J. Neurosci. 2310–2316.

Gibson, J.R., Bartley, A.F., Hays, S.A., and Huber, K.M. (2008). Imbalance of Neocortical Excitation and Inhibition and Altered UP States Reflect Network Hyperexcitability in the Mouse Model of Fragile X Syndrome. J. Neurophysiol. *100*, 2615–2626.

Hagerman, P.J., and Stafstrom, C.E. (2009). Origins of Epilepsy in Fragile X Syndrome. Epilepsy Curr. *9*, 108–112.

Hagerman, R., Lauterborn, J., Au, J., and Berry-Kravis, E. (2012). Fragile X Syndrome and Targeted Treatment Trials. In Modeling Fragile X Syndrome, (Springer, Berlin, Heidelberg), pp. 297–335.

Hall, S.S., Walter, E., Sherman, E., Hoeft, F., and Reiss, A.L. (2009). The neural basis of auditory temporal discrimination in girls with fragile X syndrome. J. Neurodev. Disord. *1*, 91–99.

He, Q., Nomura, T., Xu, J., and Contractor, A. (2014). The Developmental Switch in GABA Polarity Is Delayed in Fragile X Mice. J. Neurosci. *34*, 446–450.

Hessl, D., Berry-Kravis, E., Cordeiro, L., Yuhas, J., Ornitz, E.M., Campbell, A., Chruscinski, E., Hervey, C., Long, J.M., and Hagerman, R.J. (2009). Prepulse inhibition in fragile X syndrome: Feasibility, reliability, and implications for treatment. Am. J. Med. Genet. B Neuropsychiatr. Genet. *150B*, 545–553.

Hinds, H.L., Ashley, C.T., Sutcliffe, J.S., Nelson, D.L., Warren, S.T., Housman, D.E., and Schalling, M. (1993). Tissue specific expression of FMR–1 provides evidence for a functional role in fragile X syndrome. Nat. Genet. *3*, 36–43.

Kandler, K., Clause, A., and Noh, J. (2009). Tonotopic reorganization of developing auditory brainstem circuits. Nat. Neurosci. *12*, 711–717.

Kay, R.B., Gabreski, N.A., and Triplett, J.W. (2018). Visual subcircuit-specific dysfunction and input-specific mispatterning in the superior colliculus of fragile X mice. J. Neurodev. Disord. *10*, 23.

Keilmann, A., and Herdegen, T. (1997). The c-Fos transcription factor in the auditory pathway of the juvenile rat: effects of acoustic deprivation and repetitive stimulation. Brain Res. *753*, 291–298.

Kesner, R.P. (1966). Subcortical mechanisms of audiogenic seizures. Exp. Neurol. *15*, 192–205.

Kim, H., Gibboni, R., Kirkhart, C., and Bao, S. (2013). Impaired Critical Period Plasticity in Primary Auditory Cortex of Fragile X Model Mice. J. Neurosci. *33*, 15686–15692.

King, A.J. (2010). Auditory Neuroscience: Balancing Excitation and Inhibition during Development. Curr. Biol. *20*, R808–R810.

Knoth, I.S., and Lippe, S. (2012). Event-related potential alterations in fragile X syndrome. Front. Hum. Neurosci. *6*.

Knoth, I.S., Vannasing, P., Major, P., Michaud, J.L., and Lippé, S. (2014). Alterations of visual and auditory evoked potentials in fragile X syndrome. Int. J. Dev. Neurosci. *36*, 90–97.

Kokash, J., Alderson, E.M., Reinhard, S.M., Crawford, C.A., Binder, D.K., Ethell, I.M., and Razak, K.A. (2019). Genetic reduction of MMP-9 in the Fmr1 KO mouse partially rescues prepulse inhibition of acoustic startle response. Brain Res. *1719*, 24–29.

Kudo, M., and Niimi, K. (1980). Ascending projections of the inferior colliculus in the cat: an autoradiographic study. J. Comp. Neurol. *191*, 545–556.

Kujawa, S.G., and Liberman, M.C. (2009). Adding Insult to Injury: Cochlear Nerve Degeneration after “Temporary” Noise-Induced Hearing Loss. J. Neurosci. *29*, 14077–14085.

Leitner, D.S., and Cohen, M.E. (1985). Role of the inferior colliculus in the inhibition of acoustic startle in the rat. Physiol. Behav. *34*, 65–70.

León, A., Elgueda, D., Silva, M.A., Hamamé, C.M., and Delano, P.H. (2012). Auditory Cortex Basal Activity Modulates Cochlear Responses in Chinchillas. PLOS ONE *7*, e36203.

Lesicko, A.M.H., Hristova, T.S., Maigler, K.C., and Llano, D.A. (2016). Connectional Modularity of Top-Down and Bottom-Up Multimodal Inputs to the Lateral Cortex of the Mouse Inferior Colliculus. J. Neurosci. *36*, 11037–11050.

Li, J., Pelletier, M.R., Perez Velazquez, J.-L., and Carlen, P.L. (2002). Reduced Cortical Synaptic Plasticity and GluR1 Expression Associated with Fragile X Mental Retardation Protein Deficiency. Mol. Cell. Neurosci. *19*, 138–151.

Li, Y., Liu, H., Barta, C.L., Judge, P.D., Zhao, L., Zhang, W.J., Gong, S., Beisel, K.W., and He, D.Z.Z. (2016). Transcription Factors Expressed in Mouse Cochlear Inner and Outer Hair Cells. PLoS ONE *11*.

Liu, S.J., and Kaczmarek, L.K. (1998). Depolarization Selectively Increases the Expression of the Kv3.1 Potassium Channel in Developing Inferior Colliculus Neurons. J. Neurosci. *18*, 8758–8769.

Lovelace, J.W., Wen, T.H., Reinhard, S., Hsu, M.S., Sidhu, H., Ethell, I.M., Binder, D.K., and Razak, K.A. (2016). Matrix metalloproteinase-9 deletion rescues auditory evoked potential habituation deficit in a mouse model of Fragile X Syndrome. Neurobiol. Dis. *89*, 126–135.

Lovelace, J.W., Ethell, I.M., Binder, D.K., and Razak, K.A. (2018). Translation-relevant EEG phenotypes in a mouse model of Fragile X Syndrome. Neurobiol. Dis. *115*, 39–48.

McCullagh, E.A., Salcedo, E., Huntsman, M.M., and Klug, A. (2017). Tonotopic alterations in inhibitory input to the medial nucleus of the trapezoid body in a mouse model of Fragile X syndrome. J. Comp. Neurol. *525*, 3543–3562.

Mikaelian, D., and Ruben, R.J. (1965). Development of Hearing in the Normal Cba-J Mouse: Correlation of Physiological Observations with Behavioral Responses and with Cochlear Anatomy. Acta Otolaryngol. (Stockh.) *59*, 451–461.

Molen, M.J.W. van der, Stam, C.J., and Molen, M.W. van der (2014). Resting-State EEG Oscillatory Dynamics in Fragile X Syndrome: Abnormal Functional Connectivity and Brain Network Organization. PLOS ONE *9*, e88451.

Musumeci, S.A., Hagerman, R.J., Ferri, R., Bosco, P., Bernardina, B.D., Tassinari, C.A., De Sarro, G.B., and Elia, M. (1999). Epilepsy and EEG Findings in Males with Fragile X Syndrome. Epilepsia *40*, 1092–1099.

Musumeci, S.A., Bosco, P., Calabrese, G., Bakker, C., De Sarro, G.B., Elia, M., Ferri, R., and Oostra, B.A. (2000). Audiogenic seizures susceptibility in transgenic mice with fragile X syndrome. Epilepsia *41*, 19–23.

Nielsen, D.M., Derber, W.J., McClellan, D.A., and Crnic, L.S. (2002). Alterations in the auditory startle response in Fmr1 targeted mutant mouse models of fragile X syndrome. Brain Res. *927*, 8–17.

Nimchinsky, E.A., Oberlander, A.M., and Svoboda, K. (2001). Abnormal Development of Dendritic Spines inFMR1 Knock-Out Mice. J. Neurosci. *21*, 5139–5146.

O'Donnell, W.T., and Warren, and S.T. (2002). A Decade of Molecular Studies of Fragile X Syndrome. Annu. Rev. Neurosci. *25*, 315–338.

Oliver, D.L., and Morest, D.K. (1984). The central nucleus of the inferior colliculus in the cat. J. Comp. Neurol. *222*, 237–264.

Orefice, L.L., Zimmerman, A.L., Chirila, A.M., Sleboda, S.J., Head, J.P., and Ginty, D.D. (2016). Peripheral Mechanosensory Neuron Dysfunction Underlies Tactile and Behavioral Deficits in Mouse Models of ASDs. Cell *166*, 299–313.

Pierson, M., and Snyder-Keller, A. (1994). Development of frequency-selective domains in inferior colliculus of normal and neonatally noise-exposed rats. Brain Res. *636*, 55–67.

Rais, M., Binder, D.K., Razak, K.A., and Ethell, I.M. (2018). Sensory Processing Phenotypes in Fragile X Syndrome. ASN Neuro *10*, 1759091418801092.

Roberts, J., Hennon, E.A., Anderson, K., Roush, J., Gravel, J., Skinner, M., Misenheimer, J., and Reitz, P. (2005). Auditory Brainstem Responses in Young Males With Fragile X Syndrome. J. Speech Lang. Hear. Res. *48*, 494–500.

Rogers, S.J., Hepburn, S., and Wehner, E. (2003). Parent reports of sensory symptoms in toddlers with autism and those with other developmental disorders. J. Autism Dev. Disord. *33*, 631–642.

Rojas, D.C., Benkers, T.L., Rogers, S.J., Teale, P.D., Reite, M.L., and Hagerman, R.J. (2001). Auditory evoked magnetic fields in adults with fragile X syndrome. Neuroreport *12*, 2573–2576.

Romand, R., and Ehret, G. (1990). development of tonotopy in the inferior colliculus. I. Electrophysiological mapping in house mice. Dev. Brain Res. *54*, 221–234.

Rotschafer, S., and Razak, K. (2013). Altered auditory processing in a mouse model of fragile X syndrome. Brain Res. *1506*, 12–24.

Rotschafer, S.E., and Cramer, K.S. (2017). Developmental Emergence of Phenotypes in the Auditory Brainstem Nuclei of Fmr1 Knockout Mice. ENeuro *4*, ENEURO.0264-17.2017.

Rotschafer, S.E., and Razak, K.A. (2014). Auditory Processing in Fragile X Syndrome. Front. Cell. Neurosci. *8*.

Rotschafer, S.E., Marshak, S., and Cramer, K.S. (2015). Deletion of Fmr1 Alters Function and Synaptic Inputs in the Auditory Brainstem. PLoS ONE *10*.

Ruby, K., Falvey, K., and Kulesza, R.J. (2015). Abnormal neuronal morphology and neurochemistry in the auditory brainstem of Fmr1 knockout rats. Neuroscience *303*, 285–298.

Sakamoto, T., and Niki, H. (2001). Acoustic priming lowers the threshold for electrically induced seizures in mice inferior colliculus, but not in the deep layers of superior colliculus. Brain Res. *898*, 358–363.

Sanes, D.H., and Bao, S. (2009). Tuning up the developing auditory CNS. Curr. Opin. Neurobiol. *19*, 188–199.

Selby, L., Zhang, C., and Sun, Q.-Q. (2007). Major defects in neocortical GABAergic inhibitory circuits in mice lacking the fragile X mental retardation protein. Neurosci. Lett. *412*, 227–232.

Sinclair, D., Featherstone, R., Naschek, M., Nam, J., Du, A., Wright, S., Pance, K., Melnychenko, O., Weger, R., Akuzawa, S., et al. (2017). GABA-B Agonist Baclofen Normalizes Auditory-Evoked

Neural Oscillations and Behavioral Deficits in the Fmr1 Knockout Mouse Model of Fragile X Syndrome. ENeuro ENEURO.0380-16.2017.

Snyder-Keller, A.M., and Pierson, M.G. (1992). Audiogenic seizures induce c-fos in a model of developmental epilepsy. Neurosci. Lett. *135*, 108–112.

Sohal, V.S., Zhang, F., Yizhar, O., and Deisseroth, K. (2009). Parvalbumin neurons and gamma rhythms enhance cortical circuit performance. Nature *459*, 698–702.

Spencer, C.M., Serysheva, E., Yuva-Paylor, L.A., Oostra, B.A., Nelson, D.L., and Paylor, R. (2006). Exaggerated behavioral phenotypes in Fmr1/Fxr2 double knockout mice reveal a functional genetic interaction between Fragile X-related proteins. Hum. Mol. Genet. *15*, 1984–1994.

Strumbos, J.G., Brown, M.R., Kronengold, J., Polley, D.B., and Kaczmarek, L.K. (2010). Fragile X mental retardation protein is required for rapid experience-dependent regulation of the potassium channel Kv3.1b. J. Neurosci. Off. J. Soc. Neurosci. *30*, 10263–10271.

Till, S.M. (2010). The developmental roles of FMRP. Biochem. Soc. Trans. *38*, 507–510.

Tritsch, N.X., Yi, E., Gale, J.E., Glowatzki, E., and Bergles, D.E. (2007). The origin of spontaneous activity in the developing auditory system. Nature *450*, 50–55.

Wang, J., Ethridge, L.E., Mosconi, M.W., White, S.P., Binder, D.K., Pedapati, E.V., Erickson, C.A., Byerly, M.J., and Sweeney, J.A. (2017). A resting EEG study of neocortical hyperexcitability and altered functional connectivity in fragile X syndrome. J. Neurodev. Disord. *9*, 11.

Wang, T., de Kok, L., Willemsen, R., Elgersma, Y., and Borst, J.G.G. (2015). In vivo synaptic transmission and morphology in mouse models of Tuberous sclerosis, Fragile X syndrome, Neurofibromatosis type 1, and Costello syndrome. Front. Cell. Neurosci. *9*.

Wang, X., Zorio, D.A.R., Schecterson, L., Lu, Y., and Wang, Y. (2018). Postsynaptic FMRP Regulates Synaptogenesis In Vivo in the Developing Cochlear Nucleus. J. Neurosci. *38*, 6445–6460.

Wang, Y., Sakano, H., Beebe, K., Brown, M.R., de Laat, R., Bothwell, M., Kulesza, R.J., and Rubel, E.W. (2014). Intense and specialized dendritic localization of the fragile X mental retardation protein in binaural brainstem neurons: A comparative study in the alligator, chicken, gerbil, and human. J. Comp. Neurol. *522*, 2107–2128.

Wen, T.H., Afroz, S., Reinhard, S.M., Palacios, A.R., Tapia, K., Binder, D.K., Razak, K.A., and Ethell, I.M. (2018). Genetic Reduction of Matrix Metalloproteinase-9 Promotes Formation of Perineuronal Nets Around Parvalbumin-Expressing Interneurons and Normalizes Auditory Cortex Responses in Developing Fmr1 Knock-Out Mice. Cereb. Cortex *28*, 3951–3964.

Wisniewski, K.E., Segan, S.M., Miezejeski, C.M., Sersen, E.A., and Rudelli, R.D. (1991). The fra(X) syndrome: Neurological, electrophysiological, and neuropathological abnormalities. Am. J. Med. Genet. *38*, 476–480.

Zhang, J., Fang, Z., Jud, C., Vansteensel, M.J., Kaasik, K., Lee, C.C., Albrecht, U., Tamanini, F., Meijer, J.H., Oostra, B.A., et al. (2008). Fragile X-Related Proteins Regulate Mammalian Circadian Behavioral Rhythms. Am. J. Hum. Genet. *83*, 43–52.

Chapter 2

Abnormal development of auditory responses in the inferior colliculus of a mouse model of Fragile X Syndrome

2.1 Abstract

Sensory processing abnormalities are frequently associated with autism spectrum disorders, but the underlying mechanisms are unclear. Here we studied auditory processing in a mouse model of Fragile X Syndrome (FXS), a leading known genetic cause of autism and intellectual disability. Both humans with FXS and *Fmr1* KO mouse model of FXS show auditory hypersensitivity, with the latter showing a strong propensity for audiogenic seizures early in development. Given the literature on the relationship between midbrain abnormalities and audiogenic seizures, we investigated if the inferior colliculus (IC) of the *Fmr1* KO mouse shows abnormal auditory sensitivity and processing compared to wildtype (WT) controls. Seizures decrease with age in both humans and mice, so we determined IC responses at specific developmental time points. Using cFos staining, we found that the IC, but not the auditory cortex, of *Fmr1* KO mice show increased density of active neurons at both P21 and P34. Using *in vivo* single-unit recordings, we found that IC neurons of *Fmr1* KO mice produce a stronger response at P21, but not at P14 or P34. We also observed broader frequency tuning curves and enhanced responses to sinusoidal amplitude modulated signals in the IC of *Fmr1* KO mice. There were no differences in minimum threshold or rate-level tuning of IC neurons across genotypes. Taken together, these data show strong evidence for neural correlates of auditory hypersensitivity in the IC that is developmentally regulated in a manner consistent with developmental changes in seizure propensity. While most of the focus on human and mouse work in autism and sensory processing has centered on the forebrain, these midbrain data along with recent work on the brainstem, indicate the importance of identifying the systems level contributions to the association between sensory abnormalities and autism spectrum disorders.

2.2 Introduction

Fragile X Syndrome (FXS) is a leading genetic cause of intellectual disability and autism spectrum disorder that affects 1:4000 males and 1:8000 females. The cause of FXS is inadequate fragile X mental retardation protein (FMRP) from silencing of the fragile X mental retardation gene (*Fmr1*) through expansion and hypermethylation of CGG repeats in the X chromosome. Symptoms include cognitive and social deficits, hyperactivity, language impairments, increased susceptibility to seizures, and sensory impairments. Although caused by a monogenetic mutation, FXS phenotypes are often heterogeneous in humans (Smith et al., 2012); however, a consistent and distinctive phenotype is abnormal sensory reactivity (Rais et al., 2018), particularly hypersensitivity to sensory stimuli (Hitoglou et al., 2010; Rogers et al., 2003). Hypersensitivity manifests strongly in the auditory domain, but the underlying mechanisms are only beginning to be understood (Garcia-Pino et al., 2017; Wen et al., 2018).

An animal model of FXS, the *Fmr1* knock-out (KO) mouse, displays several core FXS-like phenotypes including hyperactivity, anxiety-like behaviors, social abnormalities, electrophysiological, and dendritic spine deficits (Bakker and Oostra, 2003; Kazdoba et al., 2014). Importantly, the *Fmr1* KO mouse also shows auditory hypersensitivity correlates including enhanced cortical responses to sounds, increased propensity for audiogenic seizures and abnormal sensory gating. The electroencephalography (EEG) phenotypes recorded using epidural and scalp electrodes in *Fmr1* KO mouse are remarkably similar to those recorded from the scalp of humans with FXS (Castrén et al., 2003; Ethridge et al., 2017; Lovelace et al., 2016, 2018; Schneider et al., 2013). These include reduced habituation of sound evoked responses, increased resting gamma power and reduced consistency in phase locking to amplitude

modulated stimuli. *In vivo* single unit recordings from the auditory cortex of *Fmr1* KO mice show abnormally increased responses to sounds during early development and in adults (Rotschafer and Razak, 2013; Wen et al., 2018). FMRP is expressed at multiple levels of the auditory system and deficits in auditory processing are predicted and indeed reported in the brainstem (Beebe et al., 2014; Garcia-Pino et al., 2017; Rotschafer and Cramer, 2017; Rotschafer et al., 2015; Wang et al., 2014). A recent study from our group deleted *Fmr1* only from forebrain excitatory neurons, and showed that increased high gamma power and reduced phase locking to sounds reported in global *Fmr1* KO are not present in the forebrain specific knockout (Lovelace et al., *In Press*). Taken together, these studies suggest that at least some of the abnormal responses recorded in the cortex are generated subcortically.

Audiogenic seizure (AGS), particularly between ~P20 and ~P30, is a robust and consistently reported phenotype in the *Fmr1* KO mouse (Dölen et al., 2007; Michalon et al., 2012; Musumeci et al., 2007; Pacey et al., 2009; Yan et al., 2005). Multiple studies have suggested that abnormalities of the midbrain inferior and superior colliculi (IC, SC) underlie specific patterns of sensitivity and behaviors noted in audiogenic seizures (Faingold, 2002; Faingold and Randall, 1999; Millan et al., 1986). These studies suggest that the responses of IC in *Fmr1* KO mouse are abnormal during development leading to auditory hypersensitivity. We recently found elevated levels of matrix metalloproteinase-9 levels in the developing IC of *Fmr1* KO mice compared to WT mice and deficits in pre-pulse inhibition of acoustic startle in *Fmr1* KO mice (Kokash et al., 2019), further suggesting early developmental deficits in IC function. The main goal of the current study is to test this hypothesis and to identify developmental changes in IC responses in *Fmr1* KO mice.

We used two different methods to quantify the development of responses in the IC of mice. The first aim was to use cFos staining to determine the number of activated cells at P21 and P34 in the IC, auditory thalamus, and auditory cortex. These studies indicated that significantly more cells in the IC, but not auditory cortex, of the *Fmr1* KO mice are activated compared to WT mice. In the second aim, we followed up with *in vivo* single unit recordings of IC responses at P14, P21, and P34 to determine minimum thresholds, response magnitudes, frequency tuning, and responses to amplitude modulated signals. We report significant genotype differences of IC responses in a manner correlated with developmental trajectory of auditory hypersensitivity in *Fmr1* KO mice.

2.3 Methods

2.3.1 Animals

All animal procedures were approved by the University of California, Riverside Institution Animal Use and Care Committee. Breeding pairs of FVB.129P2−Pde6b+Tyr$^{c\text{-}ch}$/AntJ (Wild-type, WT) and FVB.129P2−*Fmr1tm1Cgr/J (Fmr1* Knock-out, KO) were obtained from Jackson Laboratories and bred in-house. All mice were housed in a 12:12 light/dark cycle and given standard lab chow and water *ad libitum*. Male mice were used for all the experiments. cFos immunohistochemistry was done on n=16 WT (age P21-22), n=23 WT (age P34-39), n=15 *Fmr1* KO (age P21-22) and n=23 *Fmr1* KO (age P34-39) mice. Single unit electrophysiological recordings were obtained from the IC of n=9 WT (age P14-15), n=11 WT (age P21-22), n=12 WT (age P34-39), n=10 *Fmr1* KO (age P14-15), n=10 *Fmr1* KO (age P21-22), and n=9 *Fmr1* KO (age P34-39) mice.

2.3.2 Sound exposure for cFos expression

Our goal was to examine cFos expression in the auditory pathway of *Fmr1* KO mice in response to relatively loud sounds, but without any overt seizure responses. WT mice are not prone to seizures, but *Fmr1* KO mice are. Therefore, if the sound causes seizures, the motor responses involved would only be present in the KO mice and render the two groups incomparable. Therefore, we did not some pilot tests to identify the highest sound level that does not cause AGS. These pilot data showed that the AGS threshold for P34 *Fmr1* KO mice was on average ~85 dB SPL so we selected to use 80 or 90 dB for 15 minutes (500 msec upsweep followed by 500 msec downsweep). However, 90 dB sounds induced audiogenic seizure in the P21 group, so we used 85 dB SPL in this age group with 1000 msec of quiet in between each 1000 msec of sound. To perform cFos studies, up to 4 male mice aged P21-39 were placed in a standard mouse cage with no food or water. Mice used for immunohistochemistry of cFos proteins were habituated for 3 hours in a sound attenuated booth (Gretch-Ken Inc.) before stimulus presentation. This would facilitate isolation of cFos protein expression to the stimulus and minimize background cFos protein expression. In addition, these mice remained in the sound attenuation booth for 45 minutes after offset of the sound stimulus and before transcardial perfusion. Control groups underwent the same procedure except no sounds were presented. Auditory stimuli were generated with a custom software (BATLAB, Dr. Don Gans, Kent State University or Sparkle, Portfors Lab, Washington State University) and delivered through a programmable attenuator (PA5, TDT) and a speaker (FT17H, Fostex International) placed face down on top of the cage lid. Sound levels were measured with a sound level meter (735, B&K Precision) at a distance from the speaker to the cage bottom. A lamp was used to

provide light for a video camera to record behaviors during 5 minutes of baseline with no sound presentation and 15 minutes of sound presentation.

2.3.3 cFos immunohistochemistry

We examined the IC, the auditory thalamus, and core auditory cortex to determine if there are regional differences in cFos expression across genotypes and development. Sounds were presented at levels below AGS thresholds (none of the mice tested showed any overt AGS). Moreover, to maximize probability of activated cells across the tonotopic representation, we used broadband frequency (5-50 kHz) in an alternating 500 msec upsweep and 500 msec downsweep pattern for 15 minutes.

Two age groups of mice were tested for cFos: P21 and P34. Mice were euthanized with pentobarbital sodium (Fatal-Plus, i.p. 125 mg/kg) before perfusion. Transcardial perfusions were done with cold 0.1 M PBS (pH=7.4) followed by cold 4% PFA (pH=7.6). The brain tissues were extracted and post-fixed overnight in 4% PFA before storage in 0.1 M PBS at 4^{o}C until further tissue processing in the future. The brains were cryoprotected in 30% sucrose for 2 days before being cryosectioned (CM 1860, Leica Biosystems) in the coronal plane at 40 µm thickness. All immunohistochemistry steps were done on a shaker at room temperature unless otherwise noted. For each mouse, two slices for each region of interest (IC, medial geniculate body, and auditory cortex) were used for cFos immunohistochemistry. Slices were washed 3x5 minutes in 0.1 M PBS followed by blocking with 5% Normal Goat Serum for 1 hr. Slices were then washed with PBS for 10 minutes followed by 0.5% triton X-100 for 10 minutes. Next, the slices were incubated overnight in 4°C in primary antibody 1:100 cFos anti-Rabbit (SC-52, Santa Cruz) in 1% NGS and 0.1% Tween-20 in 0.1 M PBS. On the next day, the slices were washed 3x5

minutes with PBS and incubated in secondary antibody (1:500 Donkey anti-Rabbit 594) with 1% NGS and 0.1% tween in PBS for 2 hours. Then, the slices were washed in PBS 3x5 minutes and mounted on a glass slide with a mounting medium (Vectashield H-1200, Vector Laboratories) and the edges were sealed (Cytoseal 60, Richard-Allan Scientific). The slides were stored in the dark at 4°C until imaging was done. Stained sections were imaged using a confocal microscope (SP5, Leica Microsystems) at 10x objective in 1024x1024 resolutions with 20 z-steps.

Image analysis was performed using ImageJ Software (NIH). Auditory cortex was identified based on Martin del Campo et al., 2012, and the medial geniculate body (MGB) and IC was identified based on Allen Brain Atlas. Because the MGB is composed of multiple divisions involved with a range of functions, we evaluated cFos in each division separately. The dimensions of the windows used for the cell counting in the different divisions of the MGB is provided in Table 1. The sizes of these windows were selected based on sufficient coverage of the divisions of interest across all photomicrographs. A 400 µm wide window that was at 45° angle to the lateral edge of a coronal section was used as the counting window for the IC (Figure 1A, B). Large images were stitched as needed using the 'stitch' plugin (Preibisch et al., 2009) for ImageJ to obtain high resolution images for counting. A rolling ball background subtraction was done for all images (rolling ball radius =10 pixel); this removes smooth continuous backgrounds. cFos counts were based on intensity thresholding of the pixels (Geometric Triangle Function), size (greater than 20 px^2) in ImageJ. Intensity analysis were done based on selection of cFos expressing neurons as described above. The average intensity of each cFos expressing neuron was calculated and averaged per mouse.

2.3.4 *In vivo* electrophysiology recordings from IC

In vivo extracellular single unit recordings were conducted in urethane (1 g/kg) and xylazine (20 mg/kg) (i.p. injection) anesthetized mice. Supplemental doses of anesthesia were given during recording sessions, as needed. A craniotomy was performed using a micro drill (Foredom Electric Co.) with coordinates based on skull landmarks. The IC was identified based on the transverse sinus vein, auditory responses, tonotopy, and post-hoc histology from Fluoro-Ruby dye injected in the recording site. A negative feedback rectal thermometer was used to maintain the temperature of the mice at 38 ±1 °C throughout the recording session. A calibrated speaker was placed contralateral to the recorded IC at a 45° angle and 6 cm away from the ear. A glass electrode (1 M NaCl, 2-10 MΩ impedance) was advanced using a micromanipulator (Kopf 2660) to depths between 200-2000 μm in the IC. Sound stimulation and data acquisition were driven by SPARKLE software (Sparkle Data Acquisition, Portfors Lab). Single units were isolated and identified based on amplitude and constancy of spikes. Unless otherwise noted, each stimulus was repeated 20 times with a 2 Hz repetition rate. The stimulus duration was 50 msec including a 2 msec rise/fall time. The recording window used was 250 msec from stimulus onset except for the sinusoidal amplitude modulated (SAM) tones, in which the recording window were 1000 msec. Post stimulus time histogram data were analyzed offline. The number of neurons were recorded from each group: n=78 WT (age P14-15), n=77 WT (age P21-22), n=102 WT (age P34-39), n=81 *Fmr1* KO (age P14-15), n=84 *Fmr1* KO (age P21-22), and n=83 *Fmr1* KO (age P34-39). Upon isolation of a neuron, spontaneous activity and response selectivity were quantified as described below:

2.3.5 Spontaneous activity and frequency response area

Spontaneous activity was recorded within the 250 msec recording window in the absence of any stimuli. The number of action potentials within the recording window was sampled over 20 repetitions (with no sound, 2 Hz repetition rate) to obtain spontaneous activity. Frequency tuning curves were constructed by measuring responses to tone presentations of 4-48 kHz in 4 kHz steps and with sound levels between 10-90 dB SPL in 10 dB steps. Each frequency/sound level combination was repeated 20 times at 2 Hz. Characteristic frequency (CF) was defined as the frequency to which the neuron responded at the lowest sound level tested. Bandwidth (BW10, BW20, and BW30) was determined as the range of frequencies to which the neuron responded at 10 dB, 20 dB, and 30 dB above minimum threshold.

2.3.6 Rate-level functions

To determine if the response magnitudes of neurons to increasing sound levels are different across genotype, we determined the rate-level function of each neuron. The CF tone was presented at levels between 10-90 dB SPL pseudo randomly. The number of action potentials over 20 repetitions of each sound level was counted to plot the rate level function of each neuron. Percent turnover (%TO) and dynamic range were calculated from the rate-level functions as defined by (Phillips and Kelly, 1989). %TO was taken as % TO= $\frac{\text{Max Response} - \text{Response to 90 dB SPL}}{\text{Max Response}}$ X 100. A higher value of %TO indicates that the neuron's response magnitude has a non-monotonic relationship to sound level, with average response increasing and then decreasing as sound levels increase. A low %TO indicates either a response characteristic that increases continuously with sound level or reaches saturation. We hypothesized that the *Fmr1* KO IC neurons would show reduced %TO compared to WT IC

neurons. The dynamic range is the range of sound levels over which the response increases from 10% to 90% of maximum response. Across the population, the dynamic range is indicative of how rapidly the IC gets activated with increasing sound levels. We hypothesized that the *Fmr1* KO IC neurons would show narrower dynamic range compared to WT IC neurons.

2.3.7 Response magnitude and first spike latency

The average number of spikes per stimulus was calculated from the response of neurons to 20 repetitions (2 Hz rate) of CF tones presented at 15 dB and 30 dB above minimum threshold. The median first spike latency was also calculated for the 20 CF tone repetitions at every frequency and sound level tested.

2.3.8 Selectivity for sinusoidal amplitude modulated sounds

Sinusoidal amplitude modulated (SAM) tone stimulation was used to determine temporal features of single unit responses. This was motivated by the reduced phase locking of EEG responses to SAM signals seen in the *Fmr1* KO mouse auditory cortex (Lovelace et al., 2018). The carrier frequency was at CF presented 15 dB above minimum threshold and with a duration of 500 msec (2 msec rise/fall time). The recording window was 1000 msec in duration. The carrier tone was 100% depth modulated at the following frequencies: 5, 10, 20, 50, 100, and 200 Hz. Rate modulation transfer function (rMTF) was defined as the number of spikes per stimulus presentation for the duration of the stimulus presentation (500 msec). Temporal modulation transfer function (tMTF) is the vector strength (VS) as described in (Goldberg and Brown, 1969). Each spike time was correlated to the period phase (0-360 degrees). The VS was determined for every neuron at each modulation frequency (5, 10, 20, 50, 100, and 200 Hz). In

the tMTF period analysis, the first 100 msec of the recording duration was not included to omit the onset response to the sound stimulus.

2.3.9 Statistical Analysis

For the cFos data, the average of counts from 2 slices per brain region per animal was used with animal number as sample size. Because different sound levels were used for the P21 and P34 group, different statistical analyses were performed on these groups. The groups were separated into quiet and sound-exposed groups. The P21 mice received one sound level (85 dB) and the P34 groups received one of two sound levels (80 or 90 dB). The quiet group was analyzed with a Student's t-test comparing the means of *Fmr1* KO vs WT separately for P21 and P34 groups. If assumptions for the Student's t-test were not met, the nonparametric Mann-Whitney U test was performed on these groups. Meanwhile, the sound-exposed group was analyzed with a two-way ANOVA (age and genotype as factors) with Bonferroni post-hoc pairwise tests. Electrophysiology data were extracted from the acquisition software, SPARKLE. Two-way ANOVA with age and genotype as factors was performed to test main effects and interactions. The number of neurons was used as sample size for electrophysiology data. Unless otherwise noted, P value <0.05 was considered significant for all ANOVA, Student's t-test, and Mann-Whitney U test.

2.4 Results

2.4.1 Sound-evoked cFos expression is increased in the IC of Fmr1 KO mice at P21 and P34

The first major aim of the study was to determine potential genotype and age-dependent differences in sound-driven cFos expression in the IC, MGB, and auditory cortex. cFos expression was characterized in quiet and sound-exposed conditions in P21 and P34 mice of both genotypes corresponding to relatively high and low AGS susceptible ages, respectively (Musumeci et al., 2000). After habituation for 3 hours in a sound attenuated booth, a siren sound (alternating 5-50 kHz upsweep for 500 msec and 50-5 kHz downsweep for 500 msec) of calibrated sound levels was played for 15 minutes. The sound levels used did not induce overt AGS at these ages in any of the mice tested. Following perfusion, cFos immunohistochemistry, and imaging, a 400 um wide cell count window was drawn diagonally in the dorsolateral to ventromedial direction of the IC (Fig. 1 A-D) for cell counting purposes. This window was further subdivided into two halves for analysis covering 0-50% and 51-100% from lateral to medial portions of the IC.

For the quiet condition, a Student's t-test showed no significant difference in the 0-50% region of the IC for both the P21 ($t(11)=-1.186$, $p=0.261$) and P34 ($t(12)=0.841$, $p=0.417$) groups. In the 51-100% region, there was no significant difference at P21; however, there was a significant decrease in cFos density in *Fmr1* KO mice compared to WT mice at P34 ($t(12)=3.618$, $p=0.004$).

Only a single sound level (85 dB) was used for the P21 group so the data was analyzed using a Student's t-test. We could not test louder sounds because P21 KO mice showed

propensity for AGS even for sound levels of 90 dB. At P34; however, we tested mice at either 80 or 90 dB SPL and used a two-way ANOVA for the cFos analysis. For P21 in the 0-50% IC window, there was a significant increase in the sound-evoked cFos density in *Fmr1* KO mice compared to WT mice ($t(16)=-2.907$, $p=0.010$). Interestingly, for the P34 group, there was a significant decrease in the cFos density of *Fmr1* KO mice compared to the WT mice ($F(1,27)=5.415$, $p=0.028$).

In the more ventromedial (51-100%) half of the IC for the P21 group, there was no significant difference between the WT and KO groups ($t(16)=-1.444$, $p=0.168$). For the P34 group, there was significant increase in cFos density in the *Fmr1* KO group compared to the WT group ($F(1,27)=5.216$, $p=0.030$). This is seen in the example photomicrographs of Figure 1C, D. There was also a main effect of sound level with significant increase in cFos density at 90 dB compared to 80 dB sound exposure ($F(1,27)=4.998$, $p=0.034$). There was; however, no genotype x sound interaction ($F(1,27)=1.734$, $p=0.199$). These data show that at both P21 and P34, for ambient sound levels, there was no increase in cFos expression in the IC of *Fmr1* KO mice compared to WT mice. Indeed the only difference was a reduction of cFos density seen in the IC of KO mice at P34. When exposed to sound; however, there was an increase in cFos density in the IC of the *Fmr1* KO mice. The region of IC showing increased cFos expression in the KO mice shifts with age (P21→P34) from more dorsolateral IC to more ventromedial locations.

2.4.2 The MGB subnuclei show significant genotype differences in cFos density

The MGB is comprised of multiple divisions that include the medial division (MGm), the ventral division (MGv), the dorsal division (MGd), and the suprageniculate nucleus (SGN) (Fig. 2A). The adjacent peripeduncular nucleus (PP) may also be involved in auditory processing as it

reciprocally connects with the IC (Arnault and Roger, 1987). Many of these MGB divisions and adjacent regions are related to multisensory and limbic, frontal, modulate synchrony, motor, and visual modalities. The cFos expression in these areas may provide insight into how the loss of FMRP affects auditory processing and multisensory integration in the thalamus.

For the quiet condition, a Student's t-test (or Mann-Whitney U test) was used for genotype comparison in each region and age. At P21, there was a significant increase in cFos density in *Fmr1* KO mice compared to WT mice in the MGm ($t(12)=-3.152$, $p=0.008$). There was no significant difference in other regions of the thalamus studied at P21 (PP ($t(12)=-0.265$, $p=0.796$), MGv ($t(12)=1.275$, $p=0.226$), MGd ($t(12)=-0.375$, $p=0.714$), SGN ($t(12)=-1.473$, $p=0.166$)). At P34, there was a significant increase in cFos density in KO compared to WT in the MGv ($U=8$, $p=0.01$). There was no significant difference in the other regions at P34 (PP ($U=26$, $p=0.574$), MGd ($U=15.5$, $p=0.083$), MGm ($t(14)=-1.669$, $p=0.117$), SGN ($t(14)=-0.538$, $p=0.599$)).

For the sound-exposed conditions, a Student t-test was used for the P21 analysis and a two-way ANOVA (sound level and genotype as factors) was used for the analysis at P34. For the sound exposed (85 dB) condition at P21, there was a significant increase in cFos density in the SGN of the *Fmr1* KO mice compared to the WT mice ($t(16)=-4.086$, $p=0.001$). All other subnuclei showed no significance differences (PP ($t(16)=-1.491$, $p=0.155$), MGv ($t(16)=-0.367$, $p=0.718$), MGd ($t(16)=-0.792$, $p=0.440$), MGm ($t(16)=-1.758$, $p=0.098$)). At P34, no genotype-specific differences were present in any region. A sound level main effect was seen for the MGd with a significant reduction in cFos density at 90 dB compared to 80 dB sound exposure ($F(1,32)=5.522$, $p=0.025$). In addition, there was a significant sound exposure x genotype interaction

(F(1,32)=4.69, p=0.038) in the MGv. Two-way ANOVA showed no other significances in the subnuclei of the MGB (PP, MGm, SGN).

Taken together these results indicate that, in quiet, P21 KO mice had increased cFos activation in the medial division of the MGB. At P34, there was an increase in the ventral division of the MGB. It is interesting to note that the MGm is a region projecting to all cortical layers and to the amygdala. This result suggests a point of interaction between abnormal sensory processing and anxiety phenotypes in FXS during early development. When sound was presented, genotype main effects were rare, with only the SGN showing increased cFos expression in P21 *Fmr1* KO mice. The SGN is also a region receiving multisensory inputs and projects to the amygdala (LeDoux et al., 1991). At P34, there were no genotype specific differences at either 80 or 90 dB SPL.

2.4.3 cFos expression in the auditory cortex show no genotype differences

Single unit recordings from auditory cortex (Wen et al., 2018) showed higher response magnitude and spontaneous activity in P21 *Fmr1* KO mice compared to WT mice, suggesting hyperactivity of individual neurons in the auditory cortex. Here, to investigate if more neurons were activated in the auditory cortex of *Fmr1* KO mice we quantified cFos expression. A 400 µm wide rectangular window that spanned the length of cortical layers I-VI was used to quantify cFos density (Fig. 3, A1-B6).

The Student's t-test or the Mann-Whitney U test was used as appropriate. At P21, in the quiet condition, the Mann-Whitney U test showed no significant difference between WT and KO (U=16, p=0.302). For the P34 group in the quiet condition, the Student's t-test showed no significant difference between WT and KO (t(14)=-0.987, p=0.340). These data indicate that for

both ages, P21 and P34, there were no differences in the number of activated neurons in the auditory cortex in a quiet environment (Fig. 3C, left).

In the 85 dB sound-exposed condition at P21, the Mann-Whitney U test showed no significant difference between WT and KO groups (U=25, p=0.321). In the P34 group, a two-way ANOVA test showed that there was no genotype x sound interaction (F(1,29)=0.382, p=0.541) or main effect of genotype (F(1,29)=1.887, p=0.180); however, there was a significant increase in cFos density at 90 dB compared to 80 dB sound exposure (F(1,29)=8.583, p=0.007). The cFos analysis thus shows no genotype difference in the auditory cortex at P21 and P34 (Fig. 3C, right). It appears that individual neurons in the *Fmr1* KO mouse auditory cortex show increased responses at P21, but the number of neurons activated by sound is not different across genotypes. In the IC, however, more neurons are activated in the *Fmr1* KO mice. Next we tested if individual IC neurons showed increased response magnitudes and other abnormal response patterns.

2.4.4 Increase in cFos intensity of Fmr1 KO compared to WT mice at P21 in the IC when exposed to sounds

In quiet conditions at P21 of the IC, there was no significant difference between *Fmr1* KO and WT mice (t(11)=0.181, p=0.860). Similarly in quiet condition at P34, there was no significant difference between *Fmr1* KO and WT mice (t(14)=-0.553, p=0.589). At P21 when exposed to 85 dB, there was a significant increase in intensity of cFos expressing neurons in *Fmr1* KO compared to WT mice (t(13)=-4.382, p=0.001). At P34 when exposed to 80 dB or 90 dB,

there was no significant difference in sound intensity x genotype interaction (F(23,1)=0.054, p=0.818). In addition, there was no difference in sound intensity (F(23,1)=3.692, p=0.067) and no genotype difference (F(23,1)=0.063, p=0.804).

When only the dorsal-lateral region (0-50%) was analyzed for intensity of cFos expressing neurons, there was a significant genotype effect in the sound exposed condition at P21 (Appendix A, Figure A3). In the quiet condition, there was no significant difference between *Fmr1* KO and WT mice (F(23,1)=0.063, p=0.804). At P34 in the quiet condition, similarly, there was no significant difference between *Fmr1* KO and WT mice (t(14)=-0.2154, p=0.833). In sound exposed condition at 85 dB, there was a significant increase in the intensity of cFos expressing neurons of *Fmr1* KO compared to WT mice (t(13)=-4.37541, p=0.000751). At P34 sound exposed (80 or 90 dB), there was no significant sound intensity x genotype interaction (F(22,1)=0.020, p=0.890). In addition, there was no significant difference in genotype (F(22,1)=0.905, p=0.352); however, there is a significant increase at 90 dB compared to 80 dB (F(22,1)=6.251, p=0.020).

In the ventral-medial region (51-100%), there was a significant increase in the intensity of cFos expressing neurons of *Fmr1* KO compared to WT mice when exposed to 85 dB (t(13)=-4.50242, p=0.000595). At P34, there was no significant difference in sound intensity x genotype interaction (F(22,1)=0.010, p=0.922). Moreover, there is no significant difference in main effect of genotype (F(22,1)=0.041, p=0.842) nor main effect of sound intensity (F(22,1)=3.388, p=0.079).

2.4.5 No cFos intensity difference in the MGB of Fmr1 KO mice compared to WT mice

When the intensity of cFos expressing neurons were analyzed, there were no significant differences between *Fmr1* KO and WT mice in quiet conditions for both P21 and P34 (Table A1,

Figure A4). In addition, there were no significant differences between Fmr1 KO and WT mice in intensity of cFos expressing neurons at sound exposed conditions (P21 at 85 dB and P34 at 80 dB or 90 dB) except for MGd and MGm at 80 dB at P34 (Table A1, Figure A4).

2.4.6 No cFos intensity difference in AuC of *Fmr1* KO compared to WT mice

When the intensity of cFos expressing neurons were measured, there was no difference between *Fmr1* KO and WT mice (Appendix A, Figure A2). In quiet conditions at P21, there was no significant difference between *Fmr1* KO and WT mice ($t(12)=-0.812$, $p=0.433$). Similarly, in quiet condition at P34, there was no significant difference between *Fmr1* KO and WT mice ($t(14)=0.573$, $p=0.576$). In the sound exposed condition at 85 dB, the P21 group showed no significant difference between *Fmr1* KO and WT mice ($t(16)=-1.988$, $p=0.064$). The P34 group in the sound exposed condition (80 and 90 dB) showed no interaction in sound intensity x genotype ($F(27,1)=0.040$, $p=0.843$). Moreover, there was no significant main effect of genotype ($F(27,1)=0.001$, $p=0.97$) between *Fmr1* KO and WT mice; however, there was a significant difference in sound intensity ($F(27,1)=16.211$, $p=0.000413$), suggesting the intensity of cFos expression is correlated to sound level intensity.

2.4.7 Electrophysiology

Given that the cFos data showed significant genotype differences in the IC, single unit electrophysiological data were collected from this region in both genotypes at three different developmental ages: P14, P21, and P30. Spontaneous activity, rate-level functions, frequency tuning curves, and responses to SAM tones were compared across age and genotype.

2.4.8 Spontaneous activity of IC neurons shows CF-specific genotype effects

Spontaneous activity was measured by counting the number of spikes over 20 repetitions of the recording window (250 msec) with no sound stimulus. The average spontaneous activity across all recorded neurons for each genotype and age was then used in a two-way ANOVA (age and genotype as factors) to identify statistical differences. The overall spontaneous activity in the IC was low, likely due to the anesthesia (Fig. 4A). However, it was possible to detect a significant main effect of age ($F(2,499)=11.153$, $p=0.000018$) with Bonferroni post-hoc comparison showing a reduction in spontaneous activity with age (P14 vs P21, $p=0.024$; P14 vs P34, $p=0.000007$; and P21 vs P34, $p=0.124$). However, there was no main effect of genotype ($F(1, 499)=2.333$, $p=0.127$) or a genotype x age interaction ($F(2,499)=1.186$, $p=0.306$). Thus, when all the neurons were considered together, spontaneous activity decreased during development in the IC with no genotype differences.

Because the data showed a trend for genotype differences at P21 and because there was a regional difference in the cFos density data of the IC, we examined the data by classifying neurons according to CF, with low and high CF groups separated with a 20 kHz cut-off range. We chose the 20 kHz cut-off frequency because the IC tonotopic map splits approximately into two halves at this CF (Felix II et al., 2007). For neurons with CF<20 kHz, there was a significant genotype x age interaction ($F(2,167)= 4.928$, $p=0.008$) and an increased spontaneous firing rate in *Fmr1* KO mice compared to WT mice ($p=0.04$), but no significant effect of age ($p=0.08$) (Fig. 4B). For neurons with CF>=20 kHz, there was no significant genotype x age interaction ($F(2,333)=0.052$, $p=0.949$) or main effect of genotype ($F(1,333)=0.933$, $p=0.335$), but a significant main effect of age ($F(2,333)=12.938$, $p<0.0001$) with Bonferroni post-hoc comparison showing a

decrease in spontaneous activity with age (P14 vs P21, p=0.000182; P14 vs P34, p<0.0001; P21 vs P34, p=0.015) (Fig. 4B). In terms of spontaneous activity in the IC, these data indicate a larger effect of genotype in neurons with CF<20 kHz and an effect of age in neurons with CF>=20 kHz.

2.4.9 Minimum thresholds of IC neurons in *Fmr1* KO mice is decreased in a CF-dependent manner

We next compared minimum threshold, defined as the lowest sound level that evoked a response to tones. When all neurons were pooled together, there was a genotype x age interaction (F(2,501)=3.818, p=0.023), a main effect of age (F(2,501)=11.586, p=0.000012) with Bonferroni post-hoc (P14 vs P21, p=0.000115; P14 vs P34, p=1.00; P21 vs P34, p=0.000037) with the lowest mean minimum threshold at P21 compared to P14 and P34. There was no significant main effect of genotype (F(1,501)=1.834, p=0.176) (Fig. 4C).

When neurons were separated by CF, neurons with CF<20 kHz showed no genotype x age interaction (F(2,164)=1.274, p=0.282) or main effect of genotype (F(1,164)=2.915, p=0.09). However, there was a significant main effect of age (F(2,164)=13.385, p<0.0001) with Bonferroni post-hoc showing a difference between P14 vs P21 (p=0.001) and P21 vs P34 (p<0.0001), but not for P14 vs P34 (p=0.261) (Fig. 4D). For neurons with CF>=20 kHz, there was no genotype x age interaction (F(2,331)=1.211, p=0.299), but a significant main effect of genotype with a decrease in minimum threshold of *Fmr1* KO compared to WT IC (p=0.012), and a main effect of age (p<0.0001) with Bonferroni post-hoc comparison showing a difference between P14 vs P21 (p=0.000005) and P14 vs P34 (p=0.006696), but not P21 vs P34 (p=0.105169) (Fig. 4D). These data suggest that reduced minimum thresholds may be a factor involved in *Fmr1* KO mouse IC responses for high-CF neurons.

2.4.10 IC neurons in *Fmr1* KO mice are hyper-responsive to sounds

We compared IC neuronal response magnitudes to tone stimulus across age and genotype. For all neurons combined (Fig. 5A), average response magnitude at 15 dB above minimum threshold showed no significant genotype x age interaction ($F(2,481)=1.495$, $p=0.225$) but a significant main effect of genotype with an increase in the mean number of spikes/stimulus in *Fmr1* KO mice compared to WT mice ($F(1,481)=5.249$, $p=0.022$). There was also a main effect of age ($F(2,481)=6.257$, $p=0.002$) with a significant Bonferroni post-hoc comparison for P21 vs P34 ($p=0.004$) and P14 vs P34 ($p=0.005$) but not significant P14 vs P21 ($p=1.00$) (Fig. 5A). Driven response seems to decrease during development. For responses at 30 dB above minimum threshold (Fig. 5B), there was a significant genotype x age interaction ($F(2,477)=4.303$, $p=0.014$). Moreover, there was a significant increase in mean response magnitude in the *Fmr1* KO mice compared to the WT mice ($F(1,477)=4.772$, $p=0.029$) and a significant main effect of age ($F(2,477)=6.313$, $p=0.002$) with Bonferroni post-hoc tests revealing no significant differences in P14 vs P21 ($p=1.00$), but a significant reduction with age in P21 vs P34 ($p=0.001$) and P14 vs P34 ($p=0.019$) comparisons.

When the neurons were classified according to CF, comparison of response magnitude at 15 dB above minimum threshold for neurons with CF<20 kHz showed a significant increase in mean response magnitude in the *Fmr1* KO group compared to the WT group ($F(1,157)=14.878$, $p=0.00016$), but no significant main effect of age ($F(2,157)=1.256$, $p=0.288$) or genotype x age interaction ($F(2,157)=0.277$, $p=0.759$) (Fig. 5C). When the sound level was at 30 dB above minimum threshold (Fig. 5D), there was a significant increase in response magnitude of neurons with CF<20 kHz in the *Fmr1* KO group compared to the WT group ($F(1,155)=18.529$, $p=0.000030$)

(Fig. 5D). There was no significant main effect of age ($F(2,155)=1.625$, $p=0.2$) and genotype x age interaction ($F(2,155)=2.117$, $p=0.124$).

For neurons CF>=20 kHz at 15 dB above threshold (Fig. 5C), there was a main effect of age ($F(2,316)=6.132$, $p=0.002$) with no significant difference in Bonferroni post-hoc comparison of P14 vs P21 ($p=1.00$), but a significant difference for P14 vs P34 ($p=0.022$) and P21 vs P34 ($p=0.003$). There was no main effect of genotype ($F(1,316)=0.002$, $p=0.968$) or genotype x age interaction ($F(2,316)=1.534$, $p=0.217$). At 30 dB above minimum threshold (Fig. 5D), there was no main effect of genotype ($F(1,314)=0.041$, $p=0.840$). There was a main effect of age ($F(2,314)=5.390$, $p=0.005$) with no significant difference using Bonferroni post-hoc comparisons in P14 vs P21($p=1.000$) and P14 vs P34 ($p=0.092$), but a significant difference in P21 vs P34 (p=0.003). In addition, there was a significant genotype x age interaction ($F(2,314)=5.174$, $p=0.006$). Overall, response magnitude elicited by the CF tone was higher in *Fmr1* KO mice for neurons with CF<20 kHz. Neurons with CF>=20 kHz showed a reduction in response magnitude with age, but no genotype differences. These results were similar to those seen with spontaneous activity. Low frequency IC neurons, therefore, show increased responses to sounds and spontaneous activity during development.

2.4.11 Rate-level functions of IC neurons are not different between genotypes

The manner in which response magnitudes increase with sound level may predispose the *Fmr1* KO mice to AGS. To quantify the relationship between increasing sound levels and response magnitude, rate-level functions were plotted for CF response to sound levels in the 10-90 dB range. Percent turnover (%TO) is a measure of the non-monotonicity of rate-level

functions and indicates the extent to which responses are reduced with increasing sound levels. Therefore, we hypothesized that %TO is lower in *Fmr1* KO mice compared to WT mice.

When all neurons were combined (Fig. 6C), there was no main effect of genotype in the %TO ($F(1,482)=0.559$, $p=0.455$) or genotype x age interactions ($F(2,482)=0.716$, $p=0.489$). But there was a significant effect of age ($F(2,482)=6.422$, $p=0.002$) with Bonferroni post-hoc significant difference at P14 vs P21 ($p=0.011$) and P14 vs P34 ($p=0.004$) but not at P21 vs P34 ($p=1.00$). These data indicate that neurons become more monotonic with age with no main genotype differences.

For neurons with CF<20 kHz (Fig. 6D), there was no genotype x age interaction ($F(2,161)=0.405$, $p=0.668$) or main effect of genotype ($p=0.473$); however there was a main effect of age ($p=0.029$) with Bonferroni post-hoc comparisons showing no significant pairwise differences (P14 vs P21, $p=0.061$; P14 vs P34, $p=0.138$; and P21 vs P34, $p=1.00$). For neurons with CF>=20 kHz (Fig. 6D), there was no significant genotype x age interaction ($F(2,330)=2.704$, $p=0.068$) or main effect of age ($p=0.483$), but there was a significant increase in %TO in *Fmr1* KO mice compared to WT mice ($p=0.037$). This genotype effect was opposite to that hypothesized. These data suggest that abnormal sensitivity to increasing sound levels of individual IC neurons may not contribute to auditory hypersensitivity in *Fmr1* KO mice.

In addition to %TO, we quantified dynamic range as the range of SPL over which response magnitude increases from 10% to 90% of maximum response. We hypothesized that the dynamic range would be narrower in the *Fmr1* KO mice IC compared to WT. This would cause the *Fmr1* KO mice's IC to be activated to near maximal levels even with small increases in sound level. However, that hypothesis was not supported because there was no significant

genotype difference in dynamic range. For all neurons combined (Fig. 6E), there was no genotype x age interaction (F(2,356)=1.935, p=0.146) or main effect of genotype (F(1,356)=0.601, p=0.439); however, there was a main effect of age (F(2,356)=3.522, p=0.031). Bonferroni post-hoc comparisons did not show any specific pairwise differences (P14 vs P21, p= 0.189; P14 vs P34, p=0.129; and P21 vs P34, p=1.00). For neurons CF<20 kHz (Fig. 6F), there was no genotype x age interaction (F(2,127)=2.614, p=0.077) or main effect of genotype (p=0.959), but there was a significant main effect of age (p=0.0004) with a significant Bonferroni post-hoc comparison between P14 vs P21 (p=0.004) and P14 vs P34 (p=0.013) but not at P21 vs P34 (p=1.00). For neurons CF>=20 kHz, there was no significant genotype x age interaction (F(2,223)=1.719, p=0.182), main effect of genotype (p=0.915), or main effect of age (p=0.948). Together, these data do not support the hypothesis that AGS susceptibility of *Fmr1* KO mice is due to altered response magnitude and sound level relationship. However, these data do reveal an overall change in rate-level functions with age in the IC.

2.4.12 Low frequency IC neurons show longer response latency in *Fmr1* KO mice

The median first spike latency of IC neuronal response to CF tone at 15 dB and 30 dB above minimum threshold was compared to identify genotype and age effects (Fig. 7). Two-way ANOVA showed a significant main effect of age for latency 15 dB above minimum threshold (F(2, 477)=35.43, p<0.0001, Fig. 7A), but no significant main effect of genotype (F(1,477)=0.613, p=0.434) or genotype x age interaction (F(2,477)=1.262, p=0.284). Bonferroni post-hoc analysis revealed a significant difference between P14 vs P21 (p<0.0001), P14 vs P34 (p<0.0001), and P21 vs P34 (p=0.00082), with latencies decreasing with age. Likewise, for CF tones presented at 30 dB above minimum threshold (Fig. 7B), there was a significant main effect of age

(F(2,475)=114.773, p<0.0001) with Bonferroni post-hoc comparison at P14 vs P21 (p<0.0001), P14 vs P34 (p<0.0001), and P21 vs P34 (p<0.0001) showing decreasing latency with age, but no significant main effect of genotype (F(1,475)=0.904, p=0.342) or genotype x age interaction (F(2, 475)=0.087, p=0.917).

When neurons were separated by CF, neurons CF<20 kHz showed a significant main effect of genotype (p=0.029) with shorter latency in the WT compared to KO for tones at 15 dB above minimum threshold (Fig. 7C). There was also a main effect of age (p=0.000044) with Bonferroni post-hoc comparison of P14 vs P21 (p=0.0042), P14 vs P34 (p=0.00018), and P21 vs P34 (p=1.00) showing that latency decreases with age; however, there was no significant difference in genotype x age interaction (F(2,163)=0.297, p=0.743). For neurons CF>=20 kHz there was no significant main effect of genotype (p=0.065) or genotype x age (F(2,315)=0.130, p=0.878). However, there was a significant main effect of age (p<0.0001) with Bonferroni post-hoc of P14 vs P21 (p<0.0001), P14 vs P34 (p<0.0001), and P21 vs P34 (p=0.0053) showing that latency decreases with age.

Similarly at 30 dB above minimum threshold, neurons CF<20 kHz showed a main effect of genotype (p=0.044) and main effect of age (p<0.0001) with Bonferroni post-hoc at P14 vs P21 (p=0.0023), P14 vs P34 (p<0.0001), and P21 vs P34 (p=0.000055) with latency decreasing with age. There was no significant genotype x age interaction (F(2,143)=1.405, p=0.249). For neurons CF>=20 kHz, there was a significant main effect of age (p<0.0001) with Bonferroni post-hoc at P14 vs P21 (p<0.0001), P14 vs P34 (p<0.0001), and P21 vs P34 (p<0.0001) indicating faster latencies with age. There was no significant main effect of genotype (p=0.615) or genotype x age interaction (F(2,312)=0.045, p=0.956). Thus, the median first spike latency in response to CF

tones decreases during development across all CFs, with genotype differences seen for neurons with CF<20 kHz. Neurons with CF<20 kHz show more genotype differences compared to neurons with higher CF.

2.4.13 Low frequency IC neurons in the *Fmr1* KO mice show broader frequency tuning

Rotschafer and Razak (2013) suggested that a possible mechanism of increased synchrony and hyper-sensitivity to sounds may be linked to broader frequency tuning curves of individual neurons in *Fmr1* KO mice. This is because more neurons would be activated for a single tone frequency if tuning curves were broader on average. To determine if broader tuning curves are seen in the IC, we performed a genotype and age comparison of frequency response area bandwidths (BW) at three different sound levels: 10, 20, and 30 dB above minimum threshold (BW10, BW20, and BW30, respectively).

Frequency response areas (e.g., Fig. 8A) were plotted by counting responses to 20 presentations of each frequency and sound level combination ranging from 4-48 kHz (4 kHz steps) and10-90 dB SPL (10 dB steps). There was a significant genotype x age interaction ($F(2,307)=4.971$, $p=0.008$) for BW10 (Fig. 8B), but no main effect of genotype ($F(1,307)=0.679$, $p=0.410$) or age ($F(2,307)=2.556$, $p=0.079$). A main effect of genotype was seen for BW20 (Fig. 8B), with broader tuning curves in *Fmr1* KO mice compared to WT mice ($F(1,307)=3.927$, $p=0.048$). There was also a significant main effect of age ($F(2,307)=6.096$, $p=0.003$) with Bonferroni post-hoc showing a significant difference in P14 vs P21 ($p=0.002$) and P14 vs P34 ($p=0.024$) but not P21 vs P34 ($p=1.00$). There were no significant genotype x age interaction ($F(2,307)=1.095$, $p=0.336$). For BW30 (Fig. 8B), there was a significant effect of age ($F(2,307)=12.276$, $p=0.000007$) with Bonferroni post-hoc showing a significance in P14 vs P21

(*p*=0.000018) and P14 vs P34 (p=0.000066) but not in the P21 vs P34 (*p*=1.00) groups. There was no main effect of genotype (*F*(1,307)=0.860, *p*=0.354) or genotype x age interaction (*F*(2,307)=0.032, *p*=0.968).

When classified by CF, neurons with CF<20 kHz (Fig. 8C) were more broadly tuned in the *Fmr1* KO IC compared to WT IC at BW10 (*F*(1,118)=4.346, *p*=0.039), BW20 (*F*(1,118)=5.9, *p*=0.017), and BW30 (*F*(1,116)=5.806, *p*=0.018). For BW10, there was no significant genotype x age interaction (*F*(2,118)=1.771, *p*=0.175) nor main effect of age (*F*(2,118)=0.058, *p*=0.944). Similarly for BW20 and BW30, there were no significant genotype x age interaction (*F*(2,118)=0.487, *p*=0.616 and *F*(2,116)=0.387, *p*=0.68, respectively) nor main effect of age (*F*(2,118)=0.487, *p*=0.515 and *F*(2,116)=1.259, *p*=0.288, respectively). Neurons with CF>=20 kHz (Fig. 8D) showed no genotype effects for BW10 (*F*(1, 181)=0.123, *p*=0.726), BW20 (*F*(1, 182)=1.221, *p*=0.271), and BW30 (*F*(1,180)=0.225, *p*=0.636). In addition, there were no significant main effect of age for BW10 (*F*(2,181)=0.699, *p*=0.499), BW20 (*F*(2,182)=2.606, *p*=0.077), and BW30 (*F*(2,180)=4.013, *p*=0.20). A genotype x age interaction at BW10 (*F*(2,181)=3.272, *p*=0.04) was seen. These results showed that there was an increase in bandwidth (BW10, BW20, and BW30) in KO compared to WT. Yet again, it appears that neurons with CF<20 kHz show more genotype differences than neurons tuned to higher than 20 kHz.

2.4.14 *Fmr1* KO mouse IC neurons showed stronger responses to amplitude modulated tones than WT neurons

The rate modulated transfer function (rMTF) and temporal modulated transfer function (tMTF) for responses to sinusoidal amplitude modulated (SAM) tones were compared across age and genotype (Fig. 9). The rMTF was analyzed as the average number of spikes per stimulus

presentation over the duration of the stimulus. The tMTF were analyzed as the degree of synchronization to the modulations as measured by vector strength. Modulation rates of 5, 10, 20, 50, 100, and 200 Hz on carrier frequency centered at CF were used for this study. The SAM tone was presented at 15 dB above minimum threshold.

For rMTF analysis, two-way ANOVA was run with genotype and age as factors. Separate ANOVA was run for each modulation rate. The main statistics are summarized in Table 2, including analyses of all neurons pooled or separated by CF (20 kHz cut-off). In general, Table 2 and Figures 9 and 10 show a number of significant genotype differences in rMTF driven mostly by increased responses to SAM in the *Fmr1* KO mice. Figure 9 (C-E) also suggests that the increased responses are more prominent at faster modulations rates with *Fmr1* KO IC neurons showing a peak ~50 Hz modulation rates compared to WT neurons, on average. Neurons with CF<20 kHz also show more consistent genotype differences across modulation rates (Table 2, Fig. 10 A-C). No consistent patterns were seen for main effects of age or age x genotype interactions. Together, we interpret these data to indicate that responses to modulated tones are increased in the *Fmr1* KO mice, consistent with increased response to un-modulated tones, and may underlie auditory hypersensitivity in *Fmr1* KO mice.

For the tMTF (Table 3, Fig. 9F-H, 10D1-F2), main effects of genotype were rare (seen only for 10 Hz modulation rate), and the other effects do not show a consistent pattern pointing to specific developmental change or genotype x age interactions. We interpret this to mean that the temporal response properties of IC neurons when tested with SAM do not contribute to abnormal auditory sensitivity.

When the responses to the first period of the modulation function were excluded from the tMTF analysis, there was a significant difference in main genotype effect at only at 5 Hz ($F(436)=4.821$, $p=0.029$), 10 Hz ($F(439)=5.105$, $p=0.024$), and 200 Hz ($F(472)=11.848$, $p=0.001$) meanwhile all other modulation rates were not significant (Table A2).

To determine if the increased in *Fmr1* KO response to SAM stimulus was attributed to the onset response or the rest of the responses, we analyzed only the first period of the modulation compared to the response without the first period modulation. For the rMTF analysis, the responses to the first period of the modulation rate showed a main genotype effect for 5 Hz, 10 Hz, 20 Hz, and 50 Hz (Table A4). When the rMTF was analyzed without the response to the first period, there was a significant main effect of genotype at 20 Hz, 50 Hz, and 100 Hz (Table 3A). The similarity in the amount of response in the first period of the modulation compared to the rest of the response suggests that the increase in response to SAM stimulus is throughout the duration of the stimulus and not attributed to the onset or the following response.

2.4.15 Tonotopy

Given the CF specific effects observed and because of a previous study that showed tonotopic gradients of ion channel expression may be affected in the auditory brainstem, we quantified development and possible genotype differences in tonotopy in the IC. We observed the expected dorsal to ventral increase in CF representation at all three developmental ages (Fig. 11) and across genotypes. The CF representation was mostly <30 kHz at P14 and expanded to include more neurons with CF>30 kHz at P21 and P34. This is also consistent with previous studies of development of tonotopy (Romand and Ehret, 1990). There was no significant

difference in the distribution of CFs across genotypes (P14: $t(159)=0.831$, $p=0.406$), (P21: $t(164)=0.788$, $p=0.431$), and (P34: $t(188)=0.589$, $p=0.555$). Together, these data suggest that CF specific susceptibilities in *Fmr1* KO mice are not due to abnormal development of tonotopy.

2.4.16 Developmental Effects

To understand the differences in response characteristics across developmental ages in single unit recordings of the IC, *Fmr1* KO mice and WT mice were compared among age groups. We used a Student t-test with correction for multiple comparisons (Table 4-6). For the P34 age group, WT neurons with CF>= 20 kHz showed a significant increase in minimum threshold. In addition, there was a significant increase in %TO for *Fmr1* KO neurons compared to WT neurons with CF>= 20 kHz. Response magnitude at 15 dB and 30 dB above minimum threshold for *Fmr1* KO neurons with CF< 20 kHz showed a significant increase compared to WT neurons. For neurons with CF< 20 kHz in the rMTFs analysis, there were significant increase in magnitudes across all modulation frequencies for *Fmr1* KO neurons compared to WT neurons.

The IC results also show an increase in magnitude during P21 at 15 dB and 30 dB above minimum threshold, suggesting the possibility that the development of cortical hyper-responsivity is inherited from subcortical sites, including the IC. When tuning to low and high CFs were considered, only response magnitude at 30 dB above minimum threshold for CF< 20 kHz and CF>= 20 kHz were significantly larger in *Fmr1* KO neurons compared to WT neurons. *Fmr1* KO neurons with CF< 20 kHz have a significant increase at BW10 compared to WT neurons. In rMTFs with all CFs combined, there were a significant increase in response magnitudes at 50 and 100 Hz modulations. There were no significant differences at the P14 age group. Taken together, the response characteristics during development affect P21 and P34, but not at P14, suggesting

a unique developmental age when *Fmr1* KO mice have increased hypersensitivity. Moreover, the increased in response magnitude at P34 indicates a sustained hyperresponsiveness with age but for only neurons with CF < 20 kHz indicating recovery for neurons with CF >= 20 kHz.

2.5 Discussion

Analysis of cFos cell density in response to relatively loud, but sub-convulsive, sounds showed that more neurons in the *Fmr1* KO mice were activated by sounds compared to WT mice at P21 and P34. The genotype difference was in the more laterodorsal half of the IC at P21, and shifted to the medioventral half at P34. At P34, a distinct band of increased cFos activity was seen in the medioventral IC adjacent to the periacqueductal gray. There was also increased sound driven response in regions of the thalamus involved in multisensory integration, but not in the MGv, the main thalamic nucleus of the lemniscal pathway. Interestingly, there was no genotype difference in cFos density in the auditory cortex.

Only one other study has examined cFos expression in response to sounds in the *Fmr1* KO mice (Chen and Toth, 2001). Their study presented sounds that induced AGS in some of the mice. When AGS was induced in *Fmr1* KO mice, there was an increase in cFos expression in KO compared to WT (who received the same sound exposure but did not seize) in the dorsal nucleus of the lateral lemniscus, posterior intralaminar nucleus, periaqueductal grey, and MGm. However, in the IC, both the *Fmr1* KO and WT mice had a similar increase in cFos expression with exposure to noise at 115 dB (2-20 kHz). However, because the *Fmr1* KO mice showed seizures and the WT mice did not in this study, the genotype differences in cFos cell density can at least partially be due the motor responses involved in the seizure. To overcome this confound, the sound stimulus in our study was in the range of 80-90 dB, which did not induce

AGS. Under these sensory driven conditions, we found the main genotype difference in cFos expression in the IC, MGm and SGN regions. Because of the strong SGN and MGm connectivity to the amygdala, this suggest a stronger activation of auditory-emotional pathways which may lead to FXS behavioral anxiety phenotypes in response to daily environmental sounds.

Analysis of single unit responses in the IC at P14, P21, and P34 showed that the *Fmr1* KO mouse neurons showed increased responses to tone bursts and amplitude modulated tones and broader frequency tuning curves. However, the rate-level functions and temporal following of responses to the amplitude modulations were not different across genotypes. Low frequency tuned neurons (CF<20 kHz) showed a greater degree of genotype differences compared with neurons with CF>=20 kHz. Taken together, these data indicate that the midbrain IC is hyper-responsive in the *Fmr1* KO mouse during early development. More neurons are activated by sound and each neuron is activated more than in age-matched WT mice. Broader tuning curves, without a difference in average latency, suggest that more neurons will respond synchronously to a single sound in *Fmr1* KO mouse IC compared to WT IC. These data suggest that the IC may be a major source of auditory hypersensitivity seen in individuals with FXS, particularly during development.

Given the consistent and debilitating auditory hypersensitivity in individuals with FXS, there has been an increased interest in understanding the underlying the circuit and cellular pathophysiology across the auditory system and across development. FMRP is expressed across the auditory system from the brainstem to the auditory cortex across multiple species including humans. There is an increased single unit response magnitude in the *Fmr1* KO mouse auditory cortex at P21, but not at P14, suggesting that this property develops between P14 and P21. The IC results also show a greater genotype difference during P21 at 15 dB and 30 dB above

threshold, suggesting the possibility that the development of cortical hyper-responsivity is inherited from subcortical sites, including the IC. Interestingly, while the IC showed both more cells being activated and single cell hyperactivity at P21, the auditory cortex only showed the single cell hyperactivity (Wen et al., 2018). This indicates that the IC may be contributing to a greater extent to the auditory hypersensitivity phenotype in FXS.

The mechanisms that cause greater susceptibility of low-CF neurons to show hyper-responsiveness is unclear, but may point to abnormal GABA responses in the *Fmr1* KO mice. The IC tonotopic gradient is such that neurons with increasing CF are found as the electrode penetrates more ventrally into the IC. I.e., most of the neurons with CF<20 kHz are likely to be within 1000 um from the dorsal surface (~50% of total dorsoventral depth, Felix and Portfors, 2007). IC neurons receive both GABA and glycine inhibitory inputs. Across species, glycine has been suggested to be likely more dominant in shaping inhibition in ventral, high-CF regions of the IC (Choy Buentello et al., 2015; Merchán et al., 2005; Sanes et al., 1987). GAD67-labeled inputs appear to dominate more dorsomedial regions of the IC (Choy Buentello et al., 2015), suggesting a more prominent role for GABA in the dorsal half of the IC. This may suggest a deficit in GABAergic inhibitory effects because most deficits were in low CF neurons in the dorsolateral region IC. GABAa receptor deficits are related to audiogenic seizure in rodents (Faingold, 2002). In addition, there is down-regulated tonic GABAa current and a decrease in GABAa receptors in *Fmr1* KO mice (Curia et al., 2009; D'Hulst et al., 2006), suggesting impaired GABA inhibition in FXS. GABAergic inputs control discharge rates in the IC receptive field (Palombi and Caspary, 1996). Whether glycinergic inhibition is affected in the IC is unclear, but Garcia-Pino et al. (2017) showed no impact on such inhibition in the brainstem of Fmr1 KO mice.

Together these studies suggest the CF-dependent susceptibility of IC to hyper-responsiveness in early development may be related to GABA dysfunction in *Fmr1* KO mice.

2.5.1 System-wide deficits in auditory processing in FXS

FMRP is expressed at multiple levels of the auditory system from the cochlear nucleus to the auditory cortex. Global deletion of *Fmr1* would affect the development and function of each of these auditory processing stages. The impact of loss of FMRP at various levels of the auditory system is only beginning to be understood. For example neurons in the lateral superior olive (LSO) of the brainstem receive show enhanced excitatory synaptic input strength through increased convergence of cochlear nucleus input early in development. LSO neurons showed increased firing rates and broader frequency tuning curves. The abnormal IC responses may originate in the brainstem. However, this needs to be additionally verified by comparing brainstem and IC recordings conducted at similar ages. In the medial nucleus of the trapezoid body (MNTB), one of the major sources of inhibition to the LSO, the tonotopic gradient of Kv3.1b potassium ion channel is significantly flatter in *Fmr1* KO, compared to WT mice. Modeling (Strumbos et al., 2010) and electrophysiological (Brown et al., 2010) data suggest an impact on temporal precision in MNTB of Fmr1 KO mice. This may be limited to the MNTB, as our IC data do not reveal any genotype differences in tMTF, suggesting that single neuron phase locking is not affected in the IC. Cell sizes were also reduced and VGAT expression is elevated in the MNTB of the Fmr1 KO mice suggesting increased inhibitory input and disinhibition of the LSO (Rotschafer et al., 2015).

This is the first comprehensive study of the IC in developing *Fmr1* KO mice. Similar studies have not been performed in the medial geniculate body. However, the auditory cortex

has received considerable attention. Rotschafer and Razak (2013) showed increased response magnitude and broader frequency tuning in the auditory cortex of Fmr1 KO mice. Wen et al., (2018) showed that such responses are seen at P21, but not at P14, suggesting the origin of hyper-responsivity in this developmental time frame when cortical properties mature (Oswald and Reyes, 2008, 2011). Consistent with abnormal inhibition, Wen et al. (2018) showed that increased matrix metalloproteinase-9 (MMP-9) in the auditory cortex may lead to abnormal development of perineuronal nets (PNN) and parvalbumin (PV) positive inhibitory interneurons. Loss of PNNs will reduce excitability of PV cells and reduced network inhibition. This suggests that at least part of the cortical deficit arises due to PV/PNN deficits that are local to cortex, and not inherited from the IC. This notion was further supported by a recent study that showed that removal of *Fmr1* only from forebrain excitatory neurons using the *Nex1* promoter results in gamma oscillation deficits in the cortex indicating local cortical circuit deficits. Interestingly, however, the abnormal phase locking phenotype seen in previous cortical recordings was not present when *Fmr1* was removed only from forebrain. This suggests a combination of cortical and subcortical contributions give rise to the various auditory processing phenotypes studied in the *Fmr1* KO mice. The present study identifies the IC as a potentially strong hub of hypersensitive responses, at least in early development.

In conclusion, we found region specific deficits in the IC of developing *Fmr1* KO mouse. A majority of the deficits at P21, the time of high AGS susceptibility, were in the dorsolateral region and in neurons tuned to lower frequencies in the IC. This implies that FMRP affects regions low and high frequency differently. Future studies should examine AGS with stimuli that are low-pass or high-pass filtered at ~20 kHz to determine if the *Fmr1* KO mice are more sensitive to the low-pass stimulus than the high-pass. The impact of GABA receptor modulation

to reduce hyperactivity ~P21 should be tested for both acute and long lasting benefits from auditory hypersensitivity in the *Fmr1* KO mice. Future studies are also needed to examine how different classes of GABA neurons in the IC (Beebe et al., 2016) are affected in *Fmr1* KO mice.

Table 1: Window size in which cells were counted within the subnuclei in the MGB.

Medial geniculate body (MGB) subnuclei	Cell count window size (um)
Suprageniculate Nucleus (SGN)	100 x175
Dorsal division of the MGB (MGd)	250 x 200
Ventral division of the MGB (MGv)	250 x 350
Medial division of the MGB (MGm)	200 x 250
Peripeduncular Nucleus (PP)	530 x 200

Table 2: rMTF, *= $p < 0.05$

Modulation Frequency (Hz)	CF Frequency	Genotype x Age Interaction	Main effect of Genotype	Main effect of Age
5	All	F(2,412)=1.973, p=0.140	F(1,412)=2.011, p=0.157	F(2,412)=0.688, p=0.503
	CF<20 kHz	F(2,159)=1.697, p=0.187	F(1,159)=7.366, p=0.007*	F(2,159)=0.832, p=0.437
	CF>=20 kHz	F(2,315)=3.264, P=0.040*	F(2,315)=0.001, p=0.972	F(2,315)=4.279, p=0.015*
10	All	F(2,406)=1.028, p=0.359	F(1,406)=0.573, p=0.450	F(2,406)=1.119, p=0.328
	CF<20 kHz			

	CF>=20 kHz	F(2,159)=1.952, p=0.145 F(2,314)=1.224, p=0.296	F(2,159)=2.046, p=0.155 F(2,314)=0.641, p=0.424	F(2,159)=0.337, p=0.715 F(2,314)=2.351, p=0.097
20	All CF<20 kHz CF>=20 kHz	F(2,415)=0.733, p=0.481 F(2,159)=2.732, p=0.068 F(2,314)=0.334, p=0.717	F(1,415)=5.389, p=0.021* F(1,159)=5.786, p=0.017* F(1,314)=2.600, p=0.108	F(2, 415)=4.455, p=0.012* F(2,159)=1.389, p=0.252 F(2,314)=11.143, p<0.0001*
50	All CF<20 kHz CF>=20 kHz	F(2,414)=1.538, p=0.216 F(2,159)=1.778, p=0.172 F(2,315)=1.387, p=0.251	F(1,414)=16.72, p<0.0001* F(2,159)=5.013, p=0.027* F(2,315)=11.473, p=0.001*	F(2,414)=3.378, p=0.035* F(2,159)=1.008, p=0.367 F(2,315)=6.064, p=0.003*
100	All CF<20 kHz CF>=20 kHz	F(2,410)= 2.704,P=0.068 F(2,159)=3.724, p=0.026* F(2,293)=2.813, p=0.062	F(1,410)=6.729, P=0.010* F(2,159)=6.828, p=0.010* F(1,293)=1.760, p=0.186	F(2,410)=1.292, P=0.276 F(2,159)=0.367, p=0.693 F(2,293)=1.599, p=0.204

200	All	F(2,401)=2.282, p=0.103	F(2,401)=1.845, p=0.175	F(2,401)=0.262, p=0.770
	CF<20 kHz	F(2,159)=5.217, p=0.023*	F(2, 159)=5.217, p=0.024*	F(2,159)=0.413, p=0.663
	CF>=20 kHz	F(2,314)=1.709, p=0.183	F(1,314)=0.348, p=0.556	F(2,314)=1.52, p=0.220

Table 3: tMTF, *= $p < 0.05$

Modulation Frequency (Hz)	CF Frequency	Genotype x Age Interaction	Main effect of Genotype	Main effect of Age
5	All CF	F(2,390)=0.127, p=0.881	F(2,390)=2.872, p=0.091	F(2,390)=0.354, p=0.702
	CF<20 kHz	F(2,137)=0.159 p=0.853	F(1,137)=0.472, p=0.493	F(2,137)=0.275, p=0.760
	CF>=20 kHz	F(2,242)=0.052, p=0.949	F(1,242)=2.777, p=0.097	F(2,242)=1.050, p=0.351
10	All CF	F(2,383)=1.989, p=0.138	F(1,383)=4.912, p=0.027*	F(2,383)=2.001, p=0.137
	CF<20 kHz	F(2,136)=0.905, p=0.407	F(1,136)=0.759, p=0.385	F(2,136)=3.110, p=0.048*
	CF>=20 kHz	F(2,235)=1.386, p=0.252	F(1,235)=4.241, p=0.041*	F(2,235)=0.695, p=0.500
20	All CF	F(2,387)=2.353, p=0.096	F(2,387)=1.702, p=0.193	F(2,387)=4.997, p=0.007*
	CF<20 kHz	F(2,135)=0.887, p=0.414	F(1,135)=1.069, p=0.303	F(2,135)=3.287, p=0.040*
	CF>=20 kHz	F(2,240)=2.087, p=0.126	F(1,240)=0.599, p=0.440	F(2,240)=1.734, p=0.179
50	All CF	F(2,382)=2.058, p=0.129	F(1,382)=0.752, p=0.386	F(2,382)=0.609, p=0.544

	CF<20 kHz CF>=20 kHz	F(2,129)=0.918, p=0.402 F(2,241)=0.819, p=0.442	F(1,129)=0.226, p=0.636 F(1,241)=0.08, p=0.778	F(2,129)=0.836, p=0.436 F(2,241)=1.173, p=0.311
100	All CF CF<20 kHz CF>=20 kHz	F(2,388)=0.153, p=0.858 F(2,130)=0.502, p=0.607 F(2,248)=0.356, p=0.701	F(1,388)=0.061, p=0.804 F(1,130)=1.124, p=0.291 F(1,248)=0.119, p=0.731	F(2,388)=22.195, p<0.0001* F(2,130)=8.009, p=0.001 F(2,248)=12.587, p<0.0001*
200	All CF CF<20 kHz CF>=20 kHz	F(2,352)=1.356, p=0.259 F(2,120)=0.433, p=0.650 F(2,222)=1.738, p=0.178	F(1,352)=0.932, p=0.335 F(2,120)=0.027, p=0.870 F(1,222)1.245, p=0.266	F(2,352)=9.349, p=0.0001* F(2,120)=4.008, p=0.021* F(2,222)=4.665)=0.010*

Table 4: Statistical analysis of individual age group. After correction for multiple comparisons, *= $p < 0.016$.

		P14	P21	P34
Minimum Threshold	All CF	t(156)=0.054, p=0.957	t(162)=-0.730, p=0.466	t(183)=3.249, p=0.001*
	CF<20 kHz	t(67)=0.491, p=0.625	t(49)=0.204, p=0.839	t(48)=0.428, p=0.046
	CF>=20 kHz	t(87)=1.331, p=0.187	t(111)=0.424, p=0.672	t(133)=2.584, p=0.011*
Spontaneous Activity	All CF	t(157)=0.155, p=0.857	t(158)=-1.778, p=0.077	t(183)=-1.430, p=0.155
	CF<20 kHz	t(70)=1.084, p=0.282	t(49)=-2.410, p=0.020	t(48)=-2.217, p=0.031
	CF>=20 kHz	t(88)=-0.439, p=0.662	t(111)=-0.808, p=0.421	t(134)=-0.470, p=0.639
15 dB Above Threshold Magnitude	All CF	t(154)=-0.150, p=0.881	t(160)=-2.452, p=0.015*	t(167)=-1.233, p=0.219
	CF<20 kHz	t(66)=-1.914, p=0.060	t(46)=-2.036, p=0.048	t(45)=-2.884, p=0.006*
	CF>=20 kHz	t(86)=1.301, p=0.197	t(110)-1.292, p=0.199	t(120)=-0.087, p=0.931
30 dB Above Threshold Magnitude	All CF	t(152)=0.731, p=0.466	t(158)=-3.312, p=0.001*	t(167)=-1.173, p=0.242
	CF<20 kHz	t(66)=-1.332, p=0.187	t(43)=-3.353, p=0.002*	t(46)=-2.725, p=0.009*
	CF>=20 kHz	t(85)=2.058, p=0.043	t(110)=-2.484, p=0.015*	t(119)=-0.244, p=0.808
15 dB Above Threshold Latency	All CF	t(154)=-0.787, p=0.432	t(157)=0.597, p=0.551	t(166)=-1.477, p=0.142
	CF<20 kHz	t(69)=-2.184, p=0.032	t(48)=-1.759, p=0.085	t(46)=-0.498, p=0.621

	CF>=20 kHz	t(86)=-0.629, p=0.531	t(109)=-1.751, p=0.083	t(120)=-1.213, p=0.228
30 dB Above Threshold Latency	All CF	t(152)=-0.400, p=0.690	t(157)=-0.811, p=0.419	t(166)=-0.413, p=0.680
	CF<20 kHz	t(66)=-1.960, p=0.054	t(30)=-1.433, p=0.162	t(47)=0.165, p=0.870
	CF>=20 kHz	t(84)=-0.039, p=0.969	t(109)=-0.526, p=0.600	t(316)=-1.680, p=0.094
BW10	All CF	t(154)=-0.064, p=0.949	t(156)=0.083, p=0.934	t(111)=1.956, p=0.053
	CF<20 kHz	t(46)=-1.044, p=0.302	t(42)=-2.819, p=0.007*	t(30)=0.05, p=0.960
	CF>=20 kHz	t(30)=-1.099, p=0.280	t(72)=-0.990, p=0.326	t(79)=2.120, p=0.037
BW20	All CF	t(153)=-1.310, p=0.192	t(155)=-0.679, p=0.498	t(182)=.1.803, p=0.073
	CF<20 kHz	t(46)=-0.887, p=0.380	t(42)=-2.041, p=0.048	t(30)=-1.311, p=0.200
	CF>=20 kHz	t(31)=-0.828, p=0.414	t(72)=-1.159, p=0.250	t(79)-0.071, p=0.944
BW30	All CF	t(146)=-1.289, p=0.199	t(156)=-1.136, p=0.258	t(172)=-0.458, p=0.647
	CF<20 kHz	t(44)=-0.811, p=0.422	t(42)=-1.617, p=0.113	t(30)=-1.609, p=0.118
	CF>=20 kHz	t(29)=-1.197, p=0.241	t(72)=0.381, p=0.704	t(79)=0.282, p=0.778
Percent TO	All CF	t(157)=-0.426, p=0.670	t(159)=0.979, p=0.329	t(166)=1.247, p=0.214
	CF<20 kHz	t(68)=-0.25, p=0.804	t(47)=0.985, p=0.330	t(46)=0.876, p=0.386

	CF>=20 kHz	t(87)=-1.124, p=0.264	t(110)=0.298, p=0.767	t(133)=-3.063, p=0.003*
Dynamic Range	All CF	t(154)=0.74, p=0.461	t(151)=-1.343, p=0.181	t(51)=1.243, p=0.219
	CF<20 kHz	t(65)=-0.884, p=0.38	t(46)=-1.781, p=0.081	t(16)=1.892, p=0.077
	CF>=20 kHz	t(87)=1.412, p=0.161	t(103)=-1.095, p=0.276	t(33)=-0.386, p=0.702

Table 5: Statistical analysis of rMTF at individual age group. After correction for multiple comparisons, *= p < 0.016.

Modulation Frequency (Hz)	CF Frequency	P14	P21	P34
5	All	t(146)=0.687, p=0.493	t(145)=-1.888, p=0.061	t(121)=-1.612, p=0.110
	CF<20 kHz	t(67)=-0.487, p=0.628	t(47)=-1.076, p=0.288	t(45)=-3.065, p=0.004*
	CF>=20 kHz	t(87)=1.378, p=0.172	t(110)=-1.983, p=0.05	t(118)=-0.716, p=0.475
10	All	t(147)=0.132, p=0.557	t(142)=-1.870, p=0.064	t(117)=-0.451, p=0.653
	CF<20 kHz	t(67)=0.649, p=0.518	t(47)=1.161, p=0.251	t(45)=-2.632, p=0.012*
	CF>=20 kHz	t(87)=0.119, p=0.906	t(110)=-1.998, p=0.048	t(117)=0.188, p=0.851
20	All	t(147)=-0.542, p=0.589	t(145)=-1.823, p=0.070	t(123)=-1.656, p=0.1
	CF<20 kHz	t(67)=0.594, p=0.554	t(47)=-1.636, p=0.108	t(45)=-3.128, p=0.003*
	CF>=20 kHz	t(87)=-0.452, p=0.653	t(110)=-1.664, p=0.099	t(117)=-0.779, p=0.437
50	All	t(144)=-1.398, p=0.164	t(143)=-3.51, p=0.001*	t(127)=-2.131, p=0.035

	CF<20 kHz	t(67)=0.103, p=0.918	t(47)=-1.245, p=0.219	t(45)=-2.875, p=0.006*
	CF>=20 kHz	t(87)=-0.969, p=0.335	t(110)=-3.22, p=0.002*	t(118)=-1.733, p=0.086
100	All	t(143)=0.404, p=0.687	t(141)=-2.61, p=0.010*	t(125)=-1.545, p=0.125
	CF<20 kHz	t(67)=0.783, p=0.436	t(47)=-1.474, p=0.147	t(45)=-2.831, p=0.007*
	CF>=20 kHz	t(64)=1.327, p=0.189	t(110)=-2.331, p=0.022	t(119)=-1.416, p=0.160
200	All	t(140)=1.057, p=0.292	t(146)=-1.482, p=0.141	t(115)=-1.633, p=0.105
	CF<20 kHz	t(67)=1.007, p=0.317	t(47)=-1.040, p=0.304	t(45)=-3.520, p=0.001*
	CF>=20 kHz	t(87)=0.920, p=0.360	t(110)=-1.718, p=0.089	t(117)=-0.515, p=0.608

Table 6: Statistical analysis of tMTF at individual age group. After correction for multiple comparisons, *= p < 0.016.

Modulation Frequency (Hz)	CF Frequency	P14	P21	P34
5	All	t(142)=1.081, p=0.282	t(139)=0.651, p=0.516	t(109)=1.143, p=0.255
	CF<20 kHz	t(61)=0.382, p=0.704	t(42)=0.019, p=0.985	t(34)=0.701, p=0.488
	CF>=20 kHz	t(78)=0.906, p=0.368	t(92)=0.842, p=0.402	t(72)=1.098, p=0.276
10	All	t(142)=-0.328, p=0.743	t(135)=1.759, p=0.081	t(107)=2.191, p=0.031
	CF<20 kHz	t(60)=-0.459, p=0.648	t(40)=0.396, p=0.694	t(36)=1.503, p=0.142
	CF>=20 kHz	t(78)=-0.178, p=0.859	t(89)=1.645, p=0.103	t(68)=1.797, p=0.077
20	All	t(141)=-1.017, p=0.311	t(136)=1.781, p=0.077	t(110)=1.334, p=0.185
	CF<20 kHz	t(59)=-0.238, p=0.813	t(42)=1.361, p=0.181	t(34)=0.444, p=0.660
	CF>=20 kHz	t(79)=-1.246, p=0.216	t(88)=1.297, p=0.198	t(73)=1.24, p=0.219
50	All	t(141)=-1.474, p=0.143	t(136)=-1.54, p=0.125	t(105)=1.0, p=0.319

	CF<20 kHz CF>=20 kHz	t(56)=-1.045, p=0.300 t(82)=-0.895, p=0.373	t(42)=-0.86, p=0.395 t(88)=-0.668, p=0.506	t(31)=0.765, p=0.450 t(71)=0.722, p=0.473
100	All CF<20 kHz CF>=20 kHz	t(140)=-0.208, p=0.836 t(57)=0.193, p=0.847 t(80)=0.052, p=0.959	t(135)=0.048, p=0.962 t(41)=0.180, p=0.858 t(90)=0.873, p=0.385	t(113)=0.583, p=0.561 t(32)=1.441, p=0.159 t(78)=-0.308, p=0.759
200	All CF<20 kHz CF>=20 kHz	t(127)=-0.747, p=0.456 t(54)=0.234, p=0.816 t(70)=-0.981, p=0.330	t(130)=0.524, p=0.601 t(38)=-0.769, p=0.447 t(88)=1.203, p=0.232	t(95)=1.536, p=0.128 t(28)=0.321, p=0.751 t(64)=1.507, p=0.137

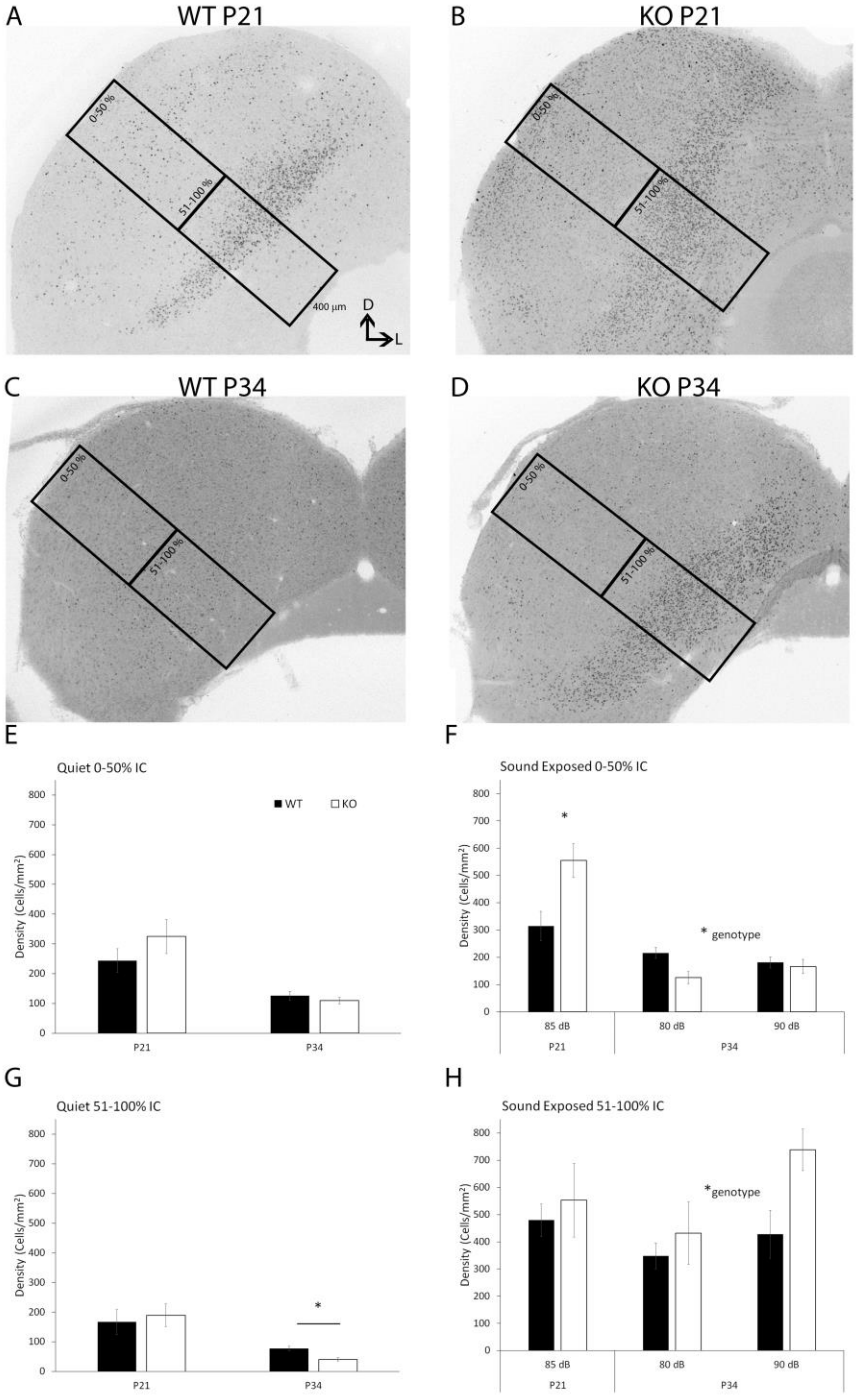

Figure 1: cFos expression is increased in the inferior colliculus of *Fmr1* KO mice. (A-B) Example photomicrograph at P34 with 90 dB sound exposure of WT (A) and *Fmr1* KO (B) WT mouse. Rectangular box shows counting window of 400 µm width that spans the IC in a dorsolateral to medioventral direction. (E) Density of cFos expressing cells within 0-50% depth of counting

window in panel (A-D). (E) Quiet group for the 0-50% depth of the IC. There was no significant differences between WT and KO for both ages. (F) In the sound-exposed group for the 0-50% depth, there was a significant increase in KO cFos density at P21 (p=0.010) and a genotype effect at P34 (p=0.028). (G) Quiet 51-100% region, there was a significant decrease in cFos density at P34 (p=0.004). (H) For sound exposed, there was an increased cFos expression in the 90 dB compared to 80 dB sound level (p=0.034) and a significant increase cFos density in KO compared to WT (p=0.030). Scale bar = 100 μm. Error bars shows STD Error.

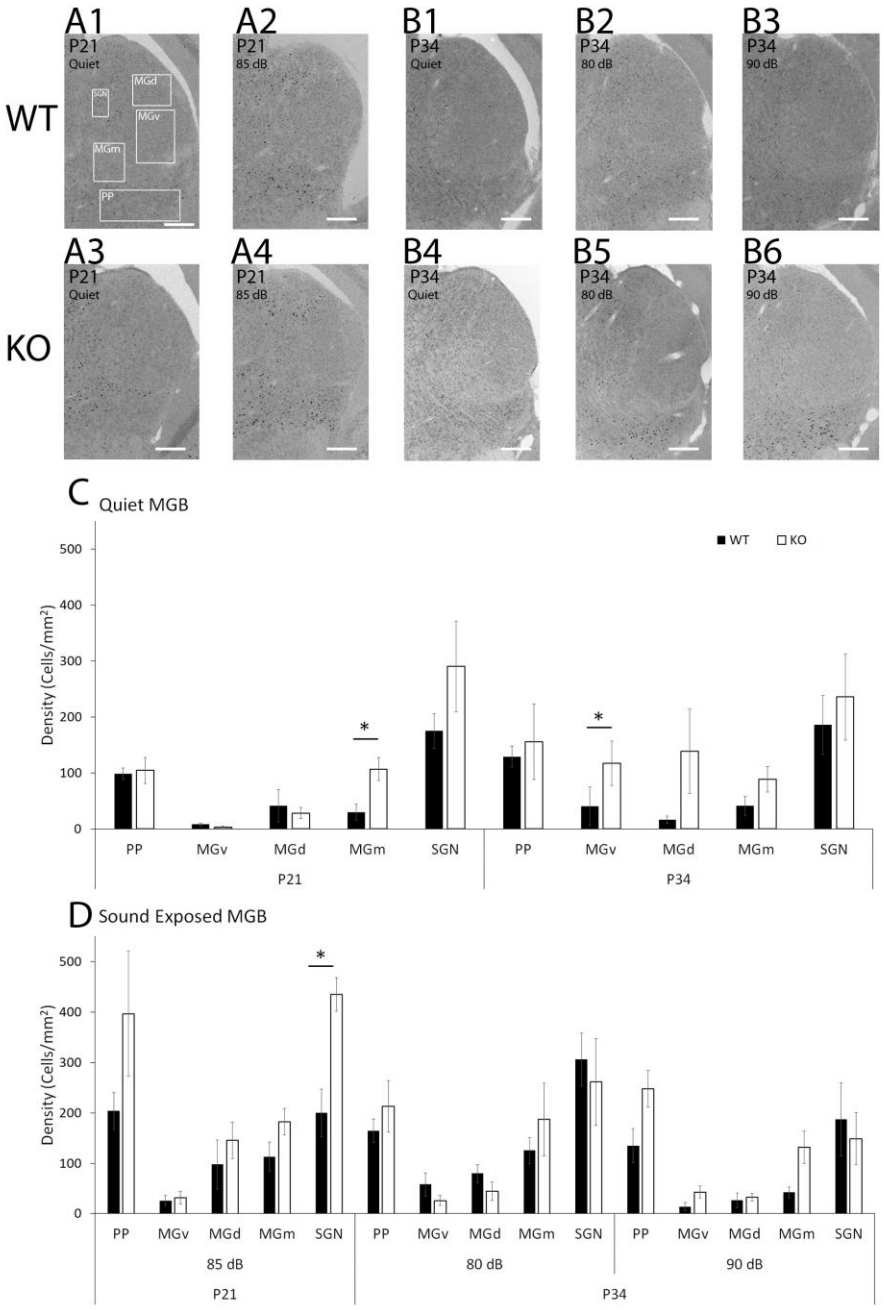

Figure 2: cFos expression in the medial geniculate body (MGB) show sub-division specific genotype differences. (A-B) Example photomicrographs of sections in the MGB (top row: WT, bottom row: KO). (A1-A4) Quiet and 85 dB sound exposure conditions at P21. (B1-B6) Quiet and sound-exposed (80 dB and 90 dB) conditions at P34. (C) Quiet group at P21 and P34. At P21, there is a significant increase in cFos density in the MGm subnuclei (p=0.008), there was no significance in all other subnuclei. For the P34 group, there was a significant increase in cFos density in the MGv subnuclei (U=8, p=0.01), there was no significance in all other subnuclei. (D)

Sound-exposed groups at P21 and P34. At P21 there was a significant increase in cFos density in the KO compared to the WT group in the SGN (p=0.001). At P34, there was a significant sound level x genotype interaction (p=0.038) in the MGV and an increase in cFos density in KO compared to WT in the MGd (p=0.025). Scale bar=200 μm. Error bars show STD Error.

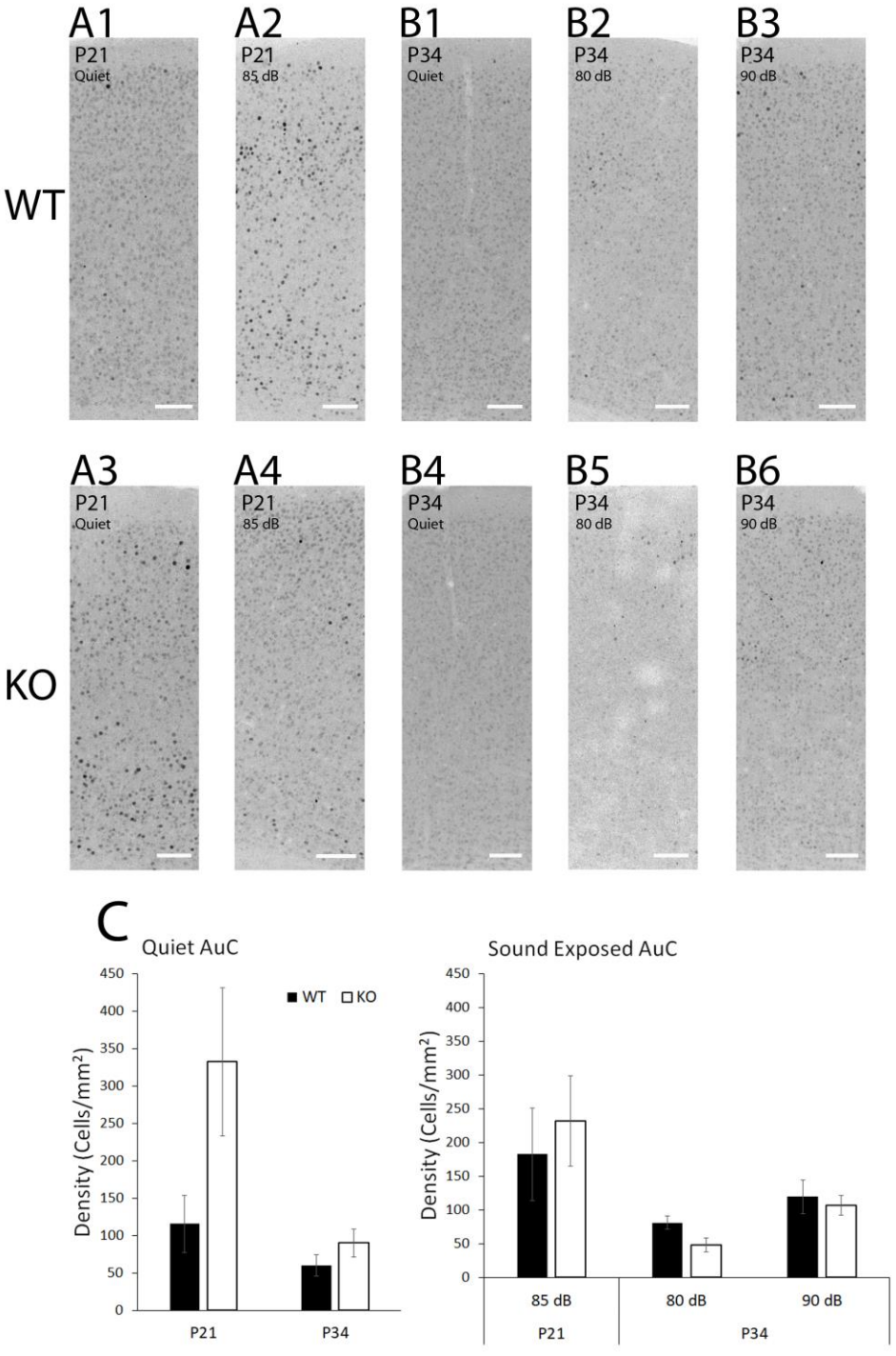

Figure 3: cFos expression in the auditory cortex. (A-B) Example photomicrograph across cortical layers I-VI, top row indicates WT and bottom row indicates KO. (A1-A4) Group P21 and (B1-B6) group P34 of quiet and noise exposed conditions. (C) In quiet condition, there was no significant differences between KO and WT at both age groups. At sound-exposed condition in the P34

group, there was an increase in cFos density at 90 dB compared to 80 dB sound level (p=0.007). Scale bar=100 µm. Error bars shows STD Error.

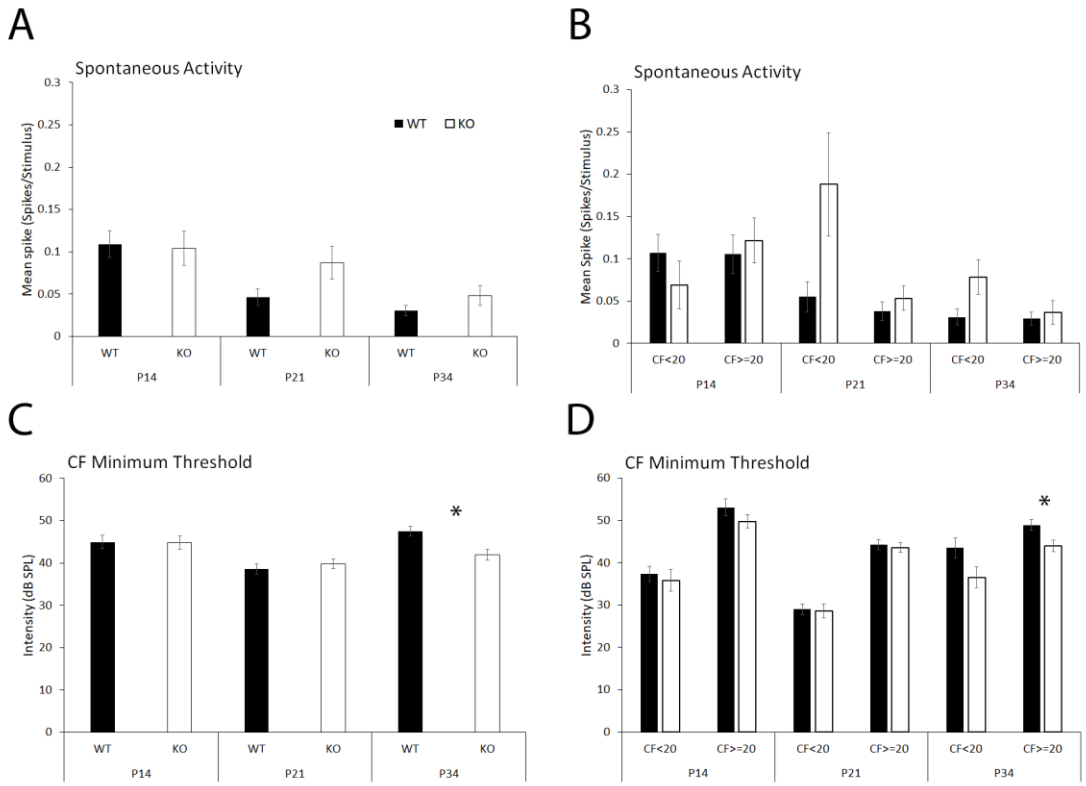

Figure 4: (A) Spontaneous activity for neurons at P14, P21, and P34. In general there was very little spontaneous activity in the IC. A two-way ANOVA (age and genotype as factors) shows a main effect of age (p=0.000018). (B) For neurons with CF under 20 kHz (CF<20 kHz), two-way ANOVA revealed significant interaction between genotype x age (p=0.008) and significant main effects of genotype but no significant main effects of age, (Genotype: p=0.04, Age: p=0.08). For neurons with CF over or equal to 20 kHz (CF>=20 kHz), there was no significant genotype x age interaction or main effects of genotype (p=0.949, p=0.335, respectively); however, there is a significant main effect of age (p=0.000004). (C) The average minimum threshold at CF for neurons in IC showed no main effects of genotype (p=0.176). There was a significant interaction between genotype x age and main effect of age (p=0.023, p=0.000012, respectively). (D) For neurons CF<20 kHz, there was no significant genotype x age interaction nor main effect of genotype (p=0.282, p=0.09, respectively); but there was a significant main effect of age (p=0.000004). For neurons CF>=20 kHz, there was no significant interaction between genotype x age (p=0.299); however, there was a significant main effect for both genotype and age (p=0.000005). Error bars shows STD Error.

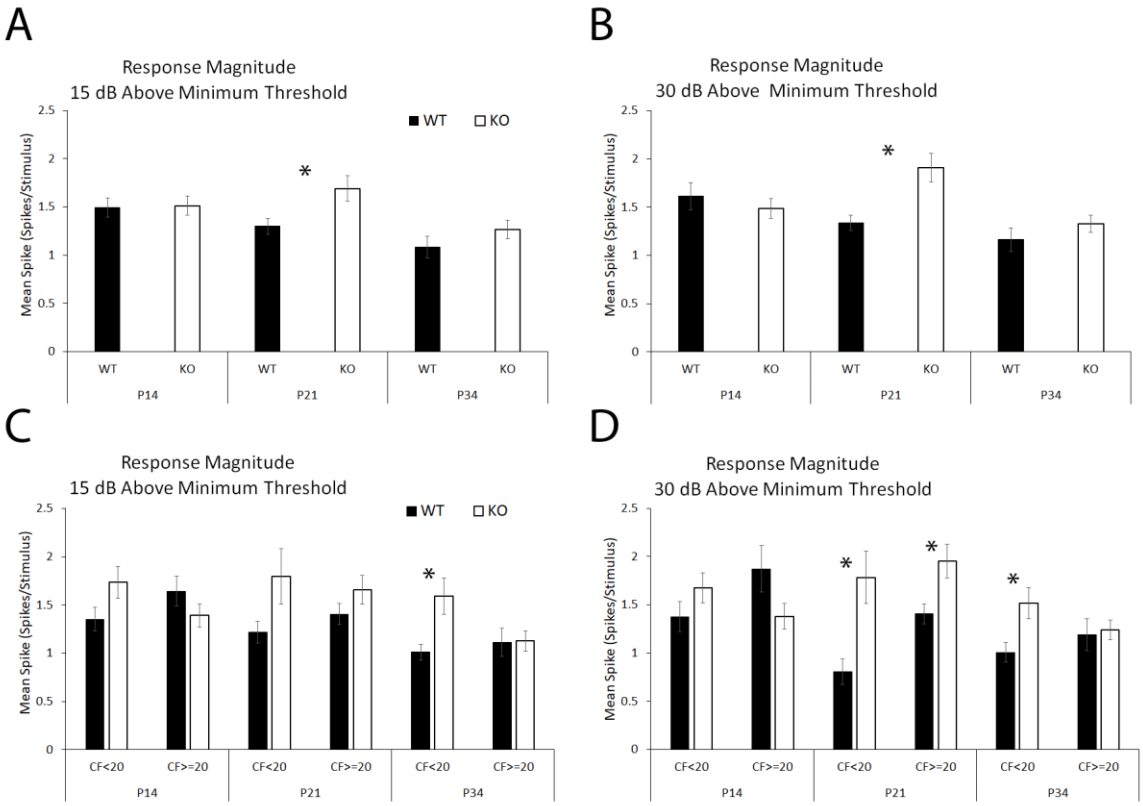

Figure 5: Response magnitude for neurons at 15 dB and 30 dB above minimum threshold. (A) All neurons at 15 dB above minimum threshold for responses during stimulus duration (0-50 msec). There was a significant main effect of genotype and age (p=0.022, p=0.002, respectively), but no significant interaction between genotype x age (p=0.225). (B) All neurons at 30 dB above minimum threshold for responses during stimulus presentation (0-50 msec). There was a significant interaction between genotype x age (p=0.014), main effect of genotype (p=0.029), and main effect of age (p=0.002). (C) Response magnitude at 15 dB above minimum threshold for neurons with CF<20 kHz and neurons with CF>= 20 kHz. For neurons with CF<20 kHz, there was no significant genotype x age interaction (p=0.759) and main effect of age (p=0.288) but a significant main effect of genotype (p=0.00016). For neurons with CF>=20 kHz, there was a significant main effect of age (p=0.002). But no significant genotype x age interaction (p=0.217) and main effect of genotype (p=0.968). (D) Response magnitude at 30 dB above minimum threshold for neurons with CF<20 kHz and neurons with CF>= 20 kHz. For CF<20 kHz, there was no significant interaction between genotype x age (p=0.124) and main effect of age (p=0.2), but there was a significant main effect of genotype (p=0.000030). For CF>=20 kHz, there was a significant interaction between genotype x age (p=0.006) and main effect of age (p=0.005), but there was no significant main effect of genotype (p=0.840).

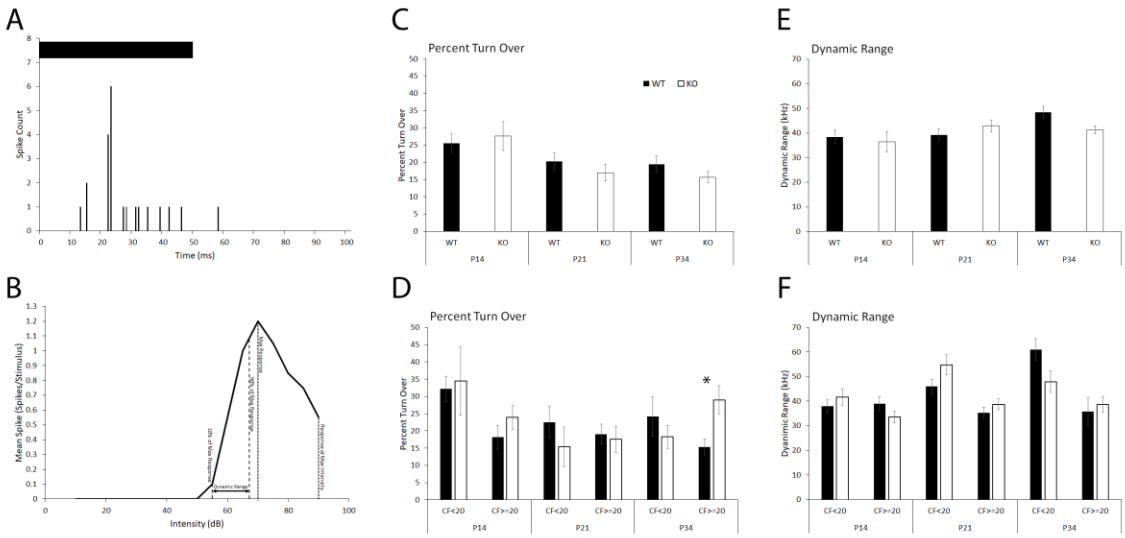

Figure 6: (A) Post-stimulus time histogram of a one IC neuron's response to a 50 msec CF tone (20 repetitions) from a P21 WT animal. Sound onset is at 0 msec and the horizontal black bar indicates tone duration. (B) Example of a rate level function of a P21 WT IC neuron. Vertical dashed lines from left to right indicate sound level for 10% of maximum response, 90% of maximum response, maximum response, and response at highest sound level tested. Dynamic range was defined as 10% to 90% of the maximum response (horizontal arrow bar shows dynamic range). %TO was defined as the maximum response subtracted by the response at the highest intensity level divided by the maximum response. (C) For %TO, there was no significant genotype x age interaction (p=0.489), nor main effect of genotype (p=0.455); however, there was a main effect of age (p=0.002). (D) When the data was split between CF<20 kHz and CF>=20 kHz, there was a main effect of age (p=0.029), and no significant interaction between genotype x age (p=0.668), nor genotype (p=0.473) for neurons CF<20 kHz. For neurons CF>=20 kHz, there was no significant genotype x age interaction (p=0.068) and main effect of age (p=0.483); but there was a main effect of genotype (p=0.037). (E, F) Dynamic range of neurons showed a main effect of age (p=0.031) but no significant genotype x age interaction (p=0.146) nor main effect of genotype (p=0.439). (F) For CF<20 kHz, there was a significant main effect of age (p=0.000452); however, there was no significant main effect of genotype (p=0.959) or genotype x age interaction (p=0.077).

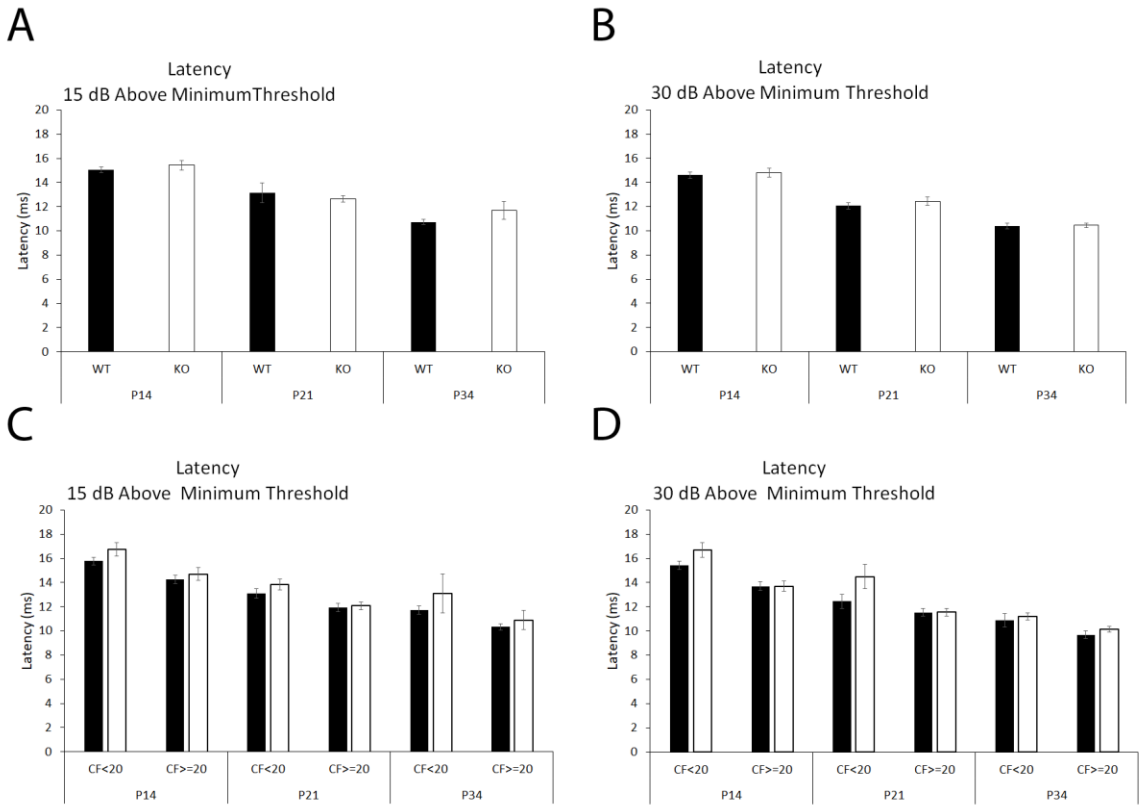

Figure 7: Median first spike latency for neuronal response to stimuli. (A) For all neurons at latency 15 dB above minimum threshold, there was no significant interaction between genotype x age (p=0.284), nor main effect of genotype (p=0.434), but there was a significant main effect of age (p<0.0001). (B) In addition, for all neurons at latency 30 dB above minimum threshold, there was no significant interaction between genotype x age (p=0.917), and main effect of genotype (p=0.342), but a significant main effect of age (p<0.0001). (C) Median first spike latency for neurons 15 dB above minimum threshold separated by neurons with CF<20 kHz and neurons with CF>=20 kHz. There was no significant interaction between genotype x age (p=0.743), but there was a significant main effect of genotype (p=0.029), and main effect of age (p<0.0001) for neurons CF<20 kHz. For neurons CF>=20 kHz, there was a significant main effect of age (p<0.001), but no significance in genotype x age interaction and main effect of genotype (p=0.878, p=0.065, respectively). (D) Median first spike latency for neurons 30 dB above minimum threshold. For CF<20 kHz, there was significant main effect of genotype and age (p=0.044, p<0.0001, respectively), but no significant in interaction of genotype x age (p=0.249). For CF>=20 kHz, there was a significant main effect of age (p<0.0001); but no significant main effect of genotype (p=0.615) and genotype x age interaction (p=0.956). Error bars shows STD Error.

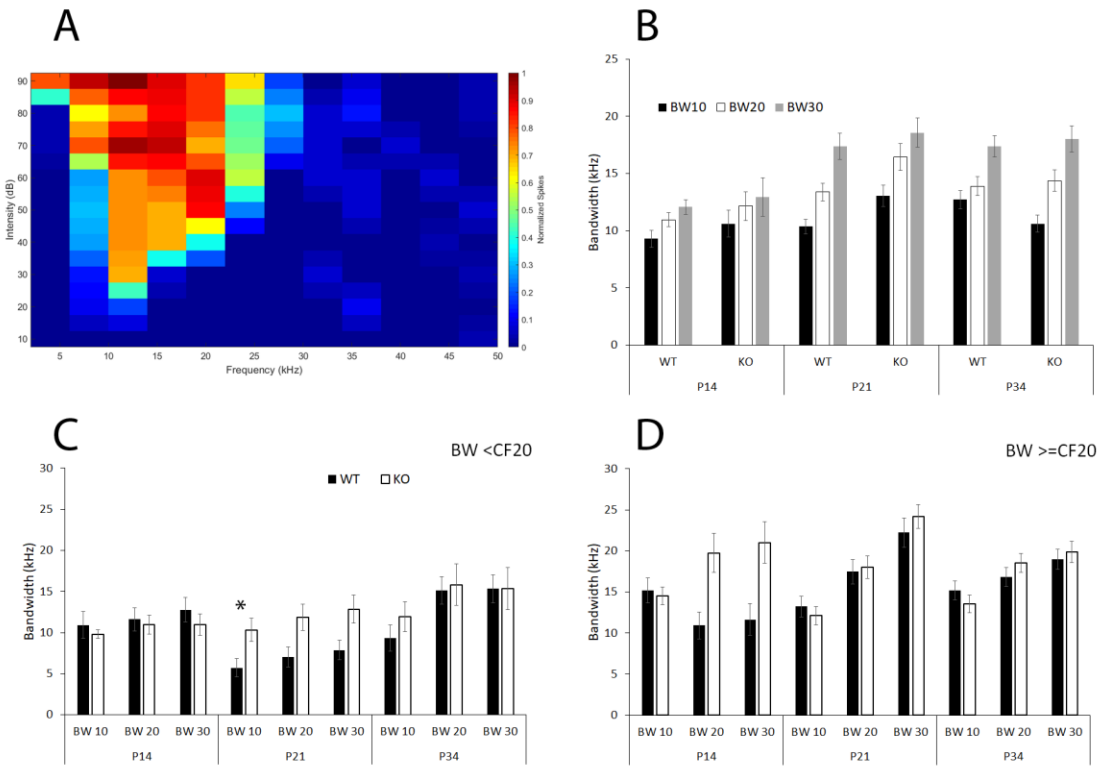

Figure 8: (A) An example of one neuron's frequency response area. (B) For neurons with all CFs combined, there was a significant interaction for BW10 (p=0.008), but not for BW20 (p=0.336) and BW30 (p=0.968). There was no significant main effect of genotype for BW10 (p=0.410), but significant for BW20 (p=0.048), but not significant for BW30 (p=0.354). For the main effect of age, there was no significant difference for BW10 (p=0.079), but there was a significant effect for BW20 (p=0.003), and BW30 (p<0.0001). (C) Bandwidth of 10 dB, 20 dB, and 30 dB above minimum threshold at CF. For CF<20 kHz, there was a significant main effect of genotype (BW10 (: *p*=0.039), BW20 (*p*=0.017), BW30 (*p*=0.018)); however, there was no genotype x age interaction (BW10 (*p*=0.175), BW20 (*p*=0.616), BW30 (*p*=0.68)) nor main effect of age (BW10 (*p*=0.944), BW20 (*p*=0.515), BW30 (*p*=0.288)). (D) For CF>=20 kHz, there was a significant interaction for BW10 (*p*=0.04) but no significant main effect of genotype (*p*=0.726) and age (*p*=0.499). All others are not significant for BW20 (Genotype x age: *p*=0.609, Genotype: *p*=0.271, Age: *p*=0.077) and BW30 (Genotype x age: *p*=0.497, Genotype: *p*=0.636, Age: *p*=0.20). Error bars shows STD Error.

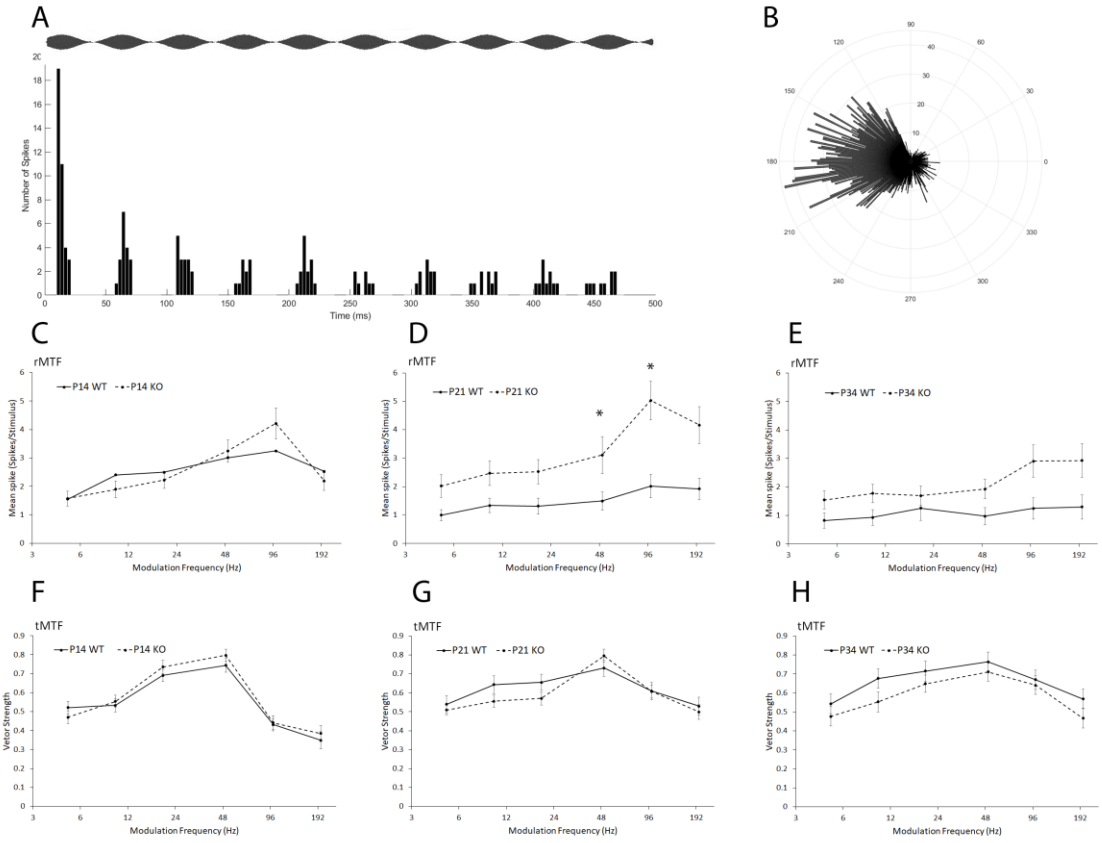

Figure 9: (A) Example of a P14 WT neuronal response to sinusoidal amplitude modulated sound at 20 Hz modulation. (B) Polar plot example of spikes of a P14 WT neuron at 20 Hz modulation along the period of the stimulus. (C-E) rMTF of P14, P21, and P34 group, respectively. (F-H) tMTF of P14, P21, and P34 group, respectively. Dashed lines indicate KO groups and solid lines indicate WT groups.

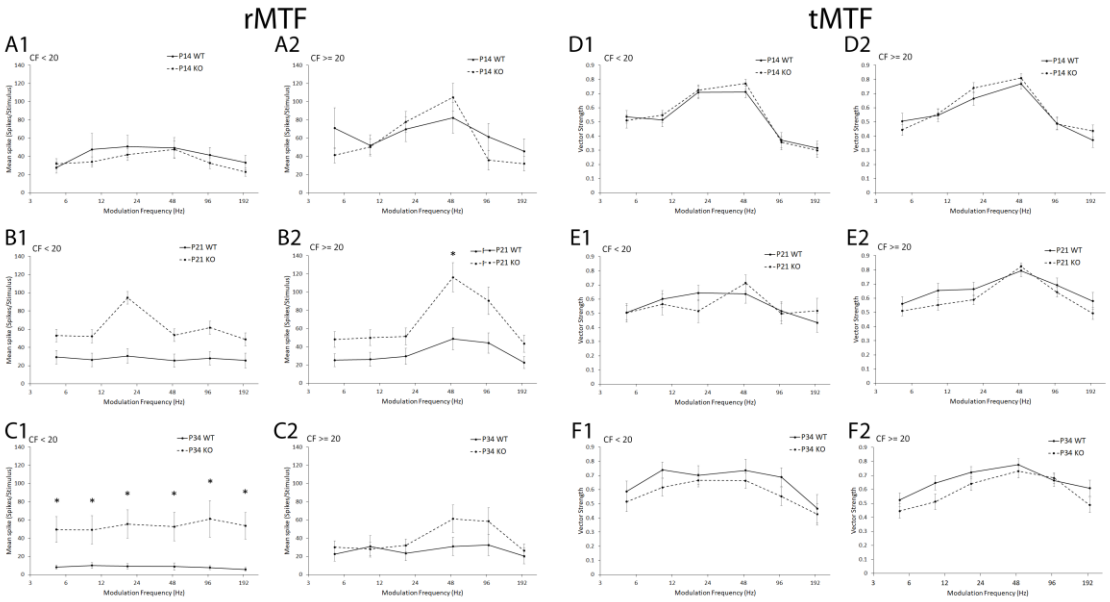

Figure 10: rMTF and tMTF subdivided into neurons with CF<20 kHz and CF>=20 kHz. The left two columns are rMTF (A-C) and the right two columns are tMTF (D-F).

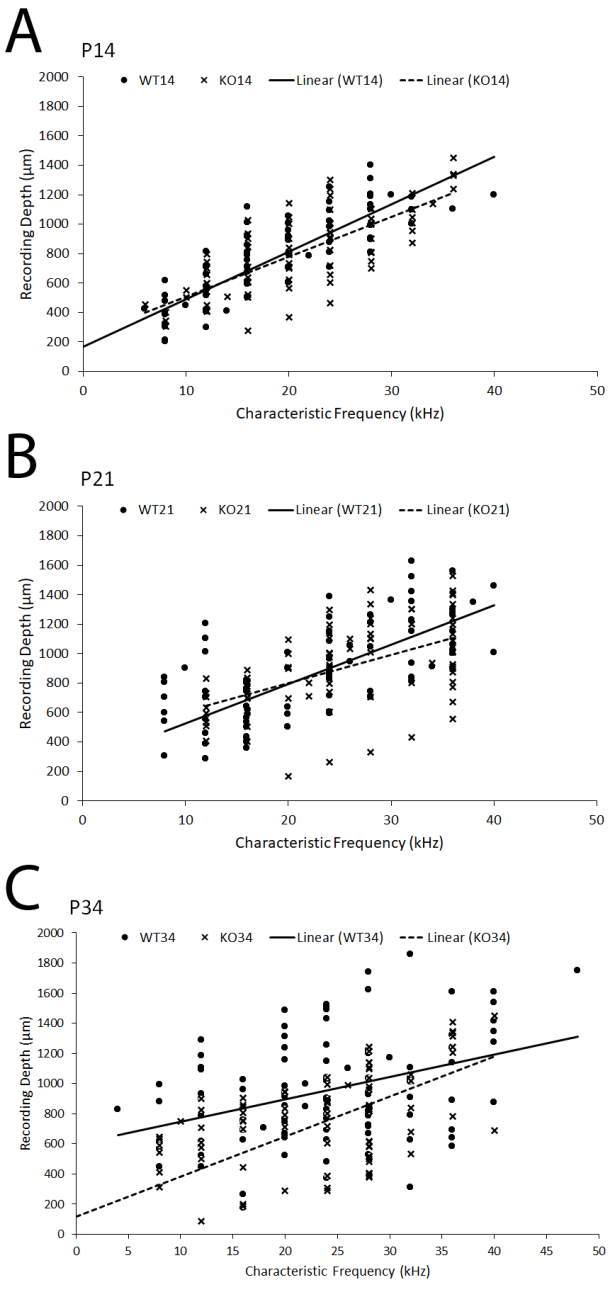

Figure 11: Distribution of CF along recording depth in the IC. There is no significant differences between WT and KO at each age group P14 (A), P21 (B), and P34 (C).

References

Arnault, P., and Roger, M. (1987). The connection of the peripeduncular area studied by retrograde and anterograde transport in the rat. J. Comp. Neurol. *258*, 463–476.

Bakker, C.E., and Oostra, B.A. (2003). Understanding fragile X syndrome: insights from animal models. Cytogenet. Genome Res. *100*, 111–123.

Beebe, K., Wang, Y., and Kulesza, R. (2014). Distribution of fragile X mental retardation protein in the human auditory brainstem. Neuroscience *273*, 79–91.

Beebe, N.L., Young, J.W., Mellott, J.G., and Schofield, B.R. (2016). Extracellular Molecular Markers and Soma Size of Inhibitory Neurons: Evidence for Four Subtypes of GABAergic Cells in the Inferior Colliculus. J. Neurosci. *36*, 3988–3999.

Brown, M.R., Kronengold, J., Gazula, V.-R., Chen, Y., Strumbos, J.G., Sigworth, F.J., Navaratnam, D., and Kaczmarek, L.K. (2010). Fragile X mental retardation protein controls gating of the sodium-activated potassium channel Slack. Nat. Neurosci. *13*, 819–821.

Castrén, M., Pääkkönen, A., Tarkka, I.M., Ryynänen, M., and Partanen, J. (2003). Augmentation of Auditory N1 in Children with Fragile X Syndrome. Brain Topogr. *15*, 165–171.

Choy Buentello, D., Bishop, D.C., and Oliver, D.L. (2015). Differential distribution of GABA and glycine terminals in the inferior colliculus of rat and mouse. J. Comp. Neurol. *523*, 2683–2697.

Curia, G., Papouin, T., Séguéla, P., and Avoli, M. (2009). Downregulation of tonic GABAergic inhibition in a mouse model of fragile X syndrome. Cereb. Cortex N. Y. N 1991 *19*, 1515–1520.

D'Hulst, C., De Geest, N., Reeve, S.P., Van Dam, D., De Deyn, P.P., Hassan, B.A., and Kooy, R.F. (2006). Decreased expression of the GABAA receptor in fragile X syndrome. Brain Res. *1121*, 238–245.

Dölen, G., Osterweil, E., Rao, B.S.S., Smith, G.B., Auerbach, B.D., Chattarji, S., and Bear, M.F. (2007). Correction of Fragile X Syndrome in Mice. Neuron *56*, 955–962.

Ethridge, L.E., White, S.P., Mosconi, M.W., Wang, J., Pedapati, E.V., Erickson, C.A., Byerly, M.J., and Sweeney, J.A. (2017). Neural synchronization deficits linked to cortical hyper-excitability and auditory hypersensitivity in fragile X syndrome. Mol. Autism *8*, 22.

Faingold, C.L. (2002). Role of GABA abnormalities in the inferior colliculus pathophysiology – audiogenic seizures. Hear. Res. *168*, 223–237.

Faingold, C.L., and Randall, M.E. (1999). Neurons in the deep layers of superior colliculus play a critical role in the neuronal network for audiogenic seizures: mechanisms for production of wild running behavior. Brain Res. *815*, 250–258.

Felix, R.A., and Portfors, C.V. (2007). Excitatory, inhibitory and facilitatory frequency response areas in the inferior colliculus of hearing impaired mice. Hear. Res. *228*, 212–229.

Garcia-Pino, E., Gessele, N., and Koch, U. (2017). Enhanced Excitatory Connectivity and Disturbed Sound Processing in the Auditory Brainstem of Fragile X Mice. J. Neurosci. *37*, 7403–7419.

Goldberg, J.M., and Brown, P.B. (1969). Response of binaural neurons of dog superior olivary complex to dichotic tonal stimuli: some physiological mechanisms of sound localization. J. Neurophysiol. *32*, 613–636.

Hitoglou, M., Ververi, A., Antoniadis, A., and Zafeiriou, D.I. (2010). Childhood Autism and Auditory System Abnormalities. Pediatr. Neurol. *42*, 309–314.

Kazdoba, T.M., Leach, P.T., Silverman, J.L., and Crawley, J.N. (2014). Modeling fragile X syndrome in the Fmr1 knockout mouse. Intractable Rare Dis. Res. *3*, 118–133.

Kokash, J., Alderson, E.M., Reinhard, S.M., Crawford, C.A., Binder, D.K., Ethell, I.M., and Razak, K.A. (2019). Genetic reduction of MMP-9 in the Fmr1 KO mouse partially rescues prepulse inhibition of acoustic startle response. Brain Res. *1719*, 24–29.

LeDoux, J.E., Farb, C.R., and Milner, T.A. (1991). Ultrastructure and synaptic associations of auditory thalamo-amygdala projections in the rat. Exp. Brain Res. *85*, 577–586.

Lovelace, J.W., Wen, T.H., Reinhard, S., Hsu, M.S., Sidhu, H., Ethell, I.M., Binder, D.K., and Razak, K.A. (2016). Matrix metalloproteinase-9 deletion rescues auditory evoked potential habituation deficit in a mouse model of Fragile X Syndrome. Neurobiol. Dis. *89*, 126–135.

Lovelace, J.W., Ethell, I.M., Binder, D.K., and Razak, K.A. (2018). Translation-relevant EEG phenotypes in a mouse model of Fragile X Syndrome. Neurobiol. Dis. *115*, 39–48.

Martin del Campo, H.N., Measor, K.R., and Razak, K.A. (2012). Parvalbumin immunoreactivity in the auditory cortex of a mouse model of presbycusis. Hear. Res. *294*, 31–39.

Merchán, M., Aguilar, L.A., Lopez-Poveda, E.A., and Malmierca, M.S. (2005). The inferior colliculus of the rat: quantitative immunocytochemical study of GABA and glycine. Neuroscience *136*, 907–925.

Michalon, A., Sidorov, M., Ballard, T.M., Ozmen, L., Spooren, W., Wettstein, J.G., Jaeschke, G., Bear, M.F., and Lindemann, L. (2012). Chronic Pharmacological mGlu5 Inhibition Corrects Fragile X in Adult Mice. Neuron *74*, 49–56.

Millan, M.H., Meldrum, B.S., and Faingold, C.L. (1986). Induction of audiogenic seizure susceptibility by focal infusion of excitant amino acid or bicuculline into the inferior colliculus of normal rats. Exp. Neurol. *91*, 634–639.

Musumeci, S.A., Bosco, P., Calabrese, G., Bakker, C., De Sarro, G.B., Elia, M., Ferri, R., and Oostra, B.A. (2000). Audiogenic seizures susceptibility in transgenic mice with fragile X syndrome. Epilepsia *41*, 19–23.

Musumeci, S.A., Calabrese, G., Bonaccorso, C.M., D'Antoni, S., Brouwer, J.R., Bakker, C.E., Elia, M., Ferri, R., Nelson, D.L., Oostra, B.A., et al. (2007). Audiogenic seizure susceptibility is reduced in fragile X knockout mice after introduction of FMR1 transgenes. Exp. Neurol. *203*, 233–240.

Oswald, A.-M.M., and Reyes, A.D. (2008). Maturation of intrinsic and synaptic properties of layer 2/3 pyramidal neurons in mouse auditory cortex. J. Neurophysiol. *99*, 2998–3008.

Oswald, A.-M.M., and Reyes, A.D. (2011). Development of Inhibitory Timescales in Auditory Cortex. Cereb. Cortex N. Y. NY *21*, 1351–1361.

Pacey, L.K.K., Heximer, S.P., and Hampson, D.R. (2009). Increased GABAB Receptor-Mediated Signaling Reduces the Susceptibility of Fragile X Knockout Mice to Audiogenic Seizures. Mol. Pharmacol. *76*, 18–24.

Palombi, P.S., and Caspary, D.M. (1996). GABA inputs control discharge rate primarily within frequency receptive fields of inferior colliculus neurons. J. Neurophysiol. *75*, 2211–2219.

Phillips, D.P., and Kelly, J.B. (1989). Coding of tone-pulse amplitude by single neurons in auditory cortex of albino rats (Rattus norvegicus). Hear. Res. *37*, 269–279.

Preibisch, S., Saalfeld, S., and Tomancak, P. (2009). Globally optimal stitching of tiled 3D microscopic image acquisitions. Bioinformatics *25*, 1463–1465.

Rais, M., Binder, D.K., Razak, K.A., and Ethell, I.M. (2018). Sensory Processing Phenotypes in Fragile X Syndrome. ASN Neuro *10*, 1759091418801092.

Rogers, S.J., Hepburn, S., and Wehner, E. (2003). Parent reports of sensory symptoms in toddlers with autism and those with other developmental disorders. J. Autism Dev. Disord. *33*, 631–642.

Romand, R., and Ehret, G. (1990). development of tonotopy in the inferior colliculus. I. Electrophysiological mapping in house mice. Dev. Brain Res. *54*, 221–234.

Rotschafer, S., and Razak, K. (2013). Altered auditory processing in a mouse model of fragile X syndrome. Brain Res. *1506*, 12–24.

Rotschafer, S.E., and Cramer, K.S. (2017). Developmental Emergence of Phenotypes in the Auditory Brainstem Nuclei of Fmr1 Knockout Mice. ENeuro *4*, ENEURO.0264-17.2017.

Rotschafer, S.E., Marshak, S., and Cramer, K.S. (2015). Deletion of Fmr1 Alters Function and Synaptic Inputs in the Auditory Brainstem. PLoS ONE *10*.

Sanes, D.H., Geary, W.A., Wooten, G.F., and Rubel, E.W. (1987). Quantitative distribution of the glycine receptor in the auditory brain stem of the gerbil. J. Neurosci. *7*, 3793–3802.

Schneider, A., Leigh, M.J., Adams, P., Nanakul, R., Chechi, T., Olichney, J., Hagerman, R., and Hessl, D. (2013). Electrocortical changes associated with minocycline treatment in fragile X syndrome. J. Psychopharmacol. (Oxf.) *27*, 956–963.

Smith, L.E., Barker, E.T., Seltzer, M.M., Abbeduto, L., and Greenberg, J.S. (2012). Behavioral Phenotype of Fragile X Syndrome in Adolescence and Adulthood. Am. J. Intellect. Dev. Disabil. *117*, 1–17.

Strumbos, J.G., Brown, M.R., Kronengold, J., Polley, D.B., and Kaczmarek, L.K. (2010). Fragile X mental retardation protein is required for rapid experience-dependent regulation of the potassium channel Kv3.1b. J. Neurosci. Off. J. Soc. Neurosci. *30*, 10263–10271.

Wang, Y., Sakano, H., Beebe, K., Brown, M.R., de Laat, R., Bothwell, M., Kulesza, R.J., and Rubel, E.W. (2014). Intense and specialized dendritic localization of the fragile X mental retardation protein in binaural brainstem neurons: A comparative study in the alligator, chicken, gerbil, and human. J. Comp. Neurol. *522*, 2107–2128.

Wen, T.H., Afroz, S., Reinhard, S.M., Palacios, A.R., Tapia, K., Binder, D.K., Razak, K.A., and Ethell, I.M. (2018). Genetic Reduction of Matrix Metalloproteinase-9 Promotes Formation of Perineuronal Nets Around Parvalbumin-Expressing Interneurons and Normalizes Auditory Cortex Responses in Developing Fmr1 Knock-Out Mice. Cereb. Cortex *28*, 3951–3964.

Yan, Q.J., Rammal, M., Tranfaglia, M., and Bauchwitz, R.P. (2005). Suppression of two major Fragile X Syndrome mouse model phenotypes by the mGluR5 antagonist MPEP. Neuropharmacology *49*, 1053–1066.

Appendix A

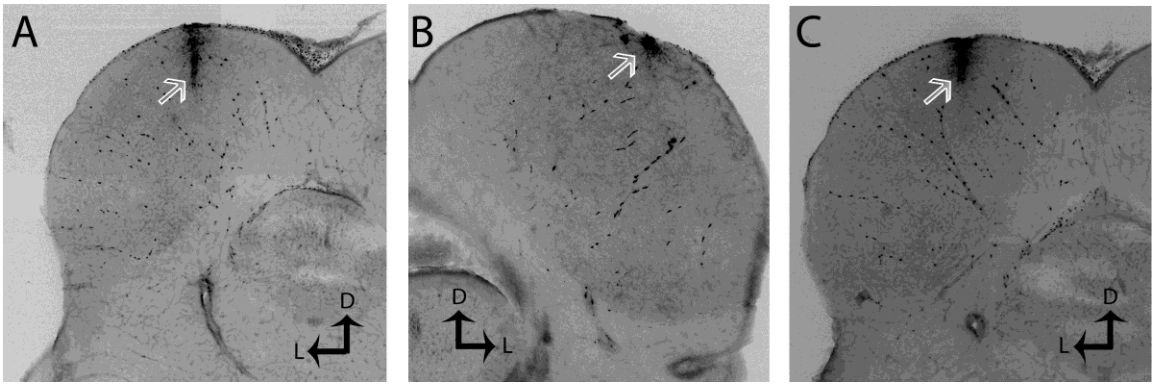

Figure A1: Fluoro-Ruby dye placement in the IC during electrophysiological recordings. The example photomicrographs are of tissue from WT P21 in the coronal plane. White arrows point to the initial electrode tract.

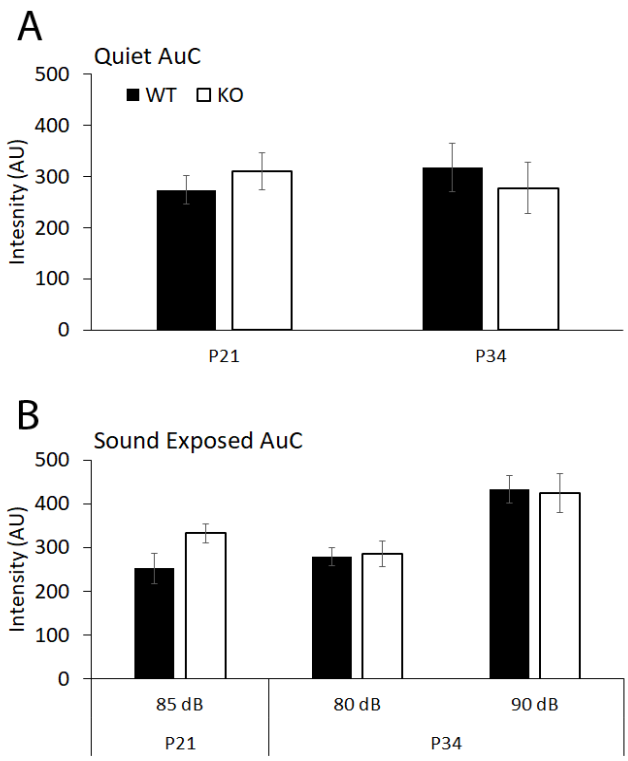

Figure A2: Intensity of cFos expressed neurons in the AuC. P21 and P34 group in the quiet condition (A) and in the sound exposed condition (B).

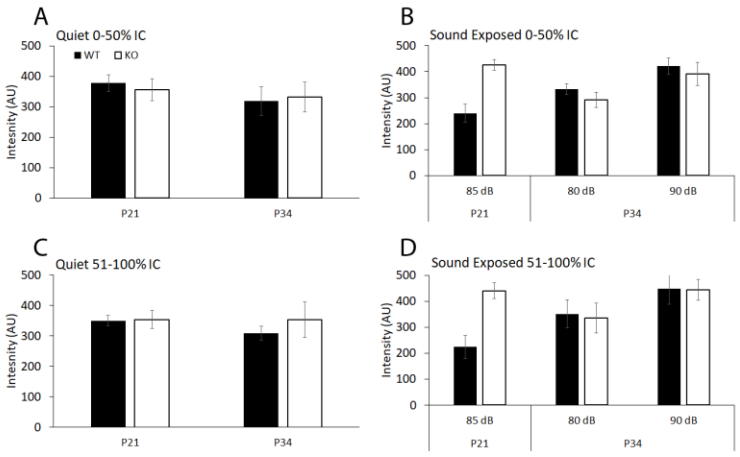

Figure A3: Intensity of cFos expressed neurons in the IC.

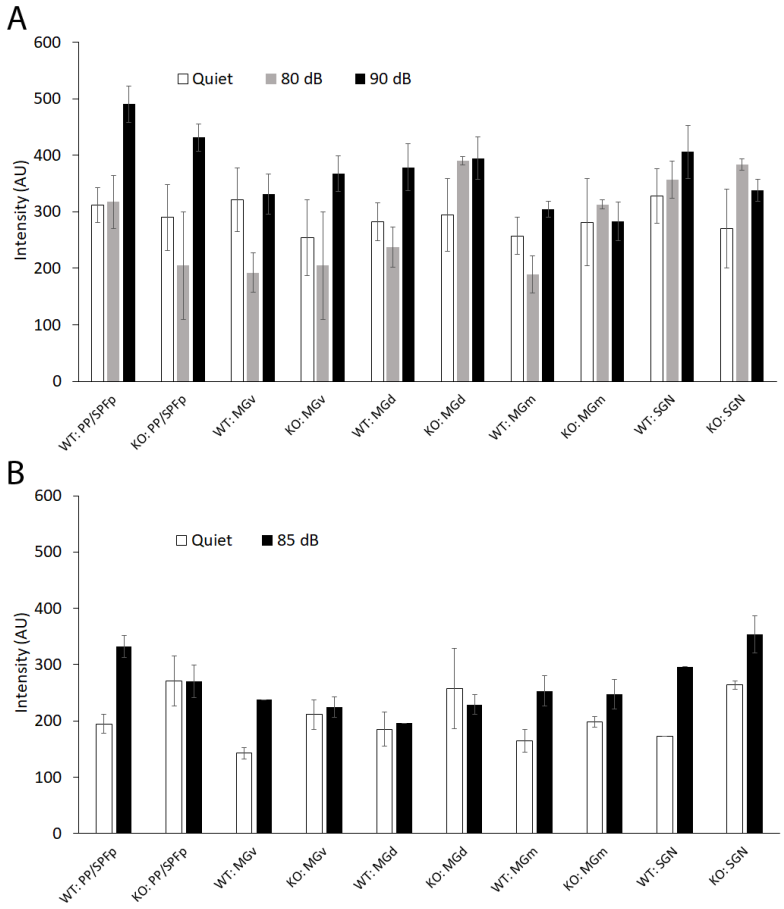

Figure A4: Intensity of cFos expressed neurons in the MGB.

Table A1: Statistics of cFos intensity analysis.

Region	Exposure	Age Group	Statistic
IC	Quiet	P21	t(11)=0.181, p=0.860
IC	Quiet	P34	t(14)=-0.553, p=0.589
IC	85 dB	P21	t(13)=-4.382, p=0.001*
IC	80 dB, 90 dB	P34	dB*genotype:F(23,1)=0.054, p=0.818 dB: F(23,1)=3.692, p=0.067 genotype: F(23,1)=0.063, p=0.804
IC (0-50%)	Quiet	P21	t(11)=0.375, p=0.71
IC (0-50%)	Quiet	P34	t(14)=-0.2154, p=0.832515
IC (0-50%)	85 dB	P21	t(13)=-4.37541, p=0.000751*
IC (0-50%)	80 dB, 90 dB	P34	dB*genotype:F(22,1)=0.020, p=0.890 genotype: F(22,1)=0.905, p=0.352 dB: F(22,1)=6.251, p=0.020*
IC (51-100%)	Quiet	P21	t(11)=-0.11042, p=0.914066
IC (51-100%)	Quiet	P34	t(14)=-0.6348, p=0.53579
IC (51-100%)	85 dB	P21	t(13)=-4.50242, p=0.000595*
IC (51-100%)	80 dB, 90 dB	P34	dB*genotype:F(22,1)=0.010, p=0.922 genotype: F(22,1)=0.041, p=0.842 dB: F(22,1)=3.388, p=0.079
MGB (PP)	Quiet	P21	t(5)=-1.388, p=0.223
MGB (MGv)	Quiet	P21	t(2)=-2.421, p=0.1364
MGB (MGd)	Quiet	P21	t(4)=-0.669, p=0.539
MGB (MGm)	Quiet	P21	t(5)=-1.673, p=0.1551
MGB (SGN)	Quiet	P21	t(1)=-6.787, p=0.09
MGB (PP)	Quiet	P34	t(13)=0.348, p=0.732
MGB (MGv)	Quiet	P34	t(10)=0.7676, p=0.460
MGB (MGd)	Quiet	P34	t(11)=-0.181, p=0.859
MGB (MGm)	Quiet	P34	t(13)=-0.297, p=0.7706
MGB (SGN)	Quiet	P34	t(10)=0.699, p=0.500
MGB (PP)	85 dB	P21	t(6)=1.156, p=0.2914
MGB (MGv)	85 dB	P21	t(5)=0.266, p=0.800

MGB (MGd)	85 dB	P21	t(7)=-0.6181, p=0.5560
MGB (MGm)	85 dB	P21	t(5)=0.126, p=0.904
MGB (SGN)	85 dB	P21	t(4)=-0.706, p=0.5190
MGB (PP)	80 dB	P34	t(5)=-1.15, p=0.301
MGB (MGv)	80 dB	P34	t(3)=-0.1447, p=0.8941
MGB (MGd)	80 dB	P34	t(4)=-2.898, p=0.0442*
MGB (MGm)	80 dB	P34	t(5)=-3.101, p=0.026*
MGB (SGN)	80 dB	P34	t(2)=-0.770, p=0.5214
MGB (PP)	90 dB	P34	t(15)=1.488, p=0.157
MGB (MGv)	90 dB	P34	t(11)=-0.742, p=0.473
MGB (MGd)	90 dB	P34	t(13)=-0.285, p=0.780
MGB (MGm)	90 dB	P34	t(12)=0.587, p=0.567
MGB (SGN)	90 dB	P34	t(12)=1.334, p=0.206
AuC	Quiet	P21	t(12)=-0.812, p=0.433
AuC	Quiet	P34	t(14)=0.573, p=0.576
AuC	85 dB	P21	t(16)=-1.988, p=0.064
AuC	80 dB, 90 dB	P34	dB*genotype:F(27,1)=0.040, p=0.843 dB: F(27,1)=16.211, p=0.000413* genotype: F(27,1)=0.001, p=0.97

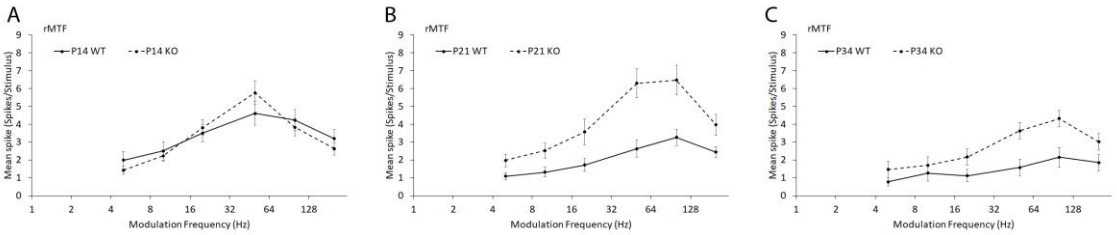

Figure A5: tMTF without first period in the analysis.

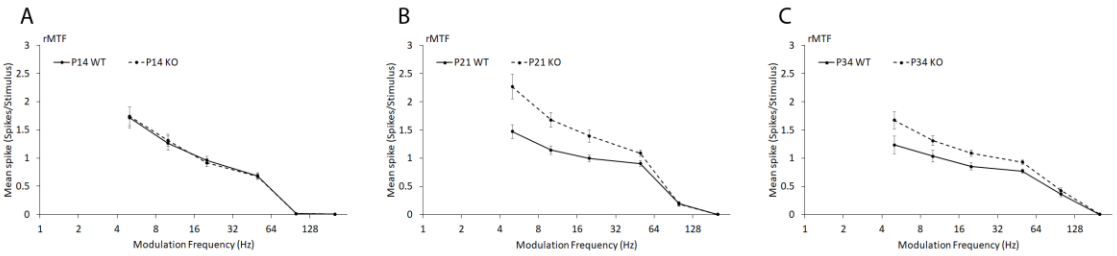

Figure A6: rMTF without first period in the analysis.

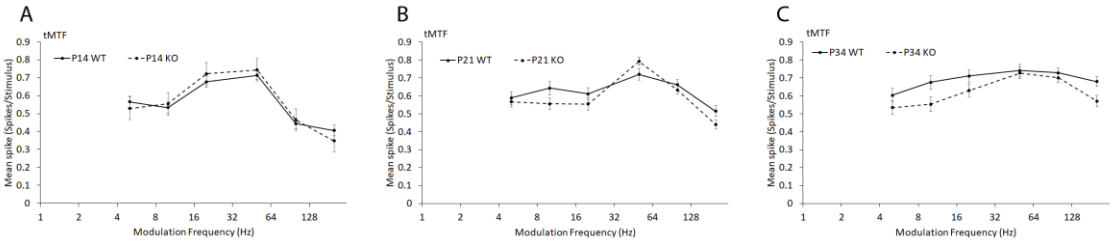

Figure A7: rMTF with first period analysis only.

Table A2: Statistics of tMTF without first period in the analysis.

Modulation Frequency (Hz)	Genotype x Age Interaction	Main effect of Genotype	Main effect of Age
5	F(436)=1.216, p=0.297	F(436)=4.821, p=0.029	F(436)=3.484, p=0.032
10	F(439)=2.416, p=0.09	F(439)=5.105, p=0.024	F(439)=3.574, p=0.029
20	F(442)=3.124, p=0.045	F(442)=2.506, p=0.114	F(442)=6.857, p=0.001

50	F(457)=6.229, p=0.002	F(457)=0.005, p=0.943	F(457)=13.171, p=0.000003
100	F(474)=2.810, p=0.061	F(474)=3.109, p=0.079	F(474)=29.419, p=9.0428E-13
200	F(472)=0.41, p=0.664	F(472)=11.848, p=0.001	F(472)=38.371, p=3.6267E-16

Table A3: Statistics of rMTF without first period in the analysis.

Modulation Frequency (Hz)	Genotype x Age Interaction	Main effect of Genotype	Main effect of Age
5	F(482)=3.124, p=0.045	F(482)=1.764, p=0.185	F(482)=1.934, p=0.146
10	F(482)=2.099, p=0.124	F(482)=4.363, p=0.0.37	F(482)=0.908, p=0.404
20	F(482)=1.183, p=0.307	F(482)=7.348, p=0.007	F(482)=3.414, p=0.034
50	F(482)=2.847, p=0.059	F(482)=16.369, p=0.000061	F(482)=11.24403, p=0.000017
100	F(482)=5.185, p=0.006	F(482)=8.425, p=0.004	F(482)=9.917, p=0.000060
200	F(482)=3.090, p=0.046	F(482)=3.765, p=0.053	F(482)=1.522, p=0.219

Table A4: Statistics of rMTF with first period analysis only.

Modulation Frequency (Hz)	Genotype x Age Interaction	Main effect of Genotype	Main effect of Age
5	F(482)=4.314, p=0.014	F(482)=6.000, p=0.015	F(482)=62.411, p=7.881E-25
10	F(478)=3.722,p=0.025	F(478)=13.256, p=0.000301	F(478)=52.375,p=2.7134E-21
20	F(477)=4.168, p=0.016	F(477)=16.899, p=0.000046	F(477)=68.176,p=9.0745E-27
50	F(478)=2.235, p=0.108	F(478)=12.867, p=0.000369	F(478)=91.939312, p=1.6491E-34
100	F(478)=0.478, p=0.621	F(478)=0.665, p=0.415	F(478)=26.364, p=1.3764E-11
200	F(478)=0.238, p=0.788	F(478)=0.383, p=0.536	F(478)=563.025, p=2.1684E-126

Chapter 3

Audiogenic seizures, Auditory brainstem response (ABR), and Distortion Product Otoacoustic Emission (DPOAE) in *Fmr1* KO Mice

3.1 Introduction

Fragile X Syndrome (FXS) is a neurodevelopmental disorder that leads to intellectual disability. The cause of FXS is inadequate Fragile X mental retardation protein (FMRP) from silencing of the Fragile X mental retardation gene (*Fmr1*). The expansion of the trinucleotide CGG repeats on the X chromosome causes hypermethylation and subsequent inactivation of *Fmr1* gene. Although caused by a monogenetic mutation, the symptoms of FXS are often heterogeneous in the human population (Smith et al., 2012). Some symptoms include intellectual disability, hyperactivity, language impairments, sensory hypersensitivity, and increased susceptibility to seizures (Rogers et al., 2003). FMRP is widely expressed in the brain and other places throughout the body (Hinds et al., 1993). A common and distinctive phenotype is abnormal sensory reactivity, particularly hypersensitivity to auditory stimuli (Hitoglou et al., 2010; Rogers et al., 2003). Here, we used the mouse model of FXS (*Fmr1* KO) which is a well-established animal model with similar phenotypes to humans with FXS. Individuals with FXS and the *Fmr1* KO mice have similar homologous gene silencing, physiology, dendritic spine structure, and seizure susceptibility (Bakker and Oostra, 2003; Kazdoba et al., 2014).

Auditory brainstem response (ABR) and distortion product otoacoustic emission (DPOAE) are audiology tests used to determine peripheral auditory functions. ABR measure auditory responses from a population of neurons which result in 5 distinct

peaks based on the latency of the waveform. The response origin of each peak is associated with: peak I, auditory nerve; peak II, cochlear nucleus; peak III, olivary complex; peak IV, nuclei of the lateral lemniscus; and peak V, inferior colliculus. The peaks can be identified based on the latency to the onset of the response. Rotschafer et al., (2015) showed through ABR tests that *Fmr1* KO mice have higher minimum threshold and decreased peak 1 amplitude compared to WT mice. Individuals with FXS showed longer peak V latency and interpeak latency for wave III-V (Arinami et al., 1988). However, Roberts et al., (2005) showed no difference in hearing sensitivity and ABR responses in normal controls compared to individuals with FXS. DPOAE measures outer hair cell function in the cochlea and is used to test the auditory descending pathway and cochlea responsiveness. Two different tone frequencies (F1 and F2) at frequency ratios of F2/F1=1.25 presented simultaneously in the ear produces a distortion product, F3, which can be measured with a microphone at the ear canal. There had been no report of DPOAE in *Fmr1* KO rodents and FXS individuals showed no impairments (Roberts et al., 2005). It is unclear whether there are peripheral auditory deficits in FXS. However, it is necessary to determine the peripheral hearing functions in order to accurately interpret central processing data in the FXS literature. Here, we describe ABR and DPOAE functions in *Fmr1* KO mice compared to WT mice. We measured ABRs with tone stimuli (4, 5.6, 8, 11, 16, 22, 32, 45, and 64 kHz at 30-75 dB SPL in steps of 5 dB) to define any possible frequency specific deficits and explored if there are outer hair cells dysfunctions in the cochlear by recording DPOAEs of *Fmr1* KO mice.

Humans and rodents with FXS have a ~20% increased susceptibility to seizures compared to the normal population (Berry-Kravis, 2002; Chen and Toth, 2001; Musumeci et al., 2000; Wisniewski et al., 1991). Audiogenic seizure (AGS) is a distinctive behavioral phenotype in rodents so this behavior is often used as a biomarker to test efficacy of potential therapeutic treatments in FXS (Dölen et al., 2007; Michalon et al., 2012; Musumeci et al., 2007; Osterweil et al., 2013; Pacey et al., 2009; Yan et al., 2005). While a number of studies have reported AGS in the *Fmr1* KO mice, there is no systematic evaluation of seizure thresholds in terms of sound levels. Therefore, we set out to quantify the relationship between sound levels and AGS to identify seizure thresholds and severities.

3.2 Methods

3.2.1 Animals

All animal work was approved by the Institutional Animal Care and Use Committee (IACUC). Breeding pairs of FVB.129P2−Pde6b+Tyr$^{c\text{-}ch}$/AntJ (Wild-type, WT) and FVB.129P2−*Fmr1tm1Cgr/J (Fmr1* Knock-out, KO) were obtained from Jackson Laboratories and bred in-house at the University of California, Riverside. The mice received *ad libitum* standard lab chow and water. Cages were changed once a week and the light-dark cycle was on a 12:12 hour cycle. Male FVB WT mice and *Fmr1* KO mice were transported to Loma Linda Veterans Affairs (Loma Linda, CA) from the University of California, Riverside (Riverside, CA) in a personal vehicle to perform ABRs and DPOAEs

experiments. After experimental procedures, the animals were transported back to the University of California, Riverside. Audiogenic seizure experiments were performed at the University of California, Riverside. Data from N=9 WT mice, N=8 *Fmr1* KO mice were used for the ABR study and data from N=9 KO and N=7 WT mice were used for the DPOAE study. Postnatal (P)30-P37 were used for the ABRs and DPOAEs experiments; the same animal were used for both the ABR and DPOAE measurements. A total of N=59 *Fmr1* KO mice were used for the audiogenic seizure experiments. Each audiogenic seizure experimental group had an N=10 except for the 95 dB level group, which had an N=9.

3.2.2 ABR and DPOAE recordings

P30-P37 day old mice were first place in a chamber and anesthetized with inhalation of 3.0% isoflurane in oxygen then injected intraperitoneally (i.p.) with a mixture of Ketamine (65mg/kg) and Xylazine (13 mg/kg). A toe pinch response was examined before the experiment and at every 5-10 minutes thereafter until the termination of the recording session; supplemental doses of anesthesia (i.p. injected) were given as needed throughout the experiment. A feedback rectal thermometer was used to maintain the temperature of the mouse at 36-38°C throughout the experiment. Sound presentations were performed in a sound attenuated booth. For the ABR recordings, 3 subdermal electrode were inserted, the ground electrode in the thigh, the reference electrode in the left cheek and the recording electrode in the vertex. An in-ear

speaker/microphone probe placed inside the left ear canal in which sound stimuli were delivered as described. ABR filter: Gain=200k; High pass filter = 300 Hz; low pass filter = 3000 Hz. For DPOAE, the F2/F1=1.25 and the F2 kHz used are: 4, 5.65, 8, 11.31, 16, 22.62, 32, 45.25, and 64. The intensity of the sound stimuli ranges from 10 to 80 dB in 5 dB steps. The ABR stimulus consisted of: 4, 5.6, 8, 11, 16, 22, 32, 45, and 64 kHz at 30-75 dB SPL in steps of 5 dB SPL.

3.2.3 Sound exposure to induce audiogenic seizure

Multiple levels of sound intensity were tested on different groups of mice to determine behavioral thresholds in audiogenic seizure. Up to 4 male mice aged P32-36 were placed in a standard mouse cage with no food or water. These mice were then exposed to sounds of calibrated sound levels within an anechoic sound attenuated booth (Gretch-Ken Inc.). Auditory stimuli were generated with a custom software (BATLAB, Dr. Don Gans, Kent State University or Sparkle, Portfors Lab, Washington State University) and delivered through a programmable attenuator (PA5, TDT) and a speaker (FT17H, Fostex International) placed face down on top of the cage lid. Sound levels were measured with a sound level meter (735, B&K Precision) at a distance from the speaker to the cage bottom. A lamp was used to provide light for a video camera to record behaviors during 5 minutes of baseline with no sound presentation and 15 minutes of sound presentation. The video recordings were used for offline analyzes of audiogenic seizure behaviors. The stimulus used to identify AGS threshold was a continuous siren

generated by presenting 1 second repetitions of up followed by down sweeps in the 6-12 kHz range presented at 80, 85, 90, 95, 100, or 105 dB SPL for 15 minutes. Separate groups of mice were exposed to each stimulus intensity with a total of N=10 for each sound level except for the 95 dB group (N=9).

3.2.4 Audiogenic seizure behavioral analysis

Audiogenic seizure behaviors were analyzed from the video recordings by an observer blinded to the group classifications (blinded to genotype and sound level exposures); a behavioral score index (SI) from Barrera-Bailón et al., 2013 was used as follows:

Table 1: Seizure index score and the corresponding behaviors.

Seizure Index Score (SI)	Audiogenic Seizure Behavior(s)
0	no seizure
1	one wild running
2	one wild running (plus jumping, plus atonic fall),
3	two wild running
4	tonic convulsion
5	tonic seizures plus generalized clonic convulsions
6	head ventral flexion plus SI-5,

7	forelimb extension plus SI-6,
8	hind limb extension plus SI-6 or death

Each mouse tested received one seizure score as the highest score possible based on the SI classifications. For example, if the mouse died from AGS, it received a score of 8, whereas if it showed only a single bout of wild running it received a score of 1. A mouse that showed multiple bouts of wild running and jumping and eventually clonic convulsions received the higher score (SI: 5) for the latter. Seizure threshold was determined as the lowest sound level needed to elicit a seizure behavioral response (a mean score > 0).

3.2.5 ABR and DPOAE Analysis

The features of the ABR response waveform, the amplitude and latency at every peak were analyzed to determine the strength of the response and the temporal characteristics. In ABR, wave I-V peaks were determined by discernable waveforms. Latency of peaks were determined at the highest point of the peak from the onset of the ABR waveform. The statistics used for the ABR data was linear mixed effect model using the statistical software (SPSS Statistics 24, IBM). The dependent variable was the latency or amplitude (as appropriate for the analysis) and the factors are genotype and intensities of the stimuli with the fixed variable as the genotype. Moreover, DPOAE response magnitude and phase were analyzed. Steeper phase is indicative of longer

latency in the emission reflected from the cochlea. DPOAE data were analyzed using custom written Matlab code. For ABR minimum thresholds, a Student's t-test was used to compare the means of WT mice and *Fmr1* KO mice. $P< 0.05$ indicates a significant difference.

3.3 Results

The main aim of this study was to identify the subcortical auditory characteristics in *Fmr1* KO mice compared to WT mice. First, audiogenic seizure severities were characterized in response to different sound intensity levels. Secondly, ABRs were tested to determine peripheral functions and subcortical activity. Third, DPOAEs were measured to explore the outer hair cell functions in the cochlea.

3.3.1 As sound levels increase, so do audiogenic seizure severity

Separate groups of P32-P36 mice were exposed to continuous 80, 85, 90, 95, 100, or 105 dB SPL siren (6-12 kHz) for 15 minutes. Each group had an N=10 except for the 95 dB level group, which had an N=9. One seizure score was given to each mouse at the highest behavioral seizure displayed for the duration of sound stimulus presentation based on the seizure index described in the methods. The mean seizure score increased with sound level (Fig. 1). At exposure to 80 dB sound level, there were no behavioral seizures observed for the duration of the sound stimulus presentation (Average SI Score=0). However, at exposure to 85 and 90 dB sound level, 5 out of 10 mice displayed

some level of seizure behaviors (Average SI Score=1.6, Average SI Score=3.4, respectively). We determined the sound level for seizure threshold to be ~85 dB in P32-P36 mice. At exposure to 95 dB, 3 out of 9 mice displayed seizure behaviors (Average SI Score=2.66); the ratio of mice that seized and the Average SI score were lower than at 90 dB. The mice that seized at exposure to 95 dB have the higher severity score (SI=8, death). At 100 dB exposure, 7 out of 10 displayed seizures (Average SI Score=5.6) and lastly at 105 dB exposure, 10 out of 10 displayed seizures (Average SI Score=4.8). In addition, we did not observed any spontaneous seizures in these mice. The data suggest that there is a dose-dependent effect of sound level on seizure severity. The sound level intensity had a direct effect on seizure behaviors in *Fmr1* KO mice indicating hypersensitivity to auditory stimulation.

3.3.2 Latency of Seizure Response

In addition to testing seizure severity in response to different sound levels, the latencies to these audiogenic seizure behavioral phenotypes were also characterized. The sound stimulus was presented for 15 mins (900 seconds) and behaviors were recorded using a video camera for offline analysis. The main rodent seizure behaviors: wild running and jumping (WRJ), tonic seizure (TS), and death were used because they are easily distinguishable phenotypes and typically occur in a serial manner during seizures (Fig. 2). Except for the lowest sound level intensity (80 dB), at least 40% of the mice exhibited WRJ during the 900 seconds of exposure to sound stimulus. For TS, the

lowest sound level to induce WRJ behavavior was 85 dB SPL, but only after 600 seconds into the sound stimulus and in 10% of mice. With louder sound stimulus (100-105 dB), 40-50% of mice exhibited TS. Death from audiogenic seizure occurs in 30-40% within 200 seconds of sound stimulus at 100-105 dB. In summary, exposure to louder sound intensity generally decreases the latency to behavioral seizures. These results suggest that there is not only an effect of sound intensity on behavioral seizure severity as describe above but there is also a factor of duration to the auditory exposure.

3.3.3 No differences in auditory minimum threshold or amplitudes of ABR

Minimum thresholds were determined as the lowest sound level at which there was an ABR peak response. Each threshold was determined for each frequency of tone tested (4, 5.65, 8, 11.31, 16, 22.62, 32, and 45.25 kHz). Male mice at P30-37 were used for unilateral ABRs to test the function of the auditory brainstem nuclei and DPOAEs were used to test the function of the outer hair cells in the cochlea. Student t-test between minimum threshold averages of WT mice compared to *Fmr1* KO mice revealed no significant differences at any frequency tested (Table 2, Fig. 4). To determine the strength of response to the frequencies tested, the amplitude of each peak response was measured. There were no statistical differences in ABR amplitude between WT mice and *Fmr1* KO mice for peaks I-V (Table 3, Fig. 5-9).

Table 2: Statistics of minimum threshold at each stimulus frequency. Student t-test showed no significant differences between *Fmr1* KO mice and WT mice at every stimulus frequency.

Stimulus Frequency	Student t-test
4	t(11)=0.054, p=0.843
5.7	t(12)=0.367, p=0.877
8	t(14)=0.212, p=0.526
11.3	t(14)=0.296, p=0.662
16	t(14)=1.521, p=0.988
22.6	t(14)=0.736, p=0.687
32	t(13)=1.740, p=0.405
45.3	t(7)=1.158, p=0.719

Table 3: Amplitudes and latencies analysis of ABR peak responses, P < 0.05 indicates statistical significance.

ABR Peak	Stimulus Frequency	Mixed Model Analysis for Latency	Latency (ms)
Peak 2	45.3	F(1,67)=4.851, p=0.031	KO>WT
Peak 3	4	F(1,63)=8.091, p=0.006	WT>KO
Peak 3	5.7	F(1, 117)=10.578, p=0.001	KO>WT
Peak 3	22.6	F(1,188)=14.497, p= 0.000190	KO>WT
Peak 3	32	F(1,189)=14.387, p= 0.0002	KO>WT
Peak 4	45.3	F(1,65)=4.410, p=0.040	KO>WT
Peak 5	4	F(1,57)=6.311, p=0.015	KO>WT
Peak 5	8	F(1,145)=11.544, p=0.001	WT>KO
Peak 5	11.3	F(1,162)=9.566, p=0.002	KO>WT

Peak 5	16	F(1,199)=6.351, p=0.013	KO>WT
Peak 5	32	F(1,203)=6.484, p= 0.000061	KO>WT
Peak 5	45.3	F(1,66)=6.484, p=0.013	KO>WT

3.3.4 *Fmr1* KO mice showed abnormal latency in mainly peak III and V of ABR response

Latency of ABR peaks were taken as the highest point of a specific peak from the onset of the ABR waveform (Fig. 3). Each peak for every tone frequency tested were analyzed using mixed model analysis with the dependent variable as the latency or amplitude and the factors as genotype and intensity of sound stimulus. Arinami et al., (1988**)** showed a difference in peak V in human subjects with FXS compared to normal controls; however, peak III was not significantly different. Here, consistent with Arinami et al., (1988), we showed a significant difference in latency of mainly peak III and V of the ABR responses (comparisons showed an overall longer latency in *Fmr1* KO mice than WT mice except for peak 3 at 4 kHz and peak 5 at 8 kHz), (Table 3, Fig. 10-14). These peak have origins to the olivary complex (peak III) and inferior colliculus (peak V) suggesting functional impairments in these auditory nuclei.

3.3.5 Magnitudes of DPOAE responses are similar between *Fmr1* KO mice and WT mice

To test the function of the outer hair cells in the cochlea, DPOAEs were measured at the ear canal. The outer hair cells receive descending inputs and produce acoustic vibrations due to the outer hair cell's physical movements. The magnitude of the otoacoustic emissions, emission phase, and input-output function (IO function) for amplitude and phase were investigated. The magnitude and phase of the emissions plotted against the F2 frequency are indicative of the response profile at that frequency on the tonotopic basilar membrane. IO functions are a measure of basilar membrane compression, measures loudness growth, and predicts hearing loss in the cochlea. There were no observable significant differences between WT mice and *Fmr1* KO mice in DPOAE response magnitude, IO functions, or emission phase (Fig. 15, 16). These results suggest that in FXS, the outer hair cells are able to produce otoacoustic emissions comparable to WT mice's levels.

3.4 Discussion

The goals of these studies were to test the peripheral audibility in WT and *Fmr1* KO mice and to characterize audiogenic seizures in *Fmr1* KO mice. The first main finding was audiogenic behavioral seizure severity and latency are correlated with sound intensity. Secondly, there was no difference in response amplitude in any of the five ABR peaks. However, there were mainly latency differences (Table 3) between WT mice and

Fmr1 KO mice for peak III and peak V, consistent with prolonged latency in Arinami et al.,'s (1988) human ABR results. Third, we observed no difference between WT mice and *Fmr1* KO mice in DPOAE measurements.

In the auditory midbrain, the inferior colliculus is the progenitor of audiogenic seizures (Sakamoto and Niki, 2001). Audiogenic seizures were prevented only when the inferior colliculus was lesioned in seizure prone rodents, in contrast, audiogenic seizures were still present when the medial geniculate body or auditory cortex was lesioned (Kesner, 1966). These evidences suggest that audiogenic seizures in *Fmr1* KO mice may also originate in the inferior colliculus. Many previous studies used audiogenic seizure behaviors in *Fmr1* KO mice as a phenotypic biomarker to demonstrate drug treatment efficacy; however, the sound used to induce audiogenic seizure were up to 135 dB SPL, the equivalent sound level of a jet engine at 50 ft away (Table 4). Here, we showed that stimulus of 105 dB SPL induced audiogenic seizure in 100% of mice and a moderately loud sound (90-95 dB) induced audiogenic seizure in 30-50% of mice. These studies suggest that even moderate levels of sound intensity can trigger an audiogenic seizure response in *Fmr1* KO mice and can adversely affect behaviors in FXS. To the best of our knowledge, this is the first study that demonstrated audiogenic seizure at moderately loud sound level. Many other studies induced audiogenic seizure with high intensity sound which may cause hearing loss and impair auditory functions (Table 4). This reflect upon the extent of auditory hypersensitivity in FXS, a moderately loud sound can evoke a behavior of reflexive aversion. A factor to note in these stimulus for audiogenic seizure

paradigms is the duration of the stimulus. A high intensity sound of 115/120 dB at 60 seconds in FVB mice (Chen and Toth, 2001; Musumeci et al., 2000, 2007) compared to 15 minutes (Dölen et al., 2007; Yan et al., 2005) and 2 minutes (Pacey et al., 2009) in C57 background mice were able to induce audiogenic seizures. As our data of audiogenic seizure latency implies, the seizure behaviors are also dependent on the stimulus duration. This implies that hypersensitivity in FXS can be due to duration of exposure to moderately loud noises in the environment. It is valuable to understand hypersensitivity at the threshold level for audiogenic seizure behaviors as it is more translationally relevant to individuals with FXS who are often exposed to moderately loud sounds (85 dB SPL).

The mechanism for audiogenic seizures can be attributed to impaired excitatory and inhibitory balance. The genetic reduction of mGluR5 expression was able to reduce the incident of audiogenic seizure in *Fmr1* KO mice (Dölen et al., 2007). In addition, the application of MPEP (Yan et al., 2005) or CTEP (Michalon et al., 2012), a mGluR5 antagonist, was able to reduce incidences of audiogenic seizures. The $GABA_b$ receptor agonist, baclofen, was able to reduce audiogenic seizures (Pacey et al., 2009). Given the multiple approaches that can rescue audiogenic seizures, it is unclear if there is only one mechanism that can induce audiogenic seizures.

The amount of susceptibility to audiogenic seizure is dependent on developmental age. Rodents at ~P21 have a higher incident of audiogenic seizure than earlier in development (<P18) or later in development (>P34) (Musumeci et al., 2000,

2007). However, it is still unknown why there is an increased in audiogenic seizure susceptibility particularly at ~P21. One hypothesis is that there is a particular molecular change in inhibition or excitation at the specific developmental age of P21. In the auditory cortex, in layers 2/3 and 4, there is reduced PV+/PNN+ (PV, parvalbumin; PNN, perineuronal nets) cell density at P21 but not at P14 or P30 (Wen et al., 2018). Alterations in PV+ neuron activity had been associated to seizure (Schwaller et al., 2004) and disruptions of PNNs formation often lead to seizures (reviewed in McRae and Porter, 2012). Given the formation of PNNs inhibitory factors in late adolescence (~P22), the disruption of inhibition due to impaired PV+ and PNN+ are candidates for the mechanism behind increase audiogenic seizure susceptibility at ~P21.

Table 4: Literature that use audiogenic seizure in *Fmr1* KO mice.

Authors	Mouse Strain	Age	Average Sound Intensity	Frequency
Dölen et al., 2007	C57Bl/6	P19-21	125 dB	18-63 kHz siren
(Yan et al., 2004)	C57 FVB Hybrid	P21 P21 P30	125 dB	18-63 kHz siren

(Yan et al., 2005)	C57 male x FVB female cross FVB	P14-180 P14-180	125 dB	18-63 kHz siren
Chen and Toth, 2001	FVB	P49-70	115 dB	2-20 kHz noise
Michalon et al., 2012	C57BL/6J FVB	P18-22 P30-60	120 dB	Modified personal alarm siren
Musumeci et al., 2000	FVB	P7, 22, 35, and 45	120 dB	Electric doorbell that generated noise
Musumeci et al., 2007	FVB	P17, 22, 35, 45, and 60	120 dB	Electric doorbell that generated noise
Osterweil et al., 2013	C57BL/6 or FVB	P14-25	130 dB	Modified personal alarm
Pacey et al., 2009	C57/Bl6	P27-30	135 dB	Piezo siren
Curia et al., 2013	C57Bl/6	P45, P90	122 dB	Doorbell
(Dansie et al., 2013)	FVB	P28-30	110 dB	2-6 kHz

There is clear evidence for sound evoked auditory cortical deficits (Lovelace et al., 2016, 2018; Rotschafer and Razak, 2013, 2014; Wen et al., 2018, 2019); however little is known about the peripheral responses in *Fmr1* KO mice. In order to fully interpret the central auditory dysfunctions, it is necessary to study how sound is processed at the site of the peripheral receptor. ABR and DPOAE are commonly used techniques to test peripheral hearing sensitivity (Abdala and Visser-Dumont, 2001). FMRP is found throughout the brainstem (Beebe et al., 2014; Wang et al., 2014) suggesting FMRP may play a role in the function of the brainstem areas. *Fmr1* mRNAs are expressed in outer hair cells of the cochlea in P26-P30 mice (Li et al., 2016); however, the levels are relatively low, suggesting FMRP does not play a large role in the function of the outer hair cells, which explain the normal DPOAE measurements in *Fmr1* KO mice. It is unknown whether FMRP plays a role in the development of the inner and outer hair cells in embryonic and early postnatal development (<P14) or in adult ages (>P30). The literature on peripheral and brainstem functions in FXS are conflicting. Although there are conflicting results, most studies showed a lower amplitude and longer peak latency in subjects with autism spectrum disorder (reviewed in Smith et al., 2019). We showed ABR latency deficits on peak III and V (comparisons showed an overall longer latency in *Fmr1* KO mice than WT mice except for peak 3 at 4 kHz and peak 5 at 8 kHz) of *Fmr1* KO mice compared to WT mice which is most consistent with Arinami et al.,'s (1988) study which showed latency differences in peak III and V. However, Arinami et al., did not show a significant difference in peak III latency. The

delay in latency of response may be explained by a delay in myelination in *Fmr1* KO mice. In the cerebellum of *Fmr1* KO mice, there was reduced MBP (myelin basic protein) at P7 and P15 followed by normal WT levels at P30, and then overexpression at 2-4 months and a decline to normal levels at 7-15 months. In addition, a decrease in OPC (oligodendrocyte precursor cell) at P7 followed by over expression at P15 (Pacey et al., 2013). These are some indications that there are delays and fluctuations in factors of myelination in *Fmr1* KO mice. The delay and instability of myelination in *Fmr1* KO mice can be the mechanism behind prolonged latency seen in ABR recordings presented here and (Arinami et al., 1988). Latency delays are also present in single unit recordings of the inferior colliculus (Chapter 2), in auditory cortex (Wen et al., 2018), and in EEG auditory evoked N2 component (Knoth et al., 2014; St. Clair et al., 1987). However, there was no delay in latency in the N1 component (St. Clair et al., 1987; Van der Molen et al., 2012a, 2012b). Latency delays in evoked potentials can be attributed to impaired formation of myelination, thus slowing down conduction speed, in *Fmr1* KO mice.

Inconsistent with our results, Rotschafer et al., 2015 showed higher threshold and smaller amplitude for peak 1 and 3 in click responses in *Fmr1* KO mice. Differences in testing procedures and environmental sound the mice were raised in may be factors that account for the inconsistencies in ABR findings. Similarly, there are also inconsistencies in ABR of humans with FXS. ABR and DPOAE in humans with FXS and ASD showed no difference from normal controls in one report (Roberts et al., 2005; Tharpe et al., 2006), which is similar to our mouse DPOAE results; however, Danesh and

Kaf, (2012) showed a reduction in DPOAE response in ASD subjects. The discrepancy in human ABR and DPOAE responses may be due to current medications that individuals were taking and some reported cases of hearing loss in the FXS population.

It is interesting that ABR latency deficits were only observed at peak III and peak V and not at any other peaks. There are known *Fmr1* KO mice deficits in the corresponding nuclei. There are synaptic and molecular deficits in the medial nucleus of the trapezoid body (MNTB), a nuclei of the olivary complex (McCullagh et al., 2017; Rotschafer et al., 2015; Ruby et al., 2015; Strumbos et al., 2010; Wang et al., 2015). The longer delay in latency deficits in peak V, corresponding to the inferior colliculus, is consistent with abnormalities in our single-unit data (Chapter 2) which shows a delay in spike latency in neurons with CF <20 kHz. Both the superior olivary complex and inferior colliculus are site of convergence from multiple nuclei. The superior olivary complex is the convergence site of the left and right ear, while the inferior colliculus receives input from almost all brainstem subnuclei and the auditory cortex. Due to FMRP's important role in regulating synaptic proteins, *Fmr1* KO mice may display more severity at nuclei which heavily depends on synaptic integrations (such as the superior olivary complex and inferior colliculus).

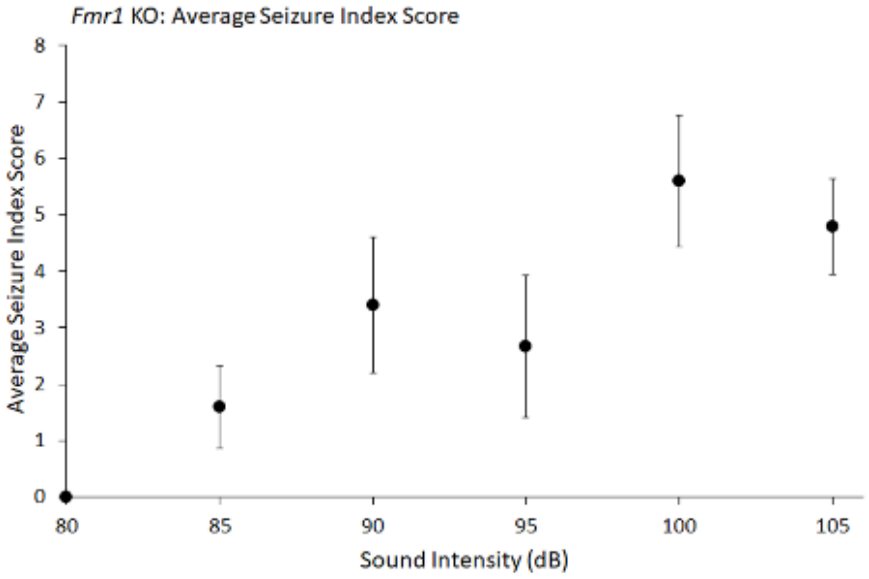

Figure 1: Average seizure index score in *Fmr1* KO mice. As the sound level intensity increase, so do the average seizure score.

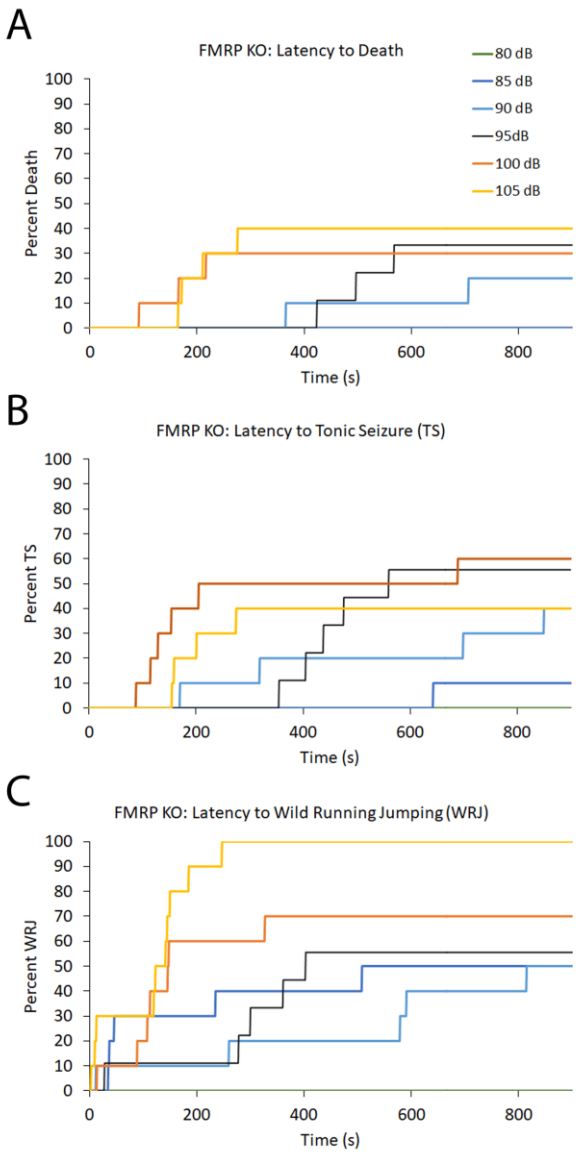

Figure 2: Percentage of mice that exhibited latency to audiogenic seizure behavioral phenotypes. (A) Latency to the highest seizure phenotype, death. (B) Latency to tonic seizure (TS) and (C) latency to wild running and jumping (WRJ).

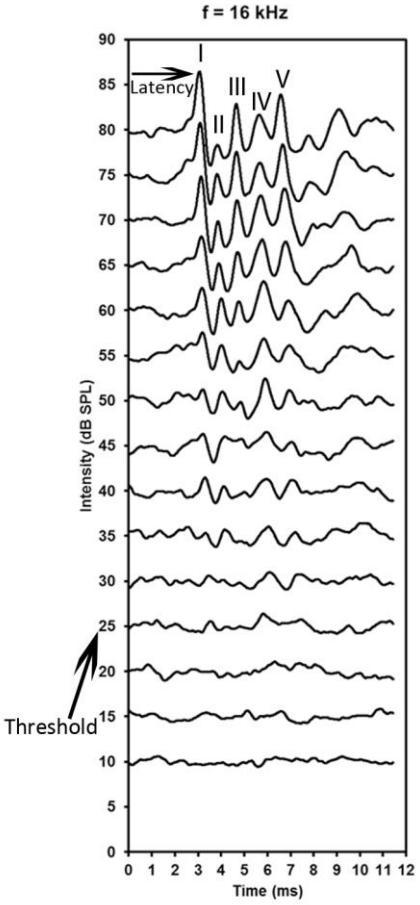

Figure 3: Example of ABR waveform of WT mice at 16 kHz tone stimulation.

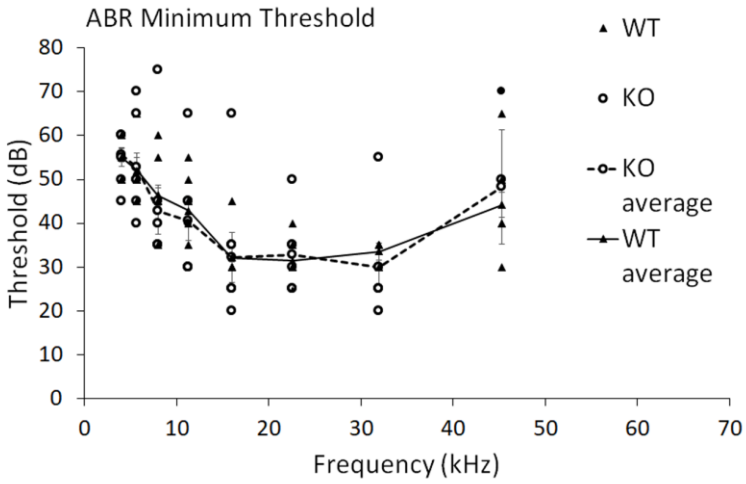

Figure 4: ABR minimum threshold at each frequency. Connected line indicates group average and error bar is STD error.

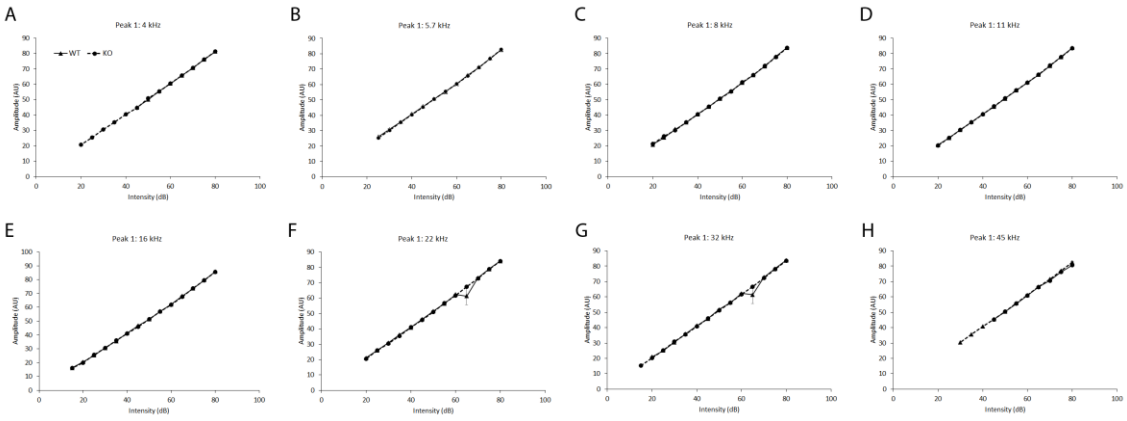

Figure 5: ABR peak 1 amplitude. (A-H) Amplitude plots at each respective frequency (4, 5.65, 8, 11.31, 16, 22.62, 32, and 45.25 kHz).

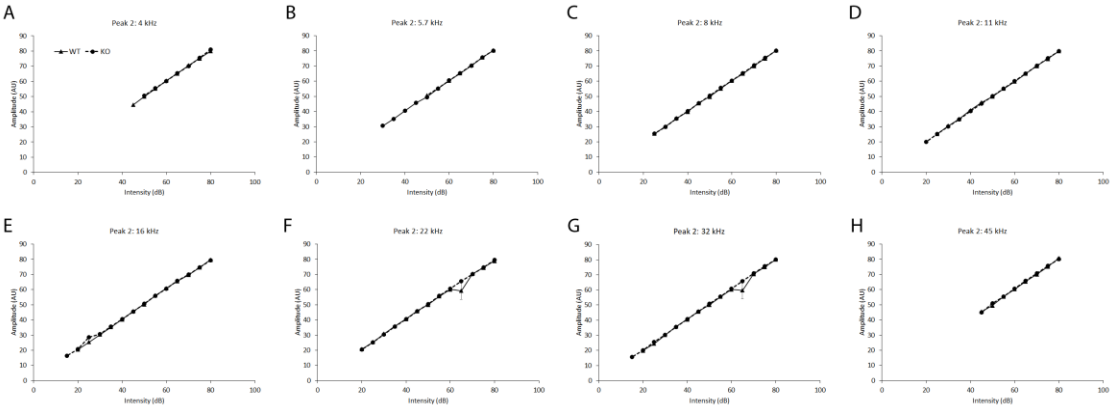

Figure 6: ABR peak 2 amplitude. (A-H) Amplitude plots at each respective frequency (4, 5.65, 8, 11.31, 16, 22.62, 32, and 45.25 kHz).

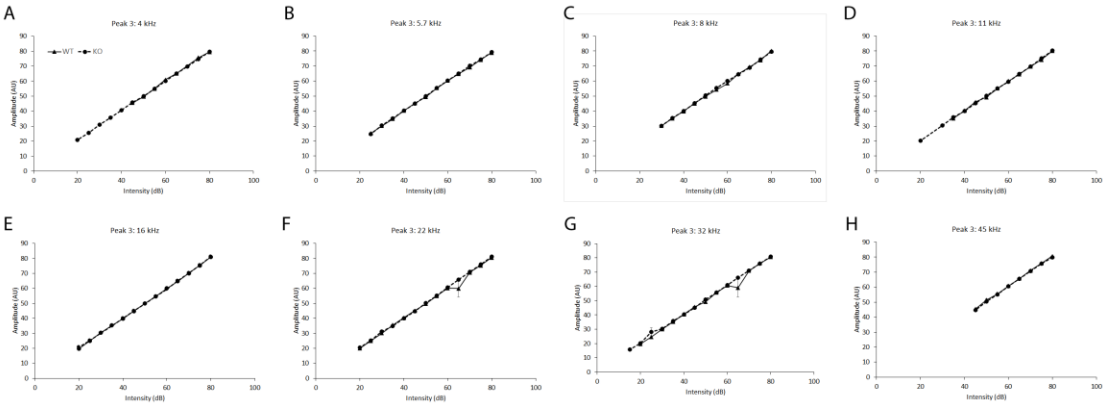

Figure 7: ABR peak 3 amplitude. (A-H) Amplitude plots at each respective frequency (4, 5.65, 8, 11.31, 16, 22.62, 32, and 45.25 kHz).

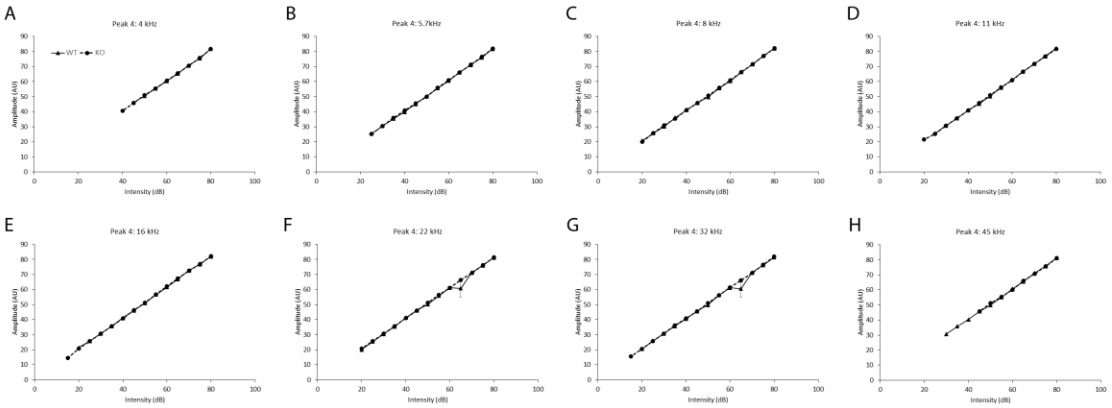

Figure 8: ABR peak 4 amplitude. (A-H) Amplitude plots at each respective frequency (4, 5.65, 8, 11.31, 16, 22.62, 32, and 45.25 kHz).

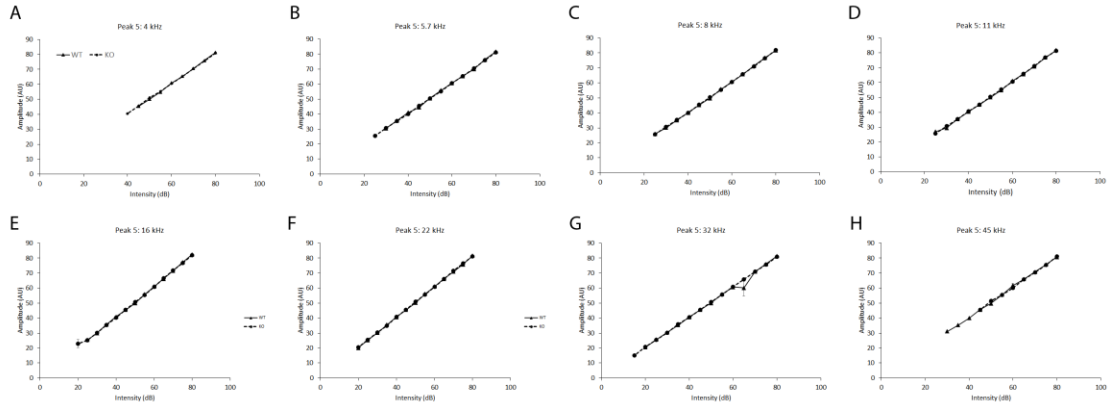

Figure 9: ABR peak 5 amplitude. (A-H) Amplitude plots at each respective frequency (4, 5.65, 8, 11.31, 16, 22.62, 32, and 45.25 kHz).

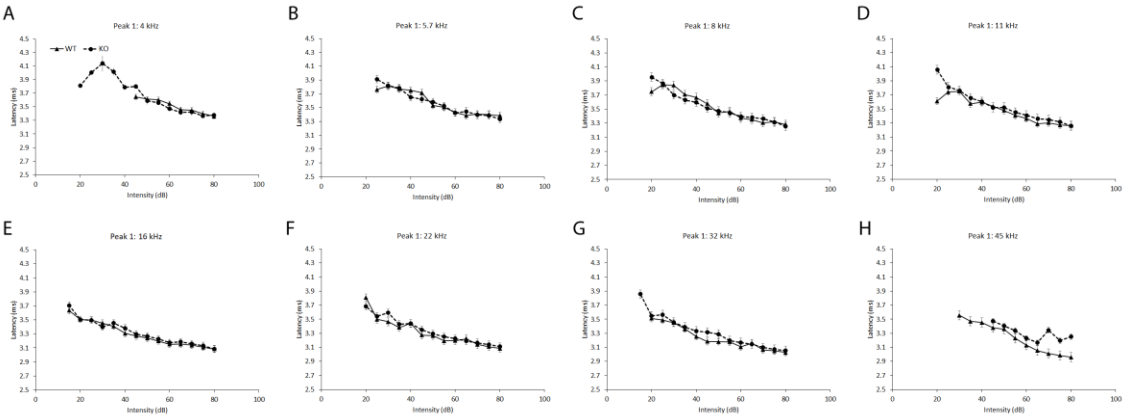

Figure 10: ABR peak 1 latency. (A-H) Latency plots at each respective frequency (4, 5.65, 8, 11.31, 16, 22.62, 32, and 45.25 kHz).

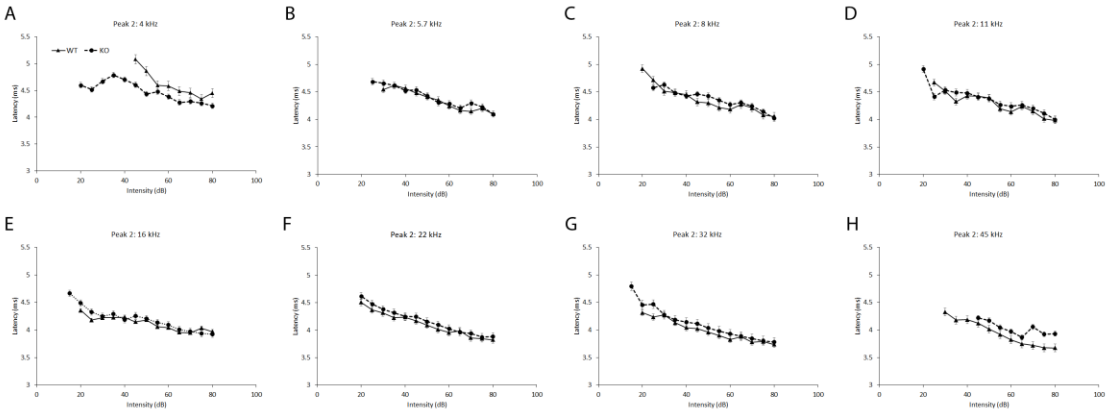

Figure 11: ABR peak 2 latency. (A-H) Latency plots at each respective frequency (4, 5.65, 8, 11.31, 16, 22.62, 32, and 45.25 kHz).

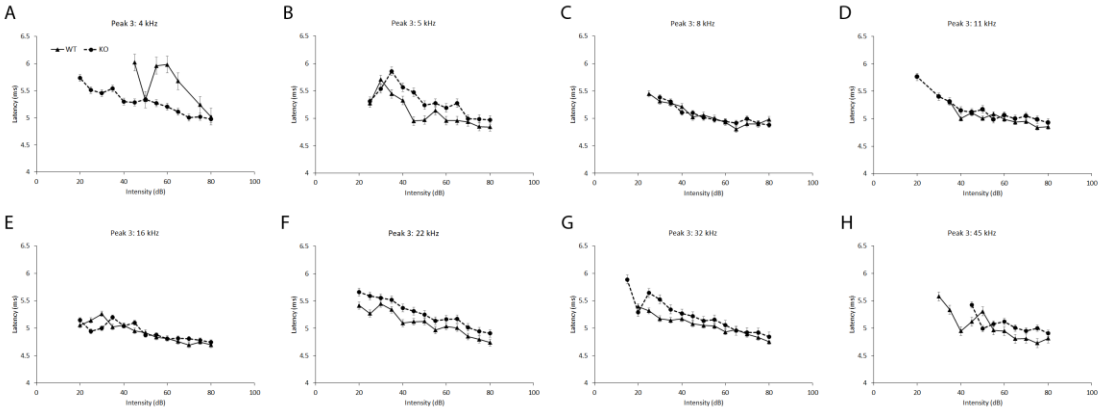

Figure 12: ABR peak 3 latency. (A-H) Latency plots at each respective frequency (4, 5.65, 8, 11.31, 16, 22.62, 32, and 45.25 kHz).

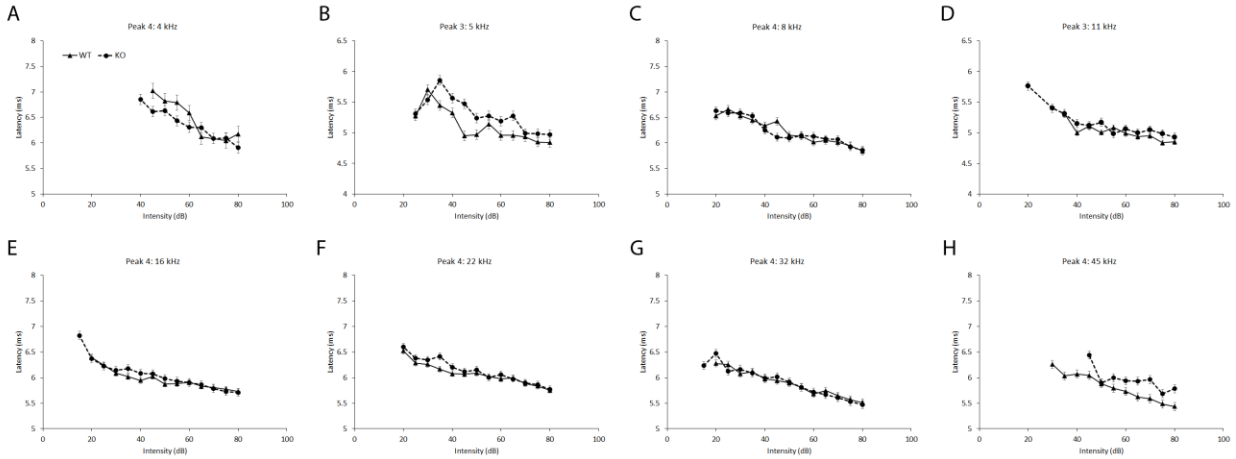

Figure 13: ABR peak 4 latency. (A-H) Latency plots at each respective frequency (4, 5.65, 8, 11.31, 16, 22.62, 32, and 45.25 kHz).

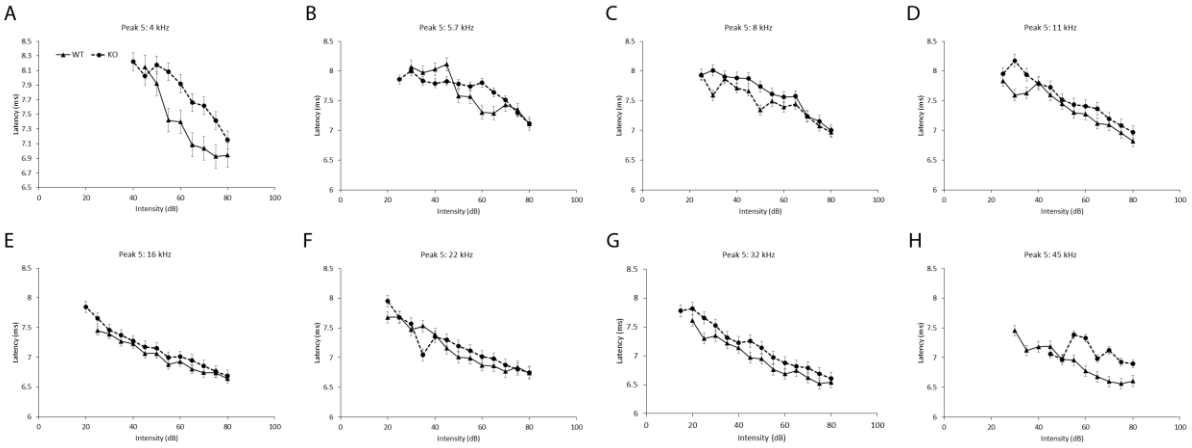

Figure 14: ABR peak 5 latency. (A-H) Latency plots at each respective frequency (4, 5.65, 8, 11.31, 16, 22.62, 32, and 45.25 kHz).

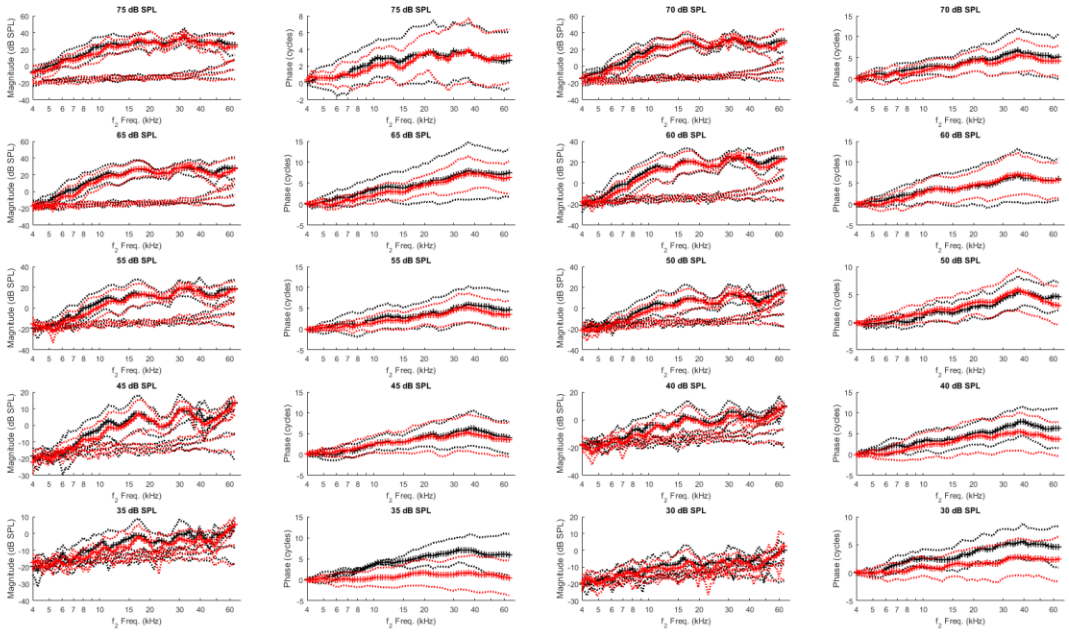

Figure 15: DPOAE response magnitude and phase plotted at each frequency.

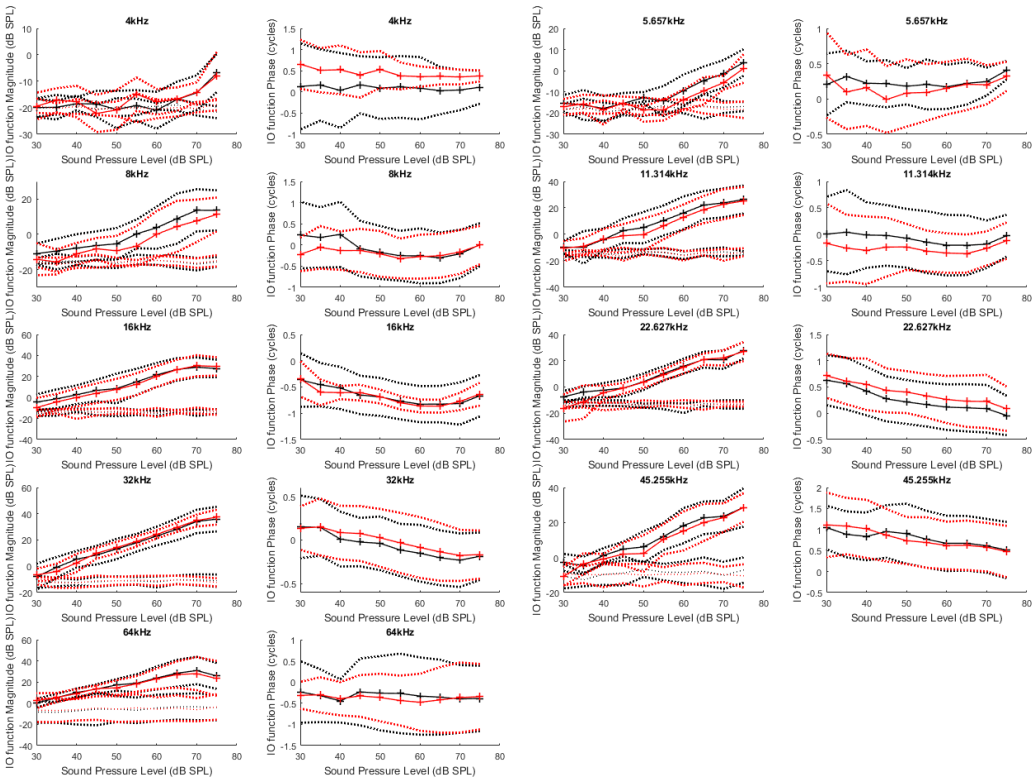

Figure 16: DPOAE response magnitude IO function and phase IO function plotted at each frequency.

References

Abdala, C., and Visser-Dumont, L. (2001). Distortion Product Otoacoustic Emissions: A Tool for Hearing Assessment and Scientific Study. Volta Rev *103*, 281–302.

Arinami, T., Sato, M., Nakajima, S., and Kondo, I. (1988). Auditory brain-stem responses in the fragile X syndrome. Am J Hum Genet *43*, 46–51.

Bakker, C.E., and Oostra, B.A. (2003). Understanding fragile X syndrome: insights from animal models. CGR *100*, 111–123.

Barrera-Bailón, B., Oliveira, J.A.C., López, D.E., Muñoz, L.J., Garcia-Cairasco, N., and Sancho, C. (2013). Pharmacological and neuroethological studies of three antiepileptic drugs in the Genetic Audiogenic Seizure Hamster (GASH:Sal). Epilepsy & Behavior *28*, 413–425.

Beebe, K., Wang, Y., and Kulesza, R. (2014). Distribution of fragile X mental retardation protein in the human auditory brainstem. Neuroscience *273*, 79–91.

Berry-Kravis, E. (2002). Epilepsy in fragile X syndrome. Dev Med Child Neurol *44*, 724–728.

Chen, L., and Toth, M. (2001). Fragile X mice develop sensory hyperreactivity to auditory stimuli. Neuroscience *103*, 1043–1050.

Curia, G., Gualtieri, F., Bartolomeo, R., Vezzali, R., and Biagini, G. (2013). Resilience to audiogenic seizures is associated with p-ERK1/2 dephosphorylation in the subiculum of Fmr1 knockout mice. Front. Cell. Neurosci. *7*.

Danesh, A.A., and Kaf, W.A. (2012). DPOAEs and contralateral acoustic stimulation and their link to sound hypersensitivity in children with autism. International Journal of Audiology *51*, 345–352.

Dansie, L.E., Phommahaxay, K., Okusanya, A.G., Uwadia, J., Huang, M., Rotschafer, S.E., Razak, K.A., Ethell, D.W., and Ethell, I.M. (2013). Long-lasting Effects of Minocycline on Behavior in Young but not Adult Fragile X Mice. Neuroscience *246*.

Dölen, G., Osterweil, E., Rao, B.S.S., Smith, G.B., Auerbach, B.D., Chattarji, S., and Bear, M.F. (2007). Correction of Fragile X Syndrome in Mice. Neuron *56*, 955–962.

Garcia-Pino, E., Gessele, N., and Koch, U. (2017). Enhanced Excitatory Connectivity and Disturbed Sound Processing in the Auditory Brainstem of Fragile X Mice. J. Neurosci. 2310–2316.

Gibson, J.R., Bartley, A.F., Hays, S.A., and Huber, K.M. (2008). Imbalance of Neocortical Excitation and Inhibition and Altered UP States Reflect Network Hyperexcitability in the Mouse Model of Fragile X Syndrome. Journal of Neurophysiology *100*, 2615–2626.

Hinds, H.L., Ashley, C.T., Sutcliffe, J.S., Nelson, D.L., Warren, S.T., Housman, D.E., and Schalling, M. (1993). Tissue specific expression of FMR–1 provides evidence for a functional role in fragile X syndrome. Nat Genet *3*, 36–43.

Hitoglou, M., Ververi, A., Antoniadis, A., and Zafeiriou, D.I. (2010). Childhood Autism and Auditory System Abnormalities. Pediatric Neurology *42*, 309–314.

Kazdoba, T.M., Leach, P.T., Silverman, J.L., and Crawley, J.N. (2014). Modeling fragile X syndrome in the Fmr1 knockout mouse. Intractable Rare Dis Res *3*, 118–133.

Kesner, R.P. (1966). Subcortical mechanisms of audiogenic seizures. Experimental Neurology *15*, 192–205.

Knoth, I.S., Vannasing, P., Major, P., Michaud, J.L., and Lippé, S. (2014). Alterations of visual and auditory evoked potentials in fragile X syndrome. International Journal of Developmental Neuroscience *36*, 90–97.

Li, Y., Liu, H., Barta, C.L., Judge, P.D., Zhao, L., Zhang, W.J., Gong, S., Beisel, K.W., and He, D.Z.Z. (2016). Transcription Factors Expressed in Mouse Cochlear Inner and Outer Hair Cells. PLoS One *11*.

Lovelace, J.W., Wen, T.H., Reinhard, S., Hsu, M.S., Sidhu, H., Ethell, I.M., Binder, D.K., and Razak, K.A. (2016). Matrix metalloproteinase-9 deletion rescues auditory evoked potential habituation deficit in a mouse model of Fragile X Syndrome. Neurobiology of Disease *89*, 126–135.

Lovelace, J.W., Ethell, I.M., Binder, D.K., and Razak, K.A. (2018). Translation-relevant EEG phenotypes in a mouse model of Fragile X Syndrome. Neurobiology of Disease *115*, 39–48.

McCullagh, E.A., Salcedo, E., Huntsman, M.M., and Klug, A. (2017). Tonotopic alterations in inhibitory input to the medial nucleus of the trapezoid body in a mouse model of Fragile X syndrome. Journal of Comparative Neurology *525*, 3543–3562.

McRae, P.A., and Porter, B.E. (2012). The perineuronal net component of the extracellular matrix in plasticity and epilepsy. Neurochemistry International *61*, 963–972.

Michalon, A., Sidorov, M., Ballard, T.M., Ozmen, L., Spooren, W., Wettstein, J.G., Jaeschke, G., Bear, M.F., and Lindemann, L. (2012). Chronic Pharmacological mGlu5 Inhibition Corrects Fragile X in Adult Mice. Neuron *74*, 49–56.

Møller, A.R., Kern, J.K., and Grannemann, B.G. (2005). Are the non-classical auditory pathways involved in autism and PDD? Neurological Research *27*, 625–629.

Musumeci, S.A., Bosco, P., Calabrese, G., Bakker, C., De Sarro, G.B., Elia, M., Ferri, R., and Oostra, B.A. (2000). Audiogenic seizures susceptibility in transgenic mice with fragile X syndrome. Epilepsia *41*, 19–23.

Musumeci, S.A., Calabrese, G., Bonaccorso, C.M., D'Antoni, S., Brouwer, J.R., Bakker, C.E., Elia, M., Ferri, R., Nelson, D.L., Oostra, B.A., et al. (2007). Audiogenic seizure susceptibility is reduced in fragile X knockout mice after introduction of FMR1 transgenes. Experimental Neurology *203*, 233–240.

Orefice, L.L., Zimmerman, A.L., Chirila, A.M., Sleboda, S.J., Head, J.P., and Ginty, D.D. (2016). Peripheral Mechanosensory Neuron Dysfunction Underlies Tactile and Behavioral Deficits in Mouse Models of ASDs. Cell *166*, 299–313.

Osterweil, E.K., Chuang, S.-C., Chubykin, A.A., Sidorov, M., Bianchi, R., Wong, R.K.S., and Bear, M.F. (2013). Lovastatin Corrects Excess Protein Synthesis and Prevents Epileptogenesis in a Mouse Model of Fragile X Syndrome. Neuron *77*, 243–250.

Pacey, L.K.K., Heximer, S.P., and Hampson, D.R. (2009). Increased GABAB Receptor-Mediated Signaling Reduces the Susceptibility of Fragile X Knockout Mice to Audiogenic Seizures. Mol Pharmacol *76*, 18–24.

Pacey, L.K.K., Xuan, I.C.Y., Guan, S., Sussman, D., Henkelman, R.M., Chen, Y., Thomsen, C., and Hampson, D.R. (2013). Delayed myelination in a mouse model of fragile X syndrome. Hum Mol Genet *22*, 3920–3930.

Roberts, J., Hennon, E.A., Anderson, K., Roush, J., Gravel, J., Skinner, M., Misenheimer, J., and Reitz, P. (2005). Auditory Brainstem Responses in Young Males With Fragile X Syndrome. J Speech Lang Hear Res *48*, 494–500.

Rogers, S.J., Hepburn, S., and Wehner, E. (2003). Parent reports of sensory symptoms in toddlers with autism and those with other developmental disorders. J Autism Dev Disord *33*, 631–642.

Rotschafer, S., and Razak, K. (2013). Altered auditory processing in a mouse model of fragile X syndrome. Brain Research *1506*, 12–24.

Rotschafer, S.E., and Razak, K.A. (2014). Auditory Processing in Fragile X Syndrome. Front Cell Neurosci *8*.

Rotschafer, S.E., Marshak, S., and Cramer, K.S. (2015). Deletion of Fmr1 Alters Function and Synaptic Inputs in the Auditory Brainstem. PLoS One *10*.

Ruby, K., Falvey, K., and Kulesza, R.J. (2015). Abnormal neuronal morphology and neurochemistry in the auditory brainstem of Fmr1 knockout rats. Neuroscience *303*, 285–298.

Sakamoto, T., and Niki, H. (2001). Acoustic priming lowers the threshold for electrically induced seizures in mice inferior colliculus, but not in the deep layers of superior colliculus. Brain Research *898*, 358–363.

Schwaller, B., Tetko, I.V., Tandon, P., Silveira, D.C., Vreugdenhil, M., Henzi, T., Potier, M.-C., Celio, M.R., and Villa, A.E.P. (2004). Parvalbumin deficiency affects network properties resulting

in increased susceptibility to epileptic seizures. Molecular and Cellular Neuroscience *25*, 650–663.

Smith, A., Storti, S., Lukose, R., and Jr, R.J.K. (2019). Structural and Functional Aberrations of the Auditory Brainstem in Autism Spectrum Disorder. J Am Osteopath Assoc *119*, 41–50.

Smith, L.E., Barker, E.T., Seltzer, M.M., Abbeduto, L., and Greenberg, J.S. (2012). Behavioral Phenotype of Fragile X Syndrome in Adolescence and Adulthood. Am J Intellect Dev Disabil *117*, 1–17.

St. Clair, D.M., Blackwood, D.H.R., Oliver, C.J., and Dickens, P. (1987). P3 Abnormality in fragile X syndrome. Biological Psychiatry *22*, 303–312.

Strumbos, J.G., Brown, M.R., Kronengold, J., Polley, D.B., and Kaczmarek, L.K. (2010). Fragile X mental retardation protein is required for rapid experience-dependent regulation of the potassium channel Kv3.1b. J. Neurosci. *30*, 10263–10271.

Tharpe, A.M., Bess, F.H., Sladen, D.P., Schissel, H., Couch, S., and Schery, T. (2006). Auditory Characteristics of Children with Autism: Ear and Hearing *27*, 430–441.

Van der Molen, M.J.W., Van der Molen, M.W., Ridderinkhof, K.R., Hamel, B.C.J., Curfs, L.M.G., and Ramakers, G.J.A. (2012a). Auditory and visual cortical activity during selective attention in fragile X syndrome: A cascade of processing deficiencies. Clinical Neurophysiology *123*, 720–729.

Van der Molen, M.J.W., Van der Molen, M.W., Ridderinkhof, K.R., Hamel, B.C.J., Curfs, L.M.G., and Ramakers, G.J.A. (2012b). Auditory change detection in fragile X syndrome males: A brain potential study. Clinical Neurophysiology *123*, 1309–1318.

Wang, T., de Kok, L., Willemsen, R., Elgersma, Y., and Borst, J.G.G. (2015). In vivo synaptic transmission and morphology in mouse models of Tuberous sclerosis, Fragile X syndrome, Neurofibromatosis type 1, and Costello syndrome. Front. Cell. Neurosci. *9*.

Wang, Y., Sakano, H., Beebe, K., Brown, M.R., de Laat, R., Bothwell, M., Kulesza, R.J., and Rubel, E.W. (2014). Intense and specialized dendritic localization of the fragile X mental retardation protein in binaural brainstem neurons: A comparative study in the alligator, chicken, gerbil, and human. J. Comp. Neurol. *522*, 2107–2128.

Wen, T.H., Afroz, S., Reinhard, S.M., Palacios, A.R., Tapia, K., Binder, D.K., Razak, K.A., and Ethell, I.M. (2018). Genetic Reduction of Matrix Metalloproteinase-9 Promotes Formation of Perineuronal Nets Around Parvalbumin-Expressing Interneurons and Normalizes Auditory Cortex Responses in Developing Fmr1 Knock-Out Mice. Cereb Cortex *28*, 3951–3964.

Wen, T.H., Lovelace, J.W., Ethell, I.M., Binder, D.K., and Razak, K.A. (2019). Developmental Changes in EEG Phenotypes in a Mouse Model of Fragile X Syndrome. Neuroscience *398*, 126–143.

Wisniewski, K.E., Segan, S.M., Miezejeski, C.M., Sersen, E.A., and Rudelli, R.D. (1991). The fra(X) syndrome: Neurological, electrophysiological, and neuropathological abnormalities. Am. J. Med. Genet. *38*, 476–480.

Yan, Q.J., Asafo-Adjei, P.K., Arnold, H.M., Brown, R.E., and Bauchwitz, R.P. (2004). A phenotypic and molecular characterization of the fmr1-tm1Cgr Fragile X mouse. Genes, Brain and Behavior *3*, 337–359.

Yan, Q.J., Rammal, M., Tranfaglia, M., and Bauchwitz, R.P. (2005). Suppression of two major Fragile X Syndrome mouse model phenotypes by the mGluR5 antagonist MPEP. Neuropharmacology *49*, 1053–1066.

Chapter 4

Effects of noise-induced hearing loss on parvalbumin and perineuronal net expression in the mouse primary auditory cortex

4.1 Abstract

Noise induced hearing loss is associated with increased excitability in the central auditory system but the cellular correlates of such changes remain to be characterized. Here we tested the hypothesis that noise-induced hearing loss causes deterioration of perineuronal nets (PNNs) in the auditory cortex of mice. PNNs are specialized extracellular matrix components that commonly enwrap cortical parvalbumin (PV) containing GABAergic interneurons. Compared to somatosensory and visual cortex, relatively less is known about PV/PNN expression patterns in the primary auditory cortex (A1). Whether changes to cortical PNNs follow acoustic trauma remains unclear. The first aim of this study was to characterize PV/PNN expression in A1 of adult mice. PNNs increase excitability of PV+ inhibitory neurons and confer protection to these neurons against oxidative stress. Decreased PV/PNN expression may therefore lead to a reduction in cortical inhibition. The second aim of this study was to examine PV/PNN expression in superficial (I-IV) and deep cortical layers (V-VI) following noise trauma. Exposing mice to loud noise caused an increase in hearing threshold that lasted at least 30 days. PV and PNN expression in A1 was analyzed at 1, 10 and 30 days following the exposure. No significant changes were observed in the density of PV+, PNN+, or PV/PNN co-localized cells following hearing loss. However, a significant layer-and cell type-specific decrease in PNN intensity was seen following hearing loss. Some changes were present even at 1 day following noise exposure. Attenuation of PNN may contribute to changes in excitability in cortex following noise trauma. The regulation of PNN may open

up a temporal window for altered excitability in the adult brain that is then stabilized at a new and potentially pathological level such as in tinnitus.

4.2 Introduction

Even relatively brief exposure to loud noise can cause hearing loss or threshold shifts. Such noise-induced threshold shifts remain a common, but preventable, hearing disorder. Noise exposure may also lead to the development of tinnitus and hyperacusis (Roberts et al., 2010). Several lines of evidence suggest that noise exposure increases excitability in the central auditory system perhaps as a consequence of damage to cochlear hair cells and the resulting reduction in afferent input. This compensatory increase in gain manifests across the auditory neuraxis and occurs over multiple and overlapping temporal trajectories suggesting complex underlying mechanisms (Berger and Coomber, 2015; Eggermont, 2015; Luo et al., 2017; Pilati et al., 2012; Syka and Rybalko, 2000; Syka et al., 1994; reviewed in Wang et al., 2011; Yang et al., 2011, 2012). The cellular correlates of these changes in excitability are not well characterized. One prominent hypothesis for noise-induced increase in excitability in the primary auditory cortex (A1) is reduced inhibition (Llano et al., 2012; Syka and Rybalko, 2000; Yang et al., 2011). While physiological studies have characterized synaptic inhibition and how inhibition changes following noise exposure, the cellular substrates that are altered are only beginning to be understood (Novák et al., 2016; Scholl and Wehr, 2008). Inhibitory

interneurons in sensory cortices can be classified based on co-expression of various markers and physiological response properties. Novak et al., (2016) showed that cortical somatostatin and parvalbumin-expressing (PV+) interneurons show relatively fast and layer specific changes in activity following noise trauma potentially leading to increased gain. Whether changes in responses of these cells are associated with circuit level or intrinsic factors remain unclear. The present study focused on perineuronal nets (PNN), a cellular structure commonly found around GABAergic cells (reviewed in Takesian and Hensch, 2013). PNNs are specialized extracellular matrix components that consist of chondroitin sulfate proteoglycans (CSPG). These CSPGs are found throughout the extra-cellular matrix, but are highly dense around cortical PV+ inhibitory interneurons (McRae et al., 2007). While PV/PNN expression has been well studied in somatosensory and visual cortex of rodents, focus on A1 is relatively recent and sparse (Brewton et al., 2016; Fader et al., 2016; Happel et al., 2014; reviewed in Sonntag et al., 2015). PNNs are involved with developmental and adult plasticity (Happel et al., 2014; Nakamura et al., 2009; Pizzorusso et al., 2002a) and provide protection against oxidative stress for PV+ cells (Cabungcal et al., 2013). These data suggest that changes in PNN expression following acoustic trauma may contribute to cortical plasticity leading to increased excitability. A loss of PNNs may decrease excitability of PV+ interneurons and thus reduce inhibition in the cortical circuit (Balmer, 2016). Therefore, the main aim of this study was to quantify cortical PNN expression following acoustic trauma that induces persistent threshold shifts. We report here that noise exposure does not change the

density of PV+, PNN+ or PV/PNN co-localized cells. However, PNN intensity is reduced in a cortical layer-and cell-type specific manner. The effect of trauma on PNN intensity appears to be relatively more severe on PNN cells that do not express PV. Some changes are seen even at the earliest examined time point (1 day post-exposure). These data suggest that altered PNN properties may be at least one of the cellular mechanisms involved in enhanced excitability of cortical neurons following acoustic trauma.

4.3 Material and methods

4.3.1 Animals

All animal procedures were approved by the University of California, Riverside Institution Animal Use and Care Committee. Female CBA/CaJ mice at 4 weeks old were received from Jackson Laboratory and housed at a 12:12 light/dark cycle. Standard lab chow and water were given *ad libitum*. All animals were housed in the same room except for the noise exposure and auditory brain-stem response (ABR) measurements. Each of the four groups (control and 1, 10, and 30 days post-exposure) consisted of n=5 mice.

4.3.2 Noise-induced hearing loss paradigm

Noise exposure was done in a sound-attenuating booth (Gretch-Ken, OR). Mice were placed in a standard cage and were able to freely move during the duration of the exposure to noise. A Fostex96TX speaker was placed facing down on top of the cage's lid. The sound stimulus used was a 102-104 dB SPL, narrowband noise (6-12 kHz) for 8 h.

No food or water was provided during the duration of the exposure to noise. The control mice spent the same amount of time in the sound-attenuating booth, but did not receive noise exposure.

4.3.3 Auditory brainstem response (ABR)

Animals were anesthetized with isoflurane inhalation for the duration of the ABR procedure at a concentration of 0.5-0.75% in air. Three platinum coated electrodes were placed under the dermis of the head: the recording electrode was on the vertex, the ground electrode was in the left cheek and the reference electrode was in the right cheek. The sound stimuli were delivered via a free field speaker (MR1 Multi-Field Magnetic Speakers, Tucker-Davis Technologies) that was placed 10 cm away from the left ear at 45° angle. Clicks of alternating ±1.4 V (duration 0.1 ms) were generated and delivered using RZ6 hardware (Tucker-Davis Technologies, FL). Intensity of the clicks ranged from 10 to 90 dB in 10 dB steps. The goal of the ABR measurement was to determine if threshold shifts occurred following noise exposure and to ensure that such shifts lasted at least 30 days. The goal was not to identify precise frequency-specific hearing levels over the course of the experiments. There-fore, clicks with a sound level resolution of 10 dB steps were used for threshold measures. The ABRs were filtered and amplified (Grass Technologies) and averaged (BioSigRZ, Tucker-Davis Technologies) before analysis. The ABR measurements were made on all mice before exposure to noise and after the noise exposure at 1 day,10 days and 30 days post-exposure (PE).

ABRs from control mice were also measured at the same four time points referenced to when they were placed in the sound booth without noise exposure.

4.3.4 Immunohistochemistry and image analysis

Mice were overdosed with sodium pentobarbital (i.p. 125 mg/kg) and perfused transcardially with cold solutions of 0.1 M phosphate buffered saline (PBS) (pH=7.4) followed by 4% paraformaldehyde (PFA) (pH=7.4). Mice were perfused for each time point (1, 10, and 30 days) post-exposure (PE) to noise. The control mice were perfused along with the 30-day PE mice. The brains were extracted from the skull and post-fixed at 20 ℃ in 4% PFA for 2 h before storage in 0.1 M PBS with sodium azide. Brain tissues were sunk in 30% sucrose for 24-48 h and coronal sections of 40mmthickness were cut with a cryostat (CM 1860, Leica Biosystems).Three to six sections containing A1 were stained and analyzed per mouse. The distance between the sections was between 40 and 480mm. It is possible that there is differential penetration of PV and WFA antibody in the 40mm thick sections. However, because our main aim was to determine how noise exposure alters PV/PNN expression, the comparison across experimental groups is unlikely to be influenced by differential antibody penetration. All immunohistochemistry was done on a shaker at room temperature unless stated otherwise. Free floating sections were washed at room temperature with 0.1 M PBS 2x for 15 min then quenched with 50 mM of NH4Cl for 15 min and then washed with 0.1 M PBS 3x for 10 min. Next, the sections were permeablized with 0.1% triton-x for10 min. Sections

incubated in blocking solution consisting of 5% normal goat serum (NGS) and 1% bovine serum albumin (BSA; Fisher BioReagents Bovine Serum Albumin, Fraction V, Cold-ethanol Precipitated; BP1605-100) in 0.1 M PBS for 1 h. The sections were then incubated overnight at 20℃ in 1% NGS, 0.5% BSA0.1% Tween-20, 1:500 agglutinin Wisteria floribunda (fluorescein conjugated, FL-1351, Vector Laboratories) and 1:5000 rabbit anti-parvalbumin (PV-25, Swant). Sections were washed with 0.5%Tween-20 3for 10 min and incubated in secondary antibody solution consisted of 1:500 donkey anti-rabbit 647 (A-31573, Life Technologies) in 0.1 M PBS. The sections were then washed with0.5% Tween-20 2for 10 min and with 0.1 M PBS for 10 min, mounted on a glass slide and allowed to air dry. The slides were cover-slipped with the mounting medium, Vectashield containing DAPI (Vector Laboratories), and the edges of the coverslip were sealed (Cytoseal 60, Richard-Allan Scientific). The location of A1 was identified as previously described by (Martin del Campo et al., 2012). In this previous study, electro-physiological mapping was used to identify tonotopy in both A1 and anterior auditory field (AAF). The boundary between A1 and AAF was identified using the reversal of tonotopy (Trujillo et al., 2011) and was marked with a dye. Coronal sections with the identified boundary were compared with sections in Paxinos mouse brain atlas. This provided the landmarks (primarily hippocampal shape) to identify A1 sections used in the present study. One challenge is that the reversal of tonotopy from A1 to AAF is not sharp. Therefore, it is possible that some of the sections analyzed include AAF. However, identical landmarks were used across experimental groups and all analyses were done

blind to the experimental group. Sections containing A1 were imaged using a confocal micro-scope (TCS SP5, Leica Microsystems) at 20. The number of PV and PNN cells from summed z-stacks were counted in A1 from a 400mmwide area across layers I-VI. The area from the pia to 50% of the cortical depth was defined as layers I-IV and from 50% depth to the white matter was defined as layer V-VI (Anderson et al., 2009). We were unable to differentiate layers more specifically because the layer boundary between layers III and IV or between V and VI cannot be distinguished with accuracy using Nissl stains. Images of PV and PNN were encoded and an experimenter blinded to the identity of the groups performed the cell counts. PNN cells were manually identified by discernible WFA staining that is circular with a hollow center. PV cells were manually identified based on the shape and size of staining. There was very little background PV staining with this protocol, facilitating identification of cells. Only cell bodies that were fully within the borders of the counting window were included in the tally.

4.3.5 Data analysis

Three aspects of PV/PNN expression were compared across the four groups (control, 1, 10 and 30 day post exposure): the density of PV/PNN expression, the overall PNN intensity across the 6 layers and the PNN intensity around cells. Cell counts and intensity measurements were obtained with ImageJ software (NIH). The number of PV+, PNN+, and co-localized (PV/PNN) cells were counted across all 6 cortical layers. The total area of the cortex was then used to calculate cell densities (cells/mm2) of each cell type.

Deterioration of PNN intensity following enzymatic PNN degradation can result in reduced excitability of PV+ neurons (Balmer, 2016). The effects of PNN deterioration may occur even without a loss of PNN+ cell density (Enwright et al., 2016). There-fore, we quantified PNN intensity following acoustic trauma. To determine the PNN intensity, a rectangle (width of 400mm and depth extending from pia to bottom of layer VI) was first drawn on the image of the cortical section (e.g., Fig. 2A and B). The average PNN intensity within the rectangle was determined as the average of all pixel intensity value in the PNN color channel. The back-ground intensity was subtracted from each image for PNN intensity analysis. Background was defined as the average pixel intensity of a4040mm area in layer 1 where there is very little PNN (Brewton et al., 2016).We also analyzed PNN intensity in the region around individual PNN cells. For this cellular PNN intensity analysis, 30% of the PNNs in each imaged A1 section were randomly (random number generator) selected. If 30% was less than 12 PNN cells, then a minimum of 12 cells was analyzed. A 40mm (66 pixels) horizontal line was drawn across the middle of the PNN surrounding each analyzed cell. The pixel intensity was plotted as a function of distance along this line. This resulted in a bimodal peaked plot (e.g., Fig. 7) with the two peaks corresponding to the locations where the line intersected the most intense part of the PNN ring structure on both sides of the cell. The area under the curve for each PNN analyzed was averaged within each image. The specific statistical tests used are reported in the results section below.

4.4 Results

4.4.1 Noise exposure causes persistent threshold shift

ABR measurement before and after noise exposure was used to quantify hearing threshold shifts. ABR measurements were made in response to clicks of 0.1 ms duration with intensities of 10e90 dB in10 dB steps. The threshold was the lowest sound level at which at least 1 peak was discernible within 7 ms from sound onset. In the example series of ABR plots from a control mouse (Fig. 1A), the threshold was between 30 and 40 dB SPL. The noise-exposed mouse (Fig. 1B) had a hearing threshold >90 dB SPL (the highest level tested in this study). The thresholds before noise exposure across all the mice in this study were in the 30-50 dB SPL range, consistent with previous ABR measurements in the mouse (Zhou et al., 2006). Change in threshold following noise exposure was quantified at 1 day (n=5 mice), 10 days (n=5 mice) and 30 days (n=5 mice) after exposure. The control mice (n=5) also had their ABRs measured at each of the same time points. The thresholds, except for one mouse, were fairly constant in the control mice across multiple days (Fig. 1C). Even in the mouse that showed increased variability across days, the threshold never exceeded50 dB SPL. Noise exposure caused an increase in threshold to >90 dB SPL at all three PE time points (Fig. 1D-F) indicating that hearing loss lasted at least 30 days PE in the noise exposed mice.

4.4.2 Expression of PV and PNN in the mouse A1

Parvalbumin and PNN expression in A1 was quantified in control and noise-exposed mice. Fig. 2A shows a photomicrograph of a coronal section through A1 from a control mouse. The area within the white rectangle is reproduced in Fig. 2B and shows the window within which the various measurements were made in this image. Fig. 2C, D, E show example PV+, PNN+ and PV/PNN co-localized neuron, respectively (arrows in Fig. 2B). Qualitative observations indicate that PV and PNN staining was essentially absent in layer I while layer II contains PV cells, but very little PNN. Consistent with Brewton et al. (2016), PNN was concentrated in layers IV-VI of A1, particularly in layer IV in which a band of cellular and neuropil staining was seen (Fig. 2B). Fig. 3 shows example photomicrographs obtained from PE mouse cortex. Qualitatively the distribution of cell types in the PE mice was similar to control A1. Quantification of control and PE cell density data are shown in Fig. 4. In control A1, there were more PNN+ cells than PV+ cells (paired two-tail t-test, $t(df)=5.925$ $p<0.0001$, $R2=0.5563$). This was true in both superficial (I-IV) and deep (V-VI) layers. A strong association between PV and PNN cells has been reported in several brain regions (Sonntag et al., 2015). Therefore, the percentage of PV+ cells that was enwrapped by PNN was calculated in A1. Approximately 46% (±0.0215 s.e.) of PV+ cells also expressed PNN in control A1. There was no difference in the percentage of PV/PNN co-localized cells between the deep and superficial layers in controlA1 (paired two-tail t-test, $t(df)=0.31$, $p=0.75$, $R2=0.003$). These data provide baseline quantification of PV/PNN expression in A1 in the control

adult CBA/CaJ mice. Persistent threshold shift does not alter the density of PV+ and PNN+ cells in A1 after noise induced hearing loss. There were no significant differences between groups in layers I-VI for PV+ (1-wayANOVA, $F(3,119)=1.06$, $p=0.37$), PNN+ (1-way ANOVA, $F(3,119)=2.57$, $p=0.08$) or PV/PNN co-localized (1-way ANOVA$F(3,119)=0.59$, $p=0.63$) cell densities. There were no differences in the density of PV+ cells in either layers I-IV or V-VI (1-way ANOVA, $F(3,119)=0.89$, $p=0.45$, $F(3,119)=0.87$, $p=0.46$, respectively). There were no significant differences in PNN+ cell density in layers I-IV (1-way ANOVA, $F(3,119)=1.178$, $p=0.3211$). A trend was seen for PNN+ cell density to be reduced in layers V-VI following noise exposure (1-way ANOVA, $F(3,119)=2.696$, $p=0.05$). The decrease in PNN+ cells density in layers I-VI ($p=0.08$), and specifically inlayers V-VI ($p=0.05$) approach statistical significance. However, we interpret these data conservatively as no significant difference with the acknowledgement that a moderate risk for type II error may be present in this interpretation. There were no significant differences in PV/PNN co-localized cell density in layers I-IV or V-VI (1-way ANOVA, $F(3,119)=0.5178$, $p=0.6708$, $F(3,119)=0.5796$, $p=0.6295$, respectively). There was also no significant differences in the percentage of PV+ cells that co-expressed PNN between the different groups (1-way ANOVA, $F(3,119)=2.063$, $p=0.1088$). Previous studies suggest that a decline in PNN intensity may reflect changes in PNN organization. This change in PNN intensity may occur independent of changes in PNN+ cell density (Balmer, 2016; Carulli et al., 2010; Enwright et al., 2016). Therefore, we compared A1 PNN intensity between control and PE mice.

Example photomicrographs of PNN are shown in Fig. 5. First, the average pixel intensity across the entire rectangle (400mm wide, pia to bottom of layer VI depth) was determined. A significant decrease in the average pixel intensity of PNN across A1 was seen following acoustic trauma (2-way ANOVA, main effect of Layer $F(1,226)=10.18$, $p=0.0016$, main effect of Group $F(3,226)=9.9338$, $p<0.0001$, interaction of Group x Layers $F(3,226)=2.168$, $p=0.0927$). When considering all 6 layers together, a significant decrease in PNN pixel intensity was observed at 1 and 10 day PE (1-way ANOVA, $F(3,230)=8.835$, $p<0.0001$, $R2=0.1033$ with Bonferroni post-hoc Control vs 1 Day PE $p<0.001$, Control vs 10 Day PE $p<0.001$, 10 Days PE vs. 30 Days PE, $p<0.05$; other pairs, $p>0.05$) (Fig. 6A). This indicates a decrease in PNN intensity even at 1 day PE. Interestingly, at day 30 PE, the intensity was similar to control levels suggesting a recovery. Layer-specific analysis shows that layer I-IV shows a decline in PNN intensity at each PE time point with no recovery (1-way ANOVA, $p=0.0001$, Bonferroni tests: Control vs. 1 Day PE, $p<0.001$; Control vs.10 Days PE, $p<0.01$; Control vs. 30 Days PE; $p<0.05$, other pairs, $p>0.05$)). Layer V-VI shows a declining in PNN intensity only at 10 day PE with recovery at 30 day PE (1-way ANOVA, $F(3,113)=4.623$, $p=0.004$, Bonferroni tests: Control vs. 10 Days PE, $p<0.05$; 10 Days PE vs. 30 Days PE; $p<0.05$, other pairs, $p>0.05$). Thus, the return of PNN intensity to control levels may be carried by changes in the deeper layers. Together these data indicate a relatively rapid and layer-specific decrease in PNN intensity in A1 following noise induced hearing loss. While the above analysis provides information about PNNs across the entire depth of A1, studies of

epileptogenesis and songbird brain development (Balmer et al., 2009; Dityatev et al., 2007) have suggested the integrity of PNN around the cell may provide additional markers of changes to PNN with functional consequences. Therefore, we analyzed PNN intensity in the region around individual cells. Fig. 7 shows examples of how such measurements were made. A 40mm line was centered on the PNN and the pixel intensity along this line was measured. The two peaks correspond to the regions of maximum cellular PNN intensity. The area under the curve was measured for 30% of randomly selected PNN+ cells, averaged across cells and compared across treatment conditions. The PNN intensity around cells in layers I-VI declined significantly following noise induced hearing loss (Fig. 8A). The decline was significant at 10 and 30 days PE exposure (1-way ANOVA $F(3,400)=8.753$, $p<0.0001$, $R2=0.0616$, Bonferroni post-hoc: Control vs 10 Days PE, $P<0.001$, Control vs 30 Days PE, $P<0.05$). Layer specific analysis indicates that there was a decline in layers I-IV that was significant at all PE days (1-way ANOVA $F(3,204)=6.402$, $p=0.0004$, $R2=0.08605$ with Bonferroni post-hoc: Control vs 1 Day PE, $P<0.05$, Control vs 10 Days PE $P<0.01$, Control vs 30 Days PE, $P<0.001$) (Fig. 8B). For layers V-VI cells, PNN intensity showed a significant decline only at 30 days PE (1-way ANOVA $F(3,192)=3.778$, $P=0.001$, $R2=0.078$ with Bonferroni post-hoc: Control vs 30 Days PE, $P<0.05$, all other pairs $P>0.05$) (Fig. 8B and C). There was no significant interaction between groups and layers (two-way ANOVA $F(3,396)=2.18$, $p=0.09$).The cellular analysis method also allows examination of whether PNN intensity changes are cell-type specific. Here we examined if PV/PNN co-localized cells were more or less

susceptible to noise exposure compared to PNN+ cells that did not have PV (Fig. 8C). For the PV/PNN co-localized cells, a significant effect of noise exposure was observed only at 30 day PE (1-way ANOVA $F(3,191)=3.778$, $p=0.0115$, $R2=0.05601$ with Bonferroni post-hoc: Control vs 30 Days PE, $p<0.05$, all others $P>0.05$), whereas the PNN cells without PV showed significantly attenuated intensity at both 10 and 30 days PE (1-way ANOVA $F(3,205)=5.930$, $P=0.0007$, $R2=0.0799$ with Bonferroni post-hoc: Control vs 1 Day PE, $P>0.05$, Control vs 10 Days PE, $P<0.01$, Control vs 30 Days PE, $P<0.01$). There was no significant interaction between group and cell type (2-way ANOVA interaction of Group x Cell Type $F(3,396)=0.59$, $P=0.62$).

4.4.3 Additional analyses

The previous analyses used individual sections as independent samples because the sections likely covered different isofrequency contours in A1. A second analysis was performed by averaging data from all sections from each mouse and using the animal number as sample size. Although this analysis is underpowered (n=5 mice per group), the interpretation that PNN intensity declines after noise exposure was supported. One-way ANOVA showed a significant decline in overall PNN intensity across layers I-VI (Fig. 6A) following noise exposure ($F(3,16)=3.3$, $P<0.05$) with post-hoc comparison showing a significant difference between control and10 Days PE ($P<0.05$). Layer-specific analyses reveals superficial layers to be more impacted than deep layers. In layer I-IV, overall PNN intensity (Fig. 6B) declined following noise exposure (one-way ANOVA,

F(3,16)=3.24, P<0.05) with post-hoc comparison showing all three noise exposure groups significantly different than control. In layer V-VI, however, there was no difference (one-way ANOVA, F(3,16)=1.63, P>0.5). When cellular PNN intensities were considered (Fig. 8), there was a trend when all six layers were considered (one-way ANOVA, F(3,16=2.6, P=0.08)). Cellular PNN intensity showed a strong trend towards exposure-related decline in both layers I-IV (one-way ANOVA, F(3,16)=2.87, P=0.06) and V-VI (one-way ANOVA, F(3,16)=2.97, P=0.06) with the control mice different than 10 and 30 days post exposure mice (P<0.05). Taken together, these data show that PNN intensity in auditory cortex declines following noise exposure.

4.5 Discussion

This study quantified the distribution of PV/PNN staining in primary auditory cortex of adult CBA strain mice, a commonly used strain to study auditory processing. We quantified the effects of persistent hearing threshold shifts on the expression of PV/PNN inA1. Consistent with previous studies of the auditory cortex (Brewton et al., 2016; Happel et al., 2014), approximately 45% of PV+ neurons in A1 are wrapped by PNNs. We tested the hypothesis that noise induced hearing loss will cause a deterioration of PNN. We show that the density of PV/PNN expressing cells does not change up to at least 30 days PE, but the intensity of PNN staining across the cortical depth and in regions around individual cells shows a relatively rapid decline following

acoustic trauma. These data have implications for involvement of cell-type specific changes in A1 following acoustic trauma that may lead to increased gain.

4.5.1 PV/PNN expression in the primary auditory cortex

Although the expression of PNN and its association with specific cell types have been well characterized in rodent visual and somatosensory cortex (Liu et al., 2013; McRae et al., 2007; Pizzorusso et al., 2002b; Takesian and Hensch, 2013) and subcortical auditory areas (Beebe et al., 2016), the expression pattern in A1 has only recently been studied (Brewton et al., 2016; Happel et al., 2014; reviewed in Sonntag et al., 2015). There is a higher density of PNN cells in layers IV-VI with a band like appearance of cellular and neuropil staining in layer IV. These data are consistent with observations made in rodent primary sensory cortices including A1 (Brewton et al., 2016; Brückner et al., 1994; Fader et al., 2016; Happel et al., 2014). The density of PNN reported here is larger than that reported by Fader et al. (2016) and Brewton et al. (2016), but is similar to that reported by Happel et al. (2014). These differences may arise due to strain differences and/or thresholds used for counting PNN. The density of PV+ cells is similar to previous reports of mouse A1 (Martin del Campo et al., 2012). The relatively strong association of PV and PNN (~45% of PV+ cells express PNN) in A1 is consistent with observations made in other brain regions (Celio, 1993; Kosaka and Heizmann, 1989; Liu et al., 2013; Pantazopoulos et al., 2006; Yamada et al., 2015). The observation that a significant percent of PV+ cells were not covered by PNN and that PNN covered many

cells that did not express PV indicate the need for future studies of A1 to identify the distribution of various cells types with PNN.

4.5.2 Effect of hearing loss on PV/PNN expression

The main aim of the study was to determine if acoustic trauma that produces long lasting increase in hearing threshold affected expression of PV/PNN in A1. The noise exposure method used in this study effectively increased hearing thresholds from <50 dB SPL pre-exposure to >90 dB SPL post-exposure. This hearing loss lasted at least 30 days suggesting a relatively persistent effect. The data did not support the hypothesis that this level of hearing loss will decrease the density of PV, PNN and/or PV/PNN double-labeled cells in A1. However, a significant layer- and cell type-specific decrease in PNN intensity was seen in the noise-exposed groups. In superficial layers (I-IV), the decline was seen even at 1 day PE. In the deep layers, a recovery of PNN intensity was observed between10 and 30 days PE. PNN cells with PV showed a decline in intensity only 30 days PE, whereas, PNN cells that did not express PV showed significant decline at 10 and 30 day PE. This suggests that PV may afford some degree of protection to PNN expression. We interpret the changes in PNN intensity to be driven by hearing loss. This interpretation has to be considered with the caveat that other areas in the cortex that are less likely to be affected by the noise trauma were not examined for PNN changes. Considerable focus has been allocated to identifying the contributions of PNNs to developmental and adult plasticity. Strong evidence suggests that PNNs provide stability

to the excitation-inhibition balance and adult plasticity can be promoted by breaking down PNNs (Happel et al., 2014; Takesian and Hensch, 2013). However, surprisingly little is known about the contribution of PNNs to the response properties of neurons they cover (Balmer, 2016). It is clear that cortical PNNs surround mostly GABAergic neurons with preference for PV+ neurons. This suggests that PNNs influence inhibition generated by fast spiking interneurons within cortical circuits. The differences between firing properties of cortical interneurons that are covered with PNN compared with those that are not remains unclear (Dityatev et al., 2007). A recent study suggests that PNN increases excitability of fast-spiking, PV+ cortical cells (Balmer, 2016). Because cortical PV+ cells are mostly inhibitory, these data indicate that deterioration of PNNs may increase network excitability. A few studies have suggested that PNNs may provide protection against oxidative stress related cell death (Cabungcal et al., 2013) and also impact the expression of PV in GABAergic cells. This is again mainly relevant for fast spiking interneurons. Integrating available data from the literature, the present study makes the suggestion that acoustic trauma causes an attenuation of PNN intensity that opens up the circuitry for changes in excitation-inhibition balance. Such acoustic experience dependent changes in PNN intensity without a change in the density of PNN expressing cells have been previously re-ported in songbird vocal learning circuits (Balmer et al., 2009). Mature PNNs contain several CSPGs in addition to hyaluronan, tenascin-C and high amounts of tenascin-R, hyaluronan synthase and link proteins (Ctrl1). The reduction in PNN intensity may reflect changes in CSPG protein levels and

composition and/or hyaluronan synthase and/or link protein levels. Changes in inhibition following noise exposure may be one of the steps in causing an increase in gain and potentially, pathological activity (e.g., tinnitus). Evidence for such pathology correlated with changes in PNN comes from studies of epileptogenesis (Dityatev, 2010; McRae et al., 2012). Decline of PNN intensity in superficial layers even within 1 day PE suggests that this may be one of the first steps of cortical structural change. The recovery of PNN intensity to control levels at 30 day PE suggests the presence of a window following trauma during which circuit plasticity may occur and be stabilized at a new homeostatically adjusted level. However, future experiments that look at additional time points are needed to determine if there is a sustained recovery. The events leading up to the decline in PNN intensity may include changes to matrix metalloproteases (MMP) and cartilage link proteins (e.g., Ctrl1). MMP-9 is an endopeptidase that cleaves extracellular matrix including PNN. MMP-9 levels are regulated by activity and high MMP-9 levels lead to increased breakdown of PNN. This suggests the hypothesis that MMP-9 levels increase within 1 day of noise exposure. This hypothesis remains to be tested. Carulli et al., 2010 showed that mice lacking Ctrl1, a PNN component, show attenuated PNNs including reduced intensity. The attenuated PNN promoted cortical plasticity in adults. Thus future studies of A1 following acoustic trauma should analyze expression levels of MMP-9 and Ctrl1 at specific time points after exposure.

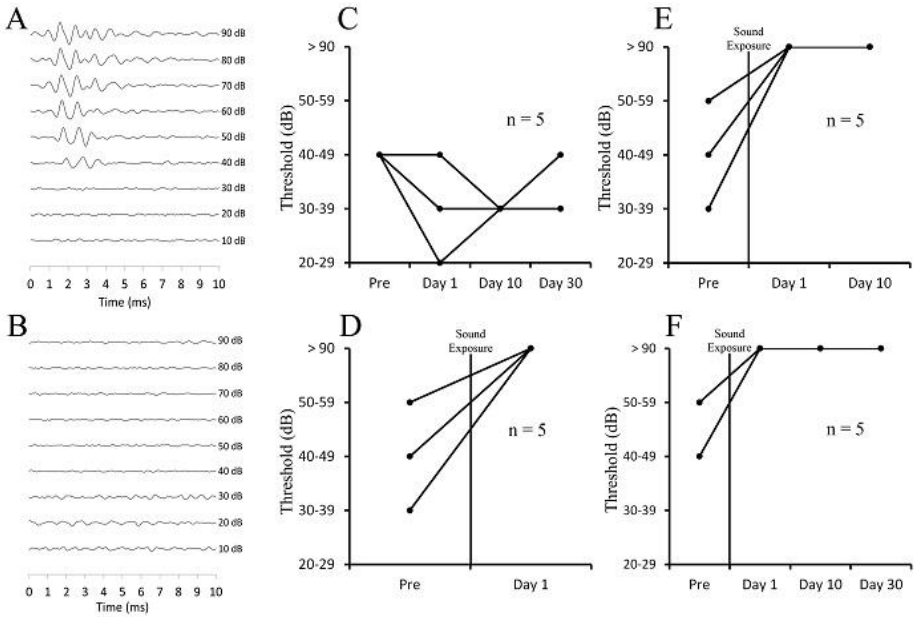

Figure 1: ABRs show that noise exposure caused considerable increase in hearing thresholds that lasted at least 30 days. (A) Example waveforms from a control mouse and (B) after 30days following noise exposure. ABR thresholds were determined using sound level steps of 10 dB SPL. The hearing threshold for the control mouse in (A) was therefore noted to be between 30 and 40 dB SPL. The noise-exposed mouse (B) did not show any ABR up to 90 dB SPL (the highest level tested). (C-F) The hearing threshold of each mouse at specified time points is shown. The symbols within a sound level bin (ordinate) are jittered for visualization purposes. N¼5 for each group. (C) The thresholds in control mice remain at<50 dB SPL throughout the course of 30 days. (D, E, F) Post exposure, the thresholds increased to>90 dB SPL (the highest level tested), indicating threshold shifts that lasted at least30 days PE.

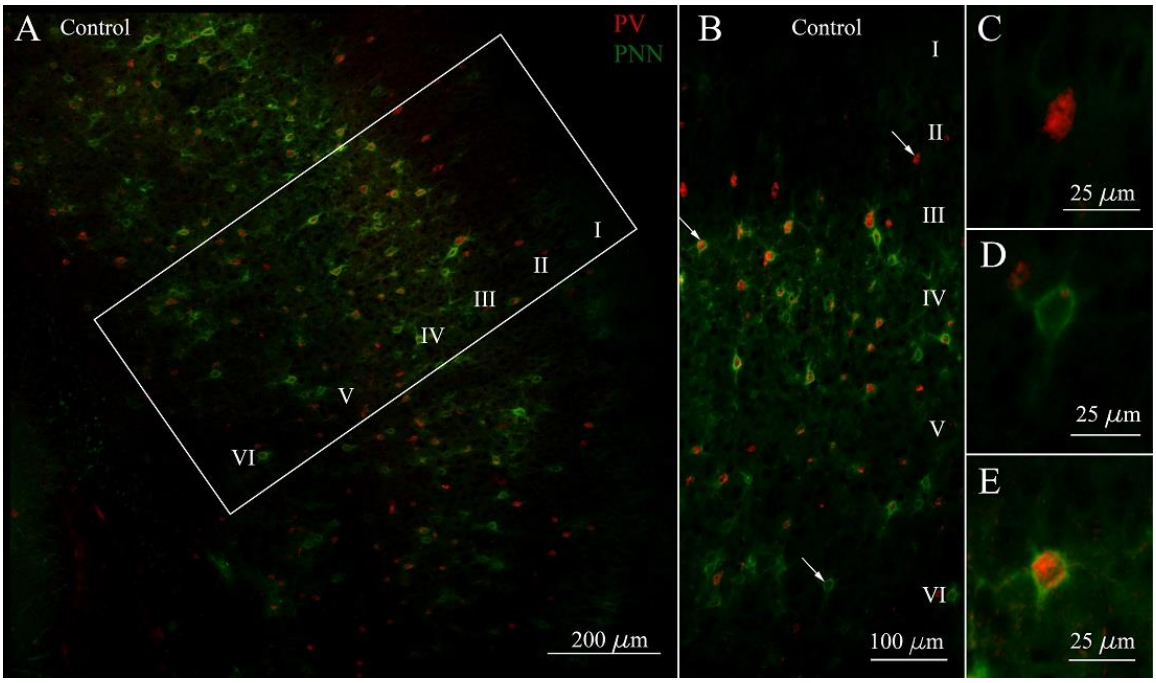

Figure 2: (A) Example photomicrograph of a coronal section through A1 stained for PV (red) and PNN (green) in a control mouse. The white rectangle indicates the 400mm wide window in A1 within which PV, PNN and co-labeled cells were quantified from this image. This rectangle is reproduced in (B) which shows that PV and PNN stained cells are present at a higher density in layers IV-VI compared to layers I-III. The highest density of PNN staining was seen in layer IV in which a banded pattern of cellular and neuropil staining was observed. Arrows point to examples of different cell types that are then shown in C, D, E. (C) PV cell without PNN, (D) PNN cell without PV, and (E) PV/PNN co-localized cell.

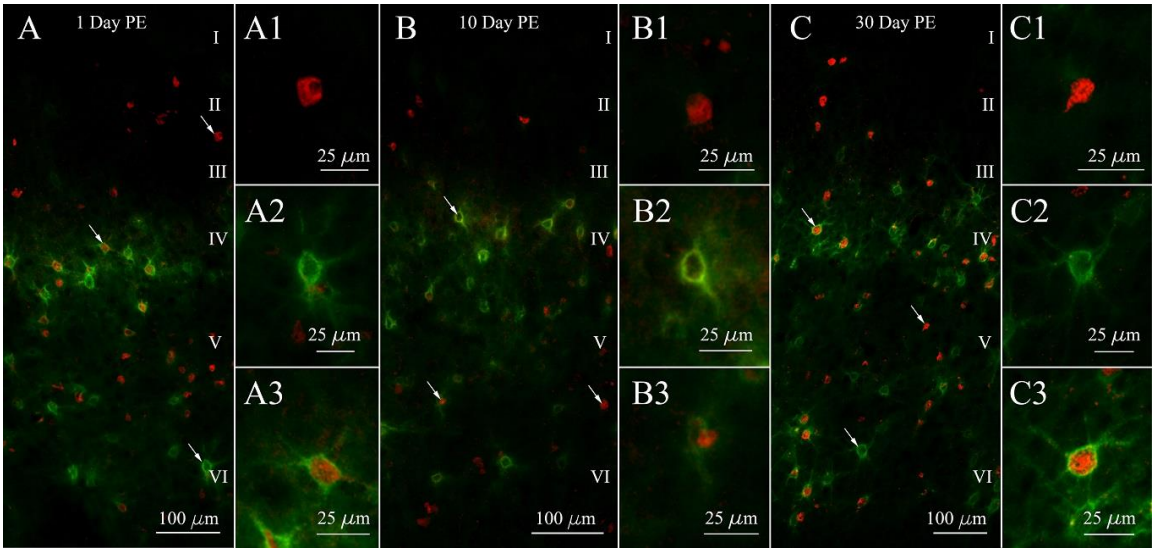

Figure 3: Photomicrographs of PV and PNN expression in the experimental groups. Arrows indicate the cells shown at a higher magnification in the insets: (A) 1 day PE, (B) 10 days PE, (C) 30 days PE. (A1, B1, C1) PV without PNN. (A2, B2, C2) PNN without PV and (A3, B3, C3) PV/PNN co-localized cells.

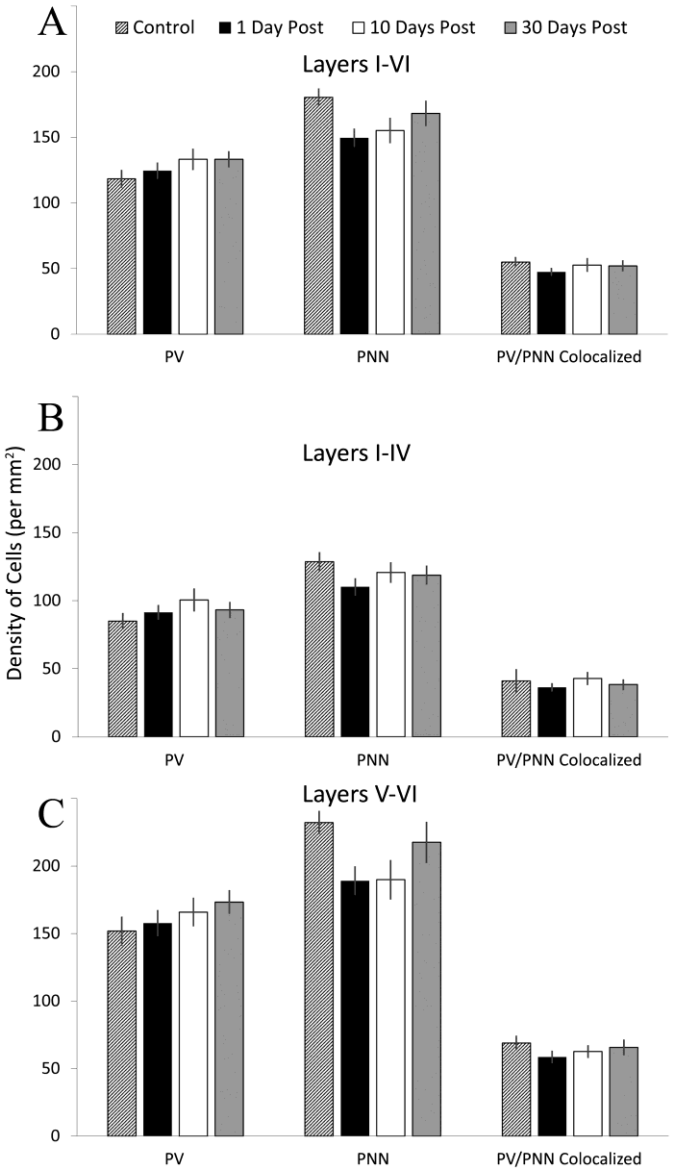

Figure 4: PV+ and PNN+ cell density in (A) layers I-VI, (B) layers I-IV and (C) layers V-VI before and 1, 10 and 30 day PE. There was no statistically significant difference in the density of stained cells following noise exposure.

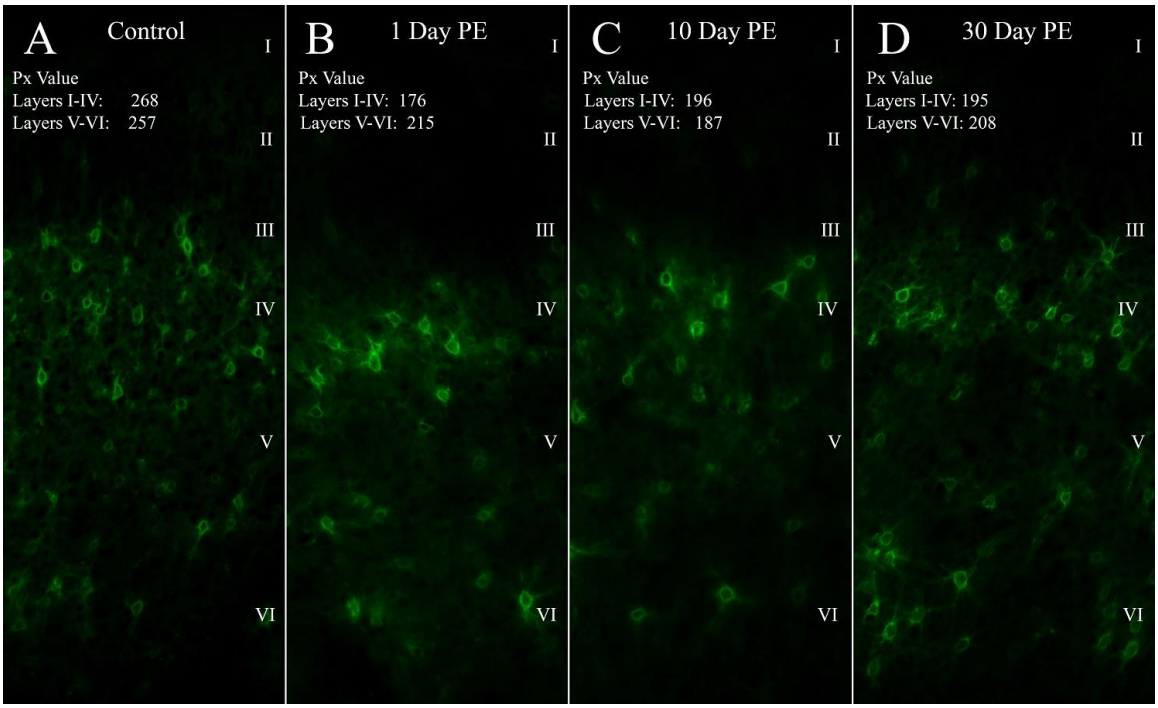

Figure 5: Example photomicrographs from the control and experimental groups from which PNN intensity was measured. Control (A) and 1 (B), 10 (C) and 30 (D) days after noise exposure.

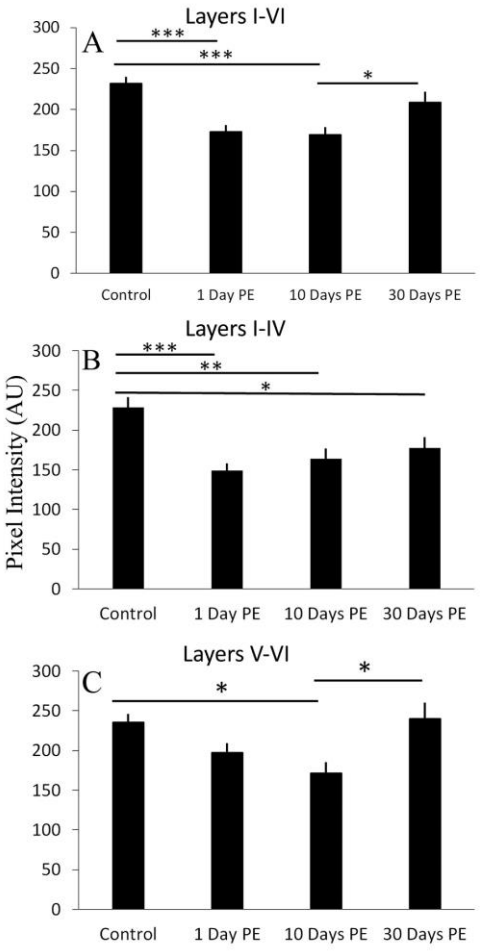

Figure 6: Decline in PNN intensity in A1 following noise exposure. (A) In all layers combined, there is a decrease in PNN intensity at 1 day PE and 10 days PE and a return to control levels at 30 day PE. (B) There is a decrease in PNN intensity in layers I-IV at 1day PE, 10 days PE and 30 days PE compared to controls (C) There is a significant decrease in PNN intensity in layers V-VI at 10 days PE followed by a significant increase by 30 days PE.

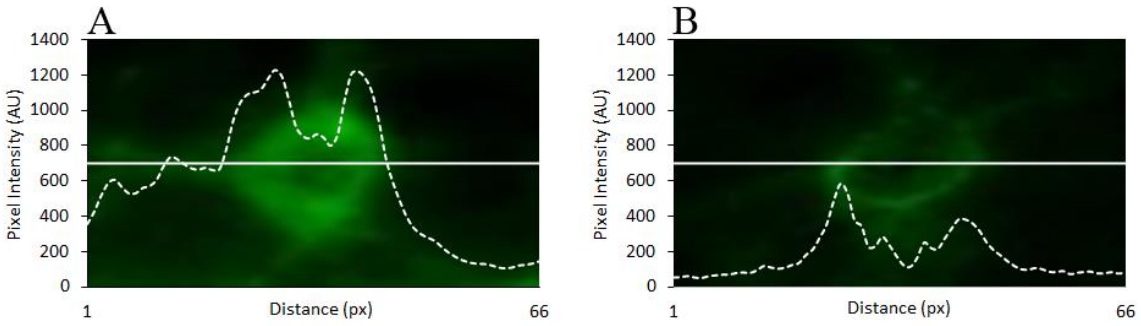

Figure 7: Examples to illustrate measurement of PNN intensity in the region around a cell. The horizontal line centered on the PNN was 40mm long. The bimodal graph shows the pixel intensity along the horizontal line. The area under the curve can be used to measure PNN intensity around cells. (A) Cell with a strong PNN label. (B) Cell with weak PNN staining.

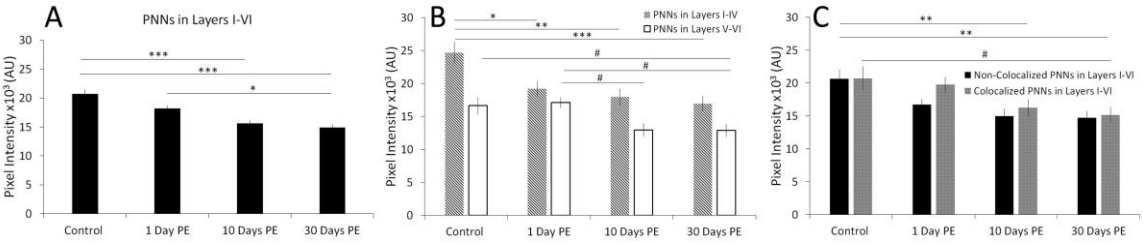

Figure 8: Noise exposure caused a decline in PNN intensity in the region around cells in A1. (A) Average PNN intensity across all layers, (B) Average PNN intensity in layers I-IV (stripe bars) and layers V-VI (white bars) (*p<0.05, **p<0.01, ***p<0.001 for layers I-VI and #p<0.05 for layers V-VI). (C) PNN intensity in cells without PV (black bars) and with PV (gray bars) (*p<0.05, **p<0.01 for non-colocalized PNNs, #p<0.05 for co-localized PNNs).

Reference

Anderson, L.A., Christianson, G.B., and Linden, J.F. (2009). Mouse auditory cortex differs from visual and somatosensory cortices in the laminar distribution of cytochrome oxidase and acetylcholinesterase. Brain Research *1252*, 130–142.

Balmer, T.S. (2016). Perineuronal nets enhance the excitability of fast-spiking neurons. Eneuro.

Balmer, T.S., Carels, V.M., Frisch, J.L., and Nick, T.A. (2009). Modulation of Perineuronal Nets and Parvalbumin with Developmental Song Learning. J. Neurosci. *29*, 12878–12885.

Beebe, N.L., Young, J.W., Mellott, J.G., and Schofield, B.R. (2016). Extracellular Molecular Markers and Soma Size of Inhibitory Neurons: Evidence for Four Subtypes of GABAergic Cells in the Inferior Colliculus. J. Neurosci. *36*, 3988–3999.

Berger, J.I., and Coomber, B. (2015). Tinnitus-Related Changes in the Inferior Colliculus. Front Neurol *6*.

Brewton, D.H., Kokash, J., Jimenez, O., Pena, E.R., and Razak, K.A. (2016). Age-Related Deterioration of Perineuronal Nets in the Primary Auditory Cortex of Mice. Frontiers in Aging Neuroscience 270.

Brückner, G., Seeger, G., Brauer, K., Härtig, W., Kacza, J., and Bigl, V. (1994). Cortical areas are revealed by distribution patterns of proteoglycan components and parvalbumin in the Mongolian gerbil and rat. Brain Research *658*, 67–86.

Cabungcal, J.-H., Steullet, P., Morishita, H., Kraftsik, R., Cuenod, M., Hensch, T.K., and Do, K.Q. (2013). Perineuronal nets protect fast-spiking interneurons against oxidative stress. Proc Natl Acad Sci U S A *110*, 9130–9135.

Carulli, D., Pizzorusso, T., Kwok, J.C.F., Putignano, E., Poli, A., Forostyak, S., Andrews, M.R., Deepa, S.S., Glant, T.T., and Fawcett, J.W. (2010). Animals lacking link protein have attenuated perineuronal nets and persistent plasticity. Brain *133*, 2331–2347.

Celio, M.R. (1993). Perineuronal nets of extracellular matrix around parvalbumin-containing neurons of the hippocampus. Hippocampus *3*, 55–60.

Dityatev, A. (2010). Remodeling of extracellular matrix and epileptogenesis. Epilepsia *51*, 61–65.

Dityatev, A., Brückner, G., Dityateva, G., Grosche, J., Kleene, R., and Schachner, M. (2007). Activity-dependent formation and functions of chondroitin sulfate-rich extracellular matrix of perineuronal nets. Devel Neurobio *67*, 570–588.

Eggermont, J.J. (2015). Animal models of spontaneous activity in the healthy and impaired auditory system. Front. Neural Circuits *9*.

Enwright, J.F., Sanapala, S., Foglio, A., Berry, R., Fish, K.N., and Lewis, D.A. (2016). Reduced Labeling of Parvalbumin Neurons and Perineuronal Nets in the Dorsolateral Prefrontal Cortex of Subjects with Schizophrenia. Neuropsychopharmacology *41*, 2206–2214.

Fader, S.M., Imaizumi, K., Yanagawa, Y., and Lee, C.C. (2016). Wisteria Floribunda Agglutinin-Labeled Perineuronal Nets in the Mouse Inferior Colliculus, Thalamic Reticular Nucleus and Auditory Cortex. Brain Sciences *6*, 13.

Happel, M.F.K., Niekisch, H., Castiblanco Rivera, L.L., Ohl, F.W., Deliano, M., and Frischknecht, R. (2014). Enhanced cognitive flexibility in reversal learning induced by removal of the extracellular matrix in auditory cortex. Proc Natl Acad Sci U S A *111*, 2800–2805.

Kosaka, T., and Heizmann, C.W. (1989). Selective staining of a population of parvalbumin-containing GABAergic neurons in the rat cerebral cortex by lectins with specific affinity for terminal N-acetylgalactosamine. Brain Research *483*, 158–163.

Liu, H., Xu, H., Yu, T., Yao, J., Zhao, C., and Yin, Z.Q. (2013). Expression of Perineuronal Nets, Parvalbumin and Protein Tyrosine Phosphatase σ in the Rat Visual Cortex During Development and After BFD. Current Eye Research *38*, 1083–1094.

Llano, D.A., Turner, J., and Caspary, D.M. (2012). Diminished cortical inhibition in an aging mouse model of chronic tinnitus. J Neurosci *32*, 16141–16148.

Luo, H., Pace, E., and Zhang, J. (2017). Blast-induced tinnitus and hyperactivity in the auditory cortex of rats. Neuroscience *340*, 515–520.

Martin del Campo, H.N., Measor, K.R., and Razak, K.A. (2012). Parvalbumin immunoreactivity in the auditory cortex of a mouse model of presbycusis. Hearing Research *294*, 31–39.

McRae, P.A., Rocco, M.M., Kelly, G., Brumberg, J.C., and Matthews, R.T. (2007). Sensory Deprivation Alters Aggrecan and Perineuronal Net Expression in the Mouse Barrel Cortex. J. Neurosci. *27*, 5405–5413.

McRae, P.A., Baranov, E., Rogers, S.L., and Porter, B.E. (2012). Persistent decrease in multiple components of the perineuronal net following status epilepticus. European Journal of Neuroscience *36*, 3471–3482.

Nakamura, M., Nakano, K., Morita, S., Nakashima, T., Oohira, A., and Miyata, S. (2009). Expression of chondroitin sulfate proteoglycans in barrel field of mouse and rat somatosensory cortex. Brain Research *1252*, 117–129.

Novák, O., Zelenka, O., Hromádka, T., and Syka, J. (2016). Immediate manifestation of acoustic trauma in the auditory cortex is layer specific and cell type dependent. Journal of Neurophysiology *115*, 1860–1874.

Pantazopoulos, H., Lange, N., Hassinger, L., and Berretta, S. (2006). Subpopulations of neurons expressing parvalbumin in the human amygdala. J. Comp. Neurol. *496*, 706–722.

Pilati, N., Ison, M.J., Barker, M., Mulheran, M., Large, C.H., Forsythe, I.D., Matthias, J., and Hamann, M. (2012). Mechanisms contributing to central excitability changes during hearing loss. PNAS *109*, 8292–8297.

Pizzorusso, T., Medini, P., Berardi, N., Chierzi, S., Fawcett, J.W., and Maffei, L. (2002a). Reactivation of Ocular Dominance Plasticity in the Adult Visual Cortex. Science *298*, 1248–1251.

Pizzorusso, T., Medini, P., Berardi, N., Chierzi, S., Fawcett, J.W., and Maffei, L. (2002b). Reactivation of Ocular Dominance Plasticity in the Adult Visual Cortex. Science *298*, 1248–1251.

Roberts, L.E., Eggermont, J.J., Caspary, D.M., Shore, S.E., Melcher, J.R., and Kaltenbach, J.A. (2010). Ringing Ears: The Neuroscience of Tinnitus. J. Neurosci. *30*, 14972–14979.

Scholl, B., and Wehr, M. (2008). Disruption of Balanced Cortical Excitation and Inhibition by Acoustic Trauma. Journal of Neurophysiology *100*, 646–656.

Sonntag, M., Blosa, M., Schmidt, S., Rübsamen, R., and Morawski, M. (2015). Perineuronal nets in the auditory system. Hearing Research *329*, 21–32.

Syka, J., and Rybalko, N. (2000). Threshold shifts and enhancement of cortical evoked responses after noise exposure in rats. Hearing Research *139*, 59–68.

Syka, J., Rybalko, N., and Popelář, J. (1994). Enhancement of the auditory cortex evoked responses in awake guinea pigs after noise exposure. Hearing Research *78*, 158–168.

Takesian, A.E., and Hensch, T.K. (2013). Chapter 1 - Balancing Plasticity/Stability Across Brain Development. In Progress in Brain Research, M.N. and T.M.V.V. Michael M. Merzenich, ed. (Elsevier), pp. 3–34.

Trujillo, M., Measor, K., Carrasco, M.M., and Razak, K.A. (2011). Selectivity for the rate of frequency-modulated sweeps in the mouse auditory cortex. Journal of Neurophysiology *106*, 2825–2837.

Wang, H., Brozoski, T.J., and Caspary, D.M. (2011). Inhibitory neurotransmission in animal models of tinnitus: Maladaptive plasticity. Hearing Research *279*, 111–117.

Yamada, J., Ohgomori, T., and Jinno, S. (2015). Perineuronal nets affect parvalbumin expression in GABAergic neurons of the mouse hippocampus. Eur J Neurosci *41*, 368–378.

Yang, S., Weiner, B.D., Zhang, L.S., Cho, S.-J., and Bao, S. (2011). Homeostatic plasticity drives tinnitus perception in an animal model. PNAS *108*, 14974–14979.

Yang, S., Su, W., and Bao, S. (2012). Long-term, but not transient, threshold shifts alter the morphology and increase the excitability of cortical pyramidal neurons. Journal of Neurophysiology *108*, 1567–1574.

Zhou, X., Jen, P.H.-S., Seburn, K.L., Frankel, W.N., and Zheng, Q.Y. (2006). Auditory brainstem responses in 10 inbred strains of mice. Brain Res *1091*, 16–26.

Chapter 5

Conclusions

5.1 Conclusions

The perception of sound is an important sensory modality which is driven by inputs into the auditory system. This dissertation explores two disorders in which conditions of auditory processing are impaired. The first condition is hearing loss brought on by exposure to loud intensity sounds in the environment (Chapter 4). We induced hearing loss in mice by exposing them to high intensity sounds to mimic noise-induced hearing loss. The second is a neurodevelopmental disorder, Fragile X Syndrome (FXS), which causes sensory dysfunction and greatly impacts the normal function of the auditory system (Chapter 2 and 3). We used a genetic knockout of the Fragile X Mental Retardation gene (*Fmr1* KO) in mice as a model of Fragile X Syndrome to study the auditory characteristics of this syndrome. Here, these studies investigated the dysfunctions in the auditory system using molecular markers, functional electrophysiology, conventional audiology test, and behavioral assessment.

Noise-induced hearing loss is a prevalent disorder affecting 40 million adults in the United States. The initial damage to the auditory system is at the peripheral through the loss of the mechanosensory receptor cells, the inner hair cells of the cochlear. We sought to investigate how the impacts of the sensory overstimulation leads to molecular changes in the auditory cortex. Molecular markers for inhibitory neurons, PV+ and PNN+, were explored to determine the central processing effects after noise-induced hearing loss. PV+ are fast spiking interneurons that are often surrounded by PNNs. We

asked if there were changes to these PV+ and PNN+ neurons because dysfunction in these cells would lead to central processing impairments. The results showed no change in the density of PV+ or PNN+ neurons. However, there was a decrease in the overall PNNs intensity in layers I-IV of the auditory cortex. This layer specific PNN degradation suggests impairments in the ascending pathway of the auditory system. Although noise induced hearing loss affects the peripheral hair cells, our results show that central processing centers are also affected. The formation of PNNs are associated with inhibition so these results indicate a disruption in central inhibition, potentially leading to more plasticity in this area of the cortex that is not receiving sensory input. It was surprising how quickly the PNN integrity deteriorated (1 day post noise exposure), showing how quickly the central molecular changes can happen after hearing loss. This leads to the question of what happens in cases of temporary hearing loss, which is more commonly experienced by the general population. In situations of temporary noise-induced hearing loss and a minimum threshold shift in audibility, we hypothesized that there is a reduction in inhibition at the auditory cortex due to degraded PNN, thus, leading to enhanced hyperactivity in the auditory cortex.

Due to the *Fmr1* KO mice's hypersensitivity to sound, we characterized the response properties using cFos, a marker for neuronal activity, and single unit electrophysiology. The cFos expression in response to sound stimulation increased in dorsal lateral region at P21 but then subsequently decreased at P34. In the ventral medial region, the expression only increased at P34. These results suggest a regional

switching of neuronal activation that is dependent on age. There may be a regulatory mechanism for neuronal activity that is unstable and over inhibits neuronal activity during this developmental stage at the dorsal-lateral region. GABA functions are impaired in *Fmr1* KO mice and the reduction in cFos expression in the dorsal-lateral region can be attributed to the high density of GABAergic markers in this region. Responses to frequencies develop from low to high on the tonotopic map and this frequency specific tonotopic development may explain the age dependent effects in the ventral medial region. At P21, the response to high frequencies may not be fully developed; however, by P34 the response to high frequencies is fully developed, hence, leading to an increase in cFos expression. To summarize, in the single-unit electrophysiology study there was higher spontaneous activity, higher response magnitude, broader frequency tuning, longer latency, greater minimum threshold, and greater response to SAM tones in neurons tuned to CF < 20 kHz in the inferior colliculus. Similar to the cFos results described above, impaired GABA functions may be the mechanism behind the hyperexcitability of neurons with CF < 20 kHz.

We systematically tested the audiogenic seizure severities in response to various sound level intensities. The audiogenic seizure phenotype in *Fmr1* KO mice are often used as a biomarker for evaluation of drug efficacy; however, there are few studies on the audiogenic seizure behaviors. Rectifying this audiogenic seizure behavior as an *Fmr1* KO mice phenotype may be key in reducing hypersensitivity in individuals with FXS. The results demonstrated the threshold for audiogenic seizure to be ~85 dB SPL and a

positive relationship between sound intensity to seizure severity. The sound level to induce audiogenic seizure (~85 dB SPL or higher) is a moderately loud sound which inform considerations in experiments which uses auditory stimulations and environmental noises for individuals with FXS.

ABR is a measurement of auditory ability in a range of frequencies and intensities. DPOAE measures acoustic emission from the outer hair cells, as an indication of the functions of the outer hair cells. There were no amplitude differences in ABR response wave form in any of the five peaks. However, there was a latency abnormality in peak III and V of the waveform. In addition, there were no differences between WT and *Fmr1* KO mice in I/O magnitude, I/O phase, magnitude, or phase in the DPOAE recordings.

FMRP is region specific and have concentration densities that changes throughout development. Approaches to develop treatments for FXS needs to consider the developmental time course during which the function of FMRP shape circuit maturation. Understanding auditory processing in FXS during a critical developmental period may reveal underlying mechanisms of how the lack of FMRP disrupt the system. These results suggest that the inferior colliculus is an important region during development which needs the role of FMRP. The impairments during development in the inferior colliculus leads to audiogenic seizures and auditory hypersensitivity.

5.2 Summary

In summary, this dissertation investigated the effects of noise-induced hearing loss on molecular markers in the auditory cortex (Chapter 4). There were degradation of PNN intensity in layers I-IV of the auditory cortex, suggesting central processing deficits after hearing loss. In Chapter 2, investigations of auditory response properties in FXS used cFos as a molecular marker of activity and single unit electrophysiological recordings. There were age and region specific differences of evoked activities in response to sound, suggesting the impairments in the auditory system are dynamic throughout development. In addition, audiogenic seizure, auditory brainstem response (ABR), and distortion product otoacoustic emission (DPOAE) were characterized in FXS. Sound stimulus at 85 dB SPL was the lowest sound level needed to evoke audiogenic seizure behaviors and 105 dB SPL evoked audiogenic seizure in all mice tested. There are behavioral deficits in response to relatively moderate intensity sound (85 dB SPL) and auditory stimulus in mice and individuals with FXS should consider this threshold. ABR and DPOAE revealed similar results in WT and *Fmr1* KO mice except for latency differences in peak III and V of ABR, corresponding to origins of the olivary complex and inferior colliculus.

5.3 Future Directions

The cFos findings in this dissertation showed age and region specific changes in the inferior colliculus for the *Fmr1* KO compared to WT mice. cFos is a molecular marker for neuronal activity but it is ambiguous as to which cell type express the cFos protein in response to sound stimulation. This leads to the question: which neuronal cell types are driven to activate through sound exposure in the inferior colliculus? To expand on the current cFos findings described in Chapter 2, we aim to stain for GAD67 (a marker for GABAergic inhibitory neurons) and vGlut1 and vGlut2 (a marker for excitatory neurons). The procedure would consists of exposing mice to sound stimuli as describe in Chapter 2. This will be followed by staining of the neural tissue in the region of interest, the inferior colliculus. The staining with the markers for cFos protein, GAD67, vGlut1, and vGlut2 which will be carried out in 2 brain slice sections that contain the inferior colliculus for each mouse. Based on previous literature of known neuronal cell types distribution in the inferior colliculus, and due to the current abnormal response properties for neurons with CF<20kHz, the hypothesis is that the activated neurons from sound exposure in the dorsal-lateral region will be GABAergic. The second hypothesizes is that there will be fewer colocalized staining of GAD67 with cFos in *Fmr1 KO* mice exposed to sounds compared to WT mice. The refinement of the cFos study with the addition of information on the cell type that are responding to sound stimuli at the region that is correlated for behavioral hypersensitivity in the Fmr1 KO mice may lead to

a mechanism for targeted treatment in FXS. Based on the results of this dissertation on across multiple age groups, mice at P21 is a critical age what presents large differences between Fmr1 KO and WT mice. Neuronal cell type that is activated in the inferior colliculus may define treatments that target GABAergic systems and treatment in early adolescence as a critical window to treat sensory hypersensitivity.

The inferior colliculus receives input from almost all brainstem subnuclei and the auditory cortex. In our previous studies, we defined abnormal response characteristics for neurons with CF<20 kHz which is specific to the dorsal-lateral region. Are the response characteristic of these nuclei in the dorsal-lateral region of the IC inherited from a lower brainstem nuclei? One possible approach is to apply the fluorescent retrograde tracer, Fluoro-Gold, in the *Fmr1* KO mouse's inferior colliculus in narrow areas (dorsal-lateral or ventral-medial areas). This method would determine if abnormal inputs are projected into the dorsal-lateral or ventral-medial regions of the IC. We hypothesize that there would be abnormal projections to the low frequency regions in the inferior colliculus. In addition, we expect a wider area of innervations and a greater overlap of brainstem terminals onto the inferior colliculus in the dorsal-later region.